

UNCLASSIFIED

AD NUMBER

AD853418

LIMITATION CHANGES

TO:

Approved for public release; distribution is unlimited.

FROM:

Distribution authorized to U.S. Gov't. agencies and their contractors;
Administrative/Operational Use; MAY 1969. Other requests shall be referred to Air Force Weapons Lab., Kirtland AFB, NM.

AUTHORITY

AFWL ltr 30 Nov 1971

THIS PAGE IS UNCLASSIFIED

AFWL-TR-68-143, Vol. I

AFWL-TR-
68-143,
Vol. I

AD853418



DISTENDED MATERIAL MODEL DEVELOPMENT

Volume I

Experiments and Theory for the Model

L. Seaman

R. K. Linde

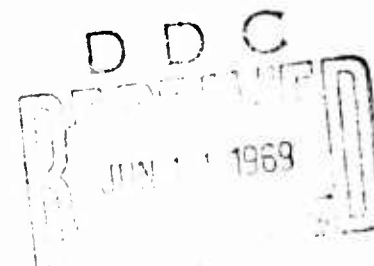
Stanford Research Institute

Menlo Park, California 94025

Contract No. F29601-67-C-0073

TECHNICAL REPORT NO. AFWL-TR-68-143, Vol. I

May 1969



AIR FORCE WEAPONS LABORATORY

Air Force Systems Command

Kirtland Air Force Base

New Mexico

This document is subject to special export controls and each transmittal to foreign governments or foreign nationals may be made only with prior approval of AFWL (WLRP), Kirtland AFB, NM, 87117.

PERMISSION FOR	
CFSTI	WHITE SECTION
DC	BUFF SECTION
UNANNOUNCED	
SIGNIFICATION	
Y	
DISTRIBUTION/AVAILABILITY CODES	
DIST.	AVAIL. CODE OR SPECIAL
2	

AIR FORCE WEAPONS LABORATORY
Air Force Systems Command
Kirtland Air Force Base
New Mexico

When U. S. Government drawings, specifications, or other data are used for any purpose other than a definitely related Government procurement operation, the Government thereby incurs no responsibility nor any obligation whatsoever, and the fact that the Government may have formulated, furnished, or in any way supplied the said drawings, specifications, or other data, is not to be regarded by implication or otherwise, as in any manner licensing the holder or any other person or corporation, or conveying any rights or permission to manufacture, use, or sell any patented invention that may in any way be related thereto.

This report is made available for study with the understanding that proprietary interests in and relating thereto will not be impaired. In case of apparent conflict or any other questions between the Government's rights and those of others, notify the Judge Advocate, Air Force Systems Command, Andrews Air Force Base, Washington, D. C. 20331.

DO NOT RETURN THIS COPY. RETAIN OR DESTROY.

AFWL-TR-68-143, Vol. I

DISTENDED MATERIAL MODEL DEVELOPMENT

Volume I

Experiments and Theory for the Model

L. Seaman

R. K. Linde

Stanford Research Institute
Menlo Park, California 94025
Contract No. F29601-67-C-0073

TECHNICAL REPORT NO. AFWL-TR-68-143, Vol. I

This document is subject to special export controls and each transmittal to foreign governments or foreign nationals may be made only with prior approval of AFWL (WLKP), Kirtland AFB, NM, 87117. Distribution is limited because of the technology discussed in the report.

FOREWORD

This report was prepared by Stanford Research Institute, Menlo Park, California, under Contract F29601-67-C-0073. The research was prepared under Program Element 6.16.46.01H, Project 5710, Subtasks 15.018 and 15.025, and was funded by the Defense Atomic Support Agency (DASA).

Inclusive dates of research were 21 April 1967 through 1 March 1969. The report was submitted 2 April 1969 by the Air Force Weapons Laboratory Project Officer, Capt Joseph B. Webster, III (WLRP).

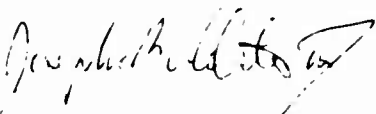
Information in this report is embargoed under the U.S. Export Control Act of 1949, administered by the Department of Commerce. This report may be released by departments or agencies of the U.S. Government to departments or agencies of foreign governments with which the United States has defense treaty commitments, subject to approval of AFWL (WLRP).

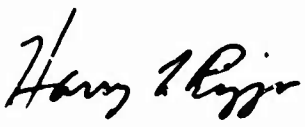
The contractor's account reference number is SRI Project PGU 6586.


The project supervisor was Dr. R. K. Linde of Poulter Laboratory and Dr. L. Seaman was project leader. The authors wish to acknowledge the advice of Dr. George Duvall of Washington State University. They are also indebted to Betty Jo Murrell, who wrote the flow charts, the section on Input-Output, and major portions of the computer program.

This volume contains a physical description of the SRI PUFF code, as well as comparisons of experimental data and computed predictions based on the model. Volume II contains test runs of the new computer code.

This technical report has been reviewed and is approved.


JOSEPH B. WEBSTER, III
Captain, USAF
Project Officer


HARRY F. RIZZO
Lt Colonel, USAF
Chief, Physics Branch


CLAUDE K. STAMBAUGH
Colonel, USAF
Chief, Research Division

ABSTRACT

The research goals were (1) to develop a dynamic response model or constitutive relations for porous materials, (2) to test this model against results from shock wave experiments, and (3) to incorporate the model into a computer program for the analysis of shock wave propagation arising either from impacts or from radiation deposition. The model developed exhibits melting, vaporization, and temperature-dependent compaction resistance, yielding, consolidation, and spalling. The model accounts for loading and unloading, heating and cooling, and any combination of these processes. The computer program (SRI PUFF 1) for analyzing shock wave propagation problems employs artificial viscosity in a modified Lax-Wendroff integration scheme.

Flyer plate impact experiments (shock attenuation tests) were conducted on samples of porous iron, copper, and tungsten, and stress histories were recorded at the rear face of the targets. Quasi-static one-dimensional compression tests were made on samples of the same porous metals, using pressures up to 10 kbar. Numerical values of parameters in the model were obtained from the quasi-static tests and from previously reported Hugoniot experiments. Stress histories computed with the code were compared with stress records obtained from the attenuation experiments. The computed (predicted) peak stresses and arrival times of the waves generally agreed to within 20 percent or better with the measured values. Precursor amplitudes and other wave front features were correctly represented in the computed histories. The model appears to adequately represent the dynamic response of porous materials, the major uncertainty being the numerical values of parameters for a given material.

(Distribution Limitation Statement No. 2)

This page intentionally left blank.

CONTENTS

<u>Section</u>	<u>Page</u>
I INTRODUCTION	1
II BACKGROUND	3
1. Theoretical	3
2. Experimental	13
III THEORETICAL MODEL FOR A POROUS MATERIAL	20
1. Introduction	20
2. Equation of State of a Solid	22
3. Constitutive Relations for a Distended Material	33
IV EXPERIMENTAL MEASUREMENTS	48
1. Quasi-Static Measurements of P-V Relations	48
2. Dynamic Measurements of Shock Attenuation	50
3. Static and Dynamic Compression of Polyurethane Foam	54
V COMPARISON OF THEORY AND EXPERIMENT	57
1. Discussions of Wave Propagation Phenomena	57
2. Computed Stress Histories	58
3. Construction of Input Data	73
4. Areas Requiring Further Effort	76
APPENDIX: INPUT DATA FOR COMPUTED STRESS RECORDS	79
REFERENCES	88
DISTRIBUTION	93

ILLUSTRATIONS

<u>Figure</u>	<u>Page</u>
1 Compression path of a porous material and four simple models for porous materials.	5
2 Energy-Pressure-Volume (E-P-V) depiction of Herrmann's Equation of State	10
3 Common Forms of Pressure and Stress Hugoniots	24
4 Energy-Pressure-Volume (E-P-V) Surface for a Solid Material	24
5 P-V Relations at Constant Internal Energy for Aluminum	30
6 Relation Between Energy and Volume for Unconfined Expansion of Solid	32
7 Hugoniot for a Porous Material	34
8 Depiction in E-P-V Space of the Constitutive Relations for a Porous Material	35
9 Constitutive Relations of a Porous Material, Emphasizing the Intermediate Surface for Elastic Response to Loading and Heating	36
10 Variation of Strength with Temperature for 1100 Aluminum	39
11 Locus of States Caused by Heating Porous Material Without Expansion	41
12 Possible Pressure Hugoniot and Variation of Yield Strength for a Porous Material	43
13 Thermal Strength Reduction Functions Employed in Computer Code	45
14 Cutaway View of Quasistatic Compression Device	49
15 Static and Dynamic Compression Data For Porous Iron	51
16 Static and Dynamic Compression Data For Porous Copper	52
17 Static and Dynamic Compression Data For Porous Tungsten	53
18 Static and Dynamic Compression Data For Polyurethane Foam	55
19 Comparison of Theoretical Isotherm with Data For Porous Iron	59
20 Comparison of Theoretical Isotherm with Data For Porous Copper	60
21 Comparison of Theoretical Isotherm with Data For Porous Tungsten	61
22 Comparison of Theoretical Isotherm with Data For Polyurethane Foam	62

ILLUSTRATIONS

<u>Figure</u>	<u>Page</u>
23 Iron/Porous Iron Impact, Shot 13,347	63
24 Iron/Porous Iron Impact, Shot 13,403	64
25 Iron/Porous Iron Impact, Shot 13,418	65
26 Copper/Porous Copper Impact, Shot 13,349	66
27 Copper/Porous Copper Impact, Shot 13,404	67
28 Copper/Porous Copper Impact, Shot 13,417	68
29 Tungsten/Porous Tungsten Impact, Shot 13,402	69
30 Tungsten/Porous Tungsten Impact, Shot 13,473	70

TABLES

I Conditions of Attenuation Experiments	55
II Hugoniot Data For Polyurethane Foam	55

NOMENCLATURE

A	Function of V
a, b	Constants in the isotherm of Kawakita and Tsutsumi (Ref. 47)
C	Bulk modulus at low pressures
COSQ	Coefficient of quadratic viscosity term
C _l	Coefficient of linear viscosity term
C _p	Specific heat at constant pressure
C _v	Specific heat at constant volume
E	Internal or deposited energy, ergs/g
E _s	Sublimation energy
F ₁ , F ₂	Stress relaxation functions of Johnson (Ref. 46)
G ₀ , G	Shear moduli of solid and porous materials, respectively, dynes/cm ²
H	$C_p/C_v - 1$
K ₀ , K	Bulk moduli of solid and porous materials, respectively, dynes/cm ²
M	Modulus for rate-independent equation of state $d\sigma = MdV/V$
N	$C/(\Gamma E_s \rho_0)$
P	Pressure, dynes/cm ²
P ₀	Pressure at previous cycle, dyne/cm ²
S	Stress, dynes/cm ²
SD	Deviator stress, dyne/cm ²
T ₁ , T ₂	Time constants for relaxation functions of Johnson (Ref. 46)
t	time, sec
U	Particle velocity, cm/sec
U _s	Shock velocity, cm/sec
V	Specific volume, cm ³ /g
V _{eq}	Equilibrium specific volume, cm ³ /g
V ₀	Initial specific volume, cm ³ /g
V _s	Specific volume of solid, cm ³ /g
Y	Yield strength, dyne/cm ²
α	Volumetric thermal expansion coefficient
γ	Ratio of specific heats
Γ	Grüneisen ratio

Γ_0	Grüneisen ratio at initial solid density
μ	$\rho/\rho_0 - 1$
ρ_s, ρ	Densities of solid and porous materials, respectively, g/cm ³
ρ_0	Initial density, g/cm ³
σ	Stress
θ	Temperature

This page intentionally left blank.

SECTION I

INTRODUCTION

Previous work (Refs. 1-5) performed for the Air Force Weapons Laboratory (AFWL) has demonstrated that porous solids (also called distended solids, or foams) can be very effective in attenuating the peak stress of a propagating stress pulse. Hence, to protect a structural material from shock damage caused by short-duration impulsive loadings, an external layer of a porous material might be used. For effective use of such porous materials, it is necessary to be able to predict the response of the material to expected shock loadings. This report provides a procedure for predicting the response.

Research performed at Stanford Research Institute (SRI) and elsewhere (see Refs. 1-20, for example) has provided a considerable body of Hugoniot* and other dynamic data on porous metals and, to some extent, on porous plastics and ceramics. To make effective use of such data in vulnerability studies and survivability design of possible reentry systems, it is necessary to employ this data to construct a mathematical model of the dynamic response of porous materials to impulsive loading. To make the needed predictions, the model must be incorporated into a computer code (such as PUFF 66) for analyzing shock-wave propagation. The present effort was initiated to develop a prediction capability for shock propagation and attenuation behavior in porous solids using data (from AFWL TR-68-33⁵) on porous copper, iron, and tungsten. This goal has been met with development of the SRI PUFF 1 computer code.

* As used in this report the term "Hugoniot" is applied to foams to mean the locus of final macroscopic pressure-volume or pressure-particle velocity states of shocked material deduced from experimental observations and invocation of the so-called "jump" conditions which express conservation of mass and momentum across a shock front. This "Hugoniot" represents actual rather than average states of the material only if the scale of porosity is such that equilibrium is attained within the time scale of the experiment.

In addition to experiments on porous metals, three exploratory dynamic experiments were performed at peak stresses below 50 kbar on "3-D" quartz phenolic material supplied by AFWL. Additional experiments are currently being performed. To present the results of these experiments in the most useful manner, the results of the three quartz phenolic experiments performed under the present contract will be presented in a later report.

SECTION II

BACKGROUND

1. THEORETICAL

The historical development of equations of state for porous materials is closely connected with the development of computer programs for wave-propagation calculations. In this section, we outline the development of wave-propagation computer programs and then describe in detail equation-of-state formulations that have been developed.

In 1950, von Neumann and Richtmyer (Ref. 21) initiated the artificial viscosity (or Q) method for using digital computer codes to solve the equations of wave propagation. With this technique, infinitely steep shock fronts are not allowed to develop and the entire field can be treated as a continuous flow. Shock fronts appear as regions of high stress gradient but not as discontinuities. The artificial viscosity tends to dampen all oscillations or perturbations in the flow field. Several integration schemes based on the Q method have been developed, notably the Lax-Wendroff method (Ref. 22), the Runge-Kutta-Gill method (Ref. 23), and the "leapfrog" scheme (Ref. 21), which is used in most PUFF codes.

The present line of PUFF-type codes originated around 1958 with the development of the SHARK (Ref. 24) and SHARP (Ref. 25) codes. With later developments at the Air Force Special Weapons Center, Kirtland Air Force Base, the generic name PUFF was given to the programs. Recent versions include PUFF (Ref. 26, 27, 28), PUFF III (Ref. 29), PUFF IV (Ref. 30), PUFF IV-EP* (Ref. 31), PUFF V-EP (Ref. 32), PUFF VTS** (Ref. 33), FOAM PUFF (Ref. 34), PUFF 66 (Ref. 35), and P PUFF 66 (Ref. 35). The present code (SRI PUFF 1) began as a modification of the last two. Most of the PUFF codes have been described in classified reports, so their characteristics cannot be outlined here. A useful review of the capabilities of each of these codes has been provided by Bothell and Archuleta (Ref. 31).

* EP stands for elastic-plastic.

** Variable time step.

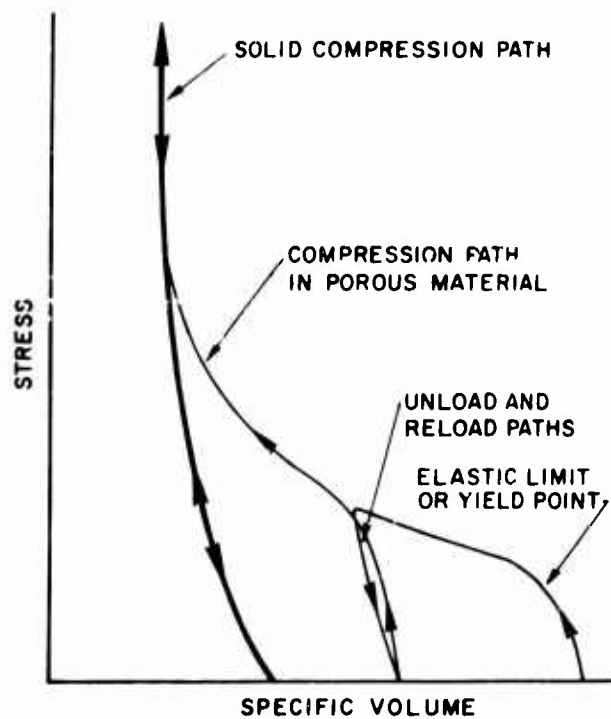
Other PUFF-type codes are available under the names of WONDY (Ref. 36), AFOAM (Ref. 4), and ARTON (Ref. 37). All of the PUFF-type codes use artificial viscosity and the leapfrog integration scheme.

The attempt to insert into a PUFF code a so-called equation of state for a porous material* has in the past met with considerable difficulty. First, the formulation of the equation of state has been hampered by a lack of specific information on material behavior. Most attempts to develop so-called equations of state for porous materials have been directed toward plate-impact problems. Hence, radiation deposition was not included, and it was assumed sufficient to provide only Hugoniot paths rather than the more complete P-V-E (pressure-volume-energy) equation of state. Second, the computations have been fraught with oscillations and instabilities associated with the large compressibilities of the porous materials. This problem with the computations points out an advantage of developing the computer program and the equation of state concurrently.

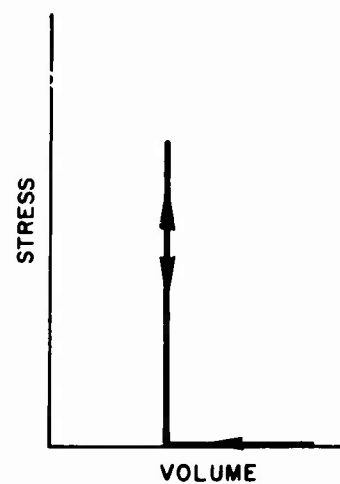
The equations of state postulated for porous materials have grown progressively more complex as more has been learned about the materials themselves. At present, the material behavior during shock compression in plate impact experiments is the aspect best understood. The thermodynamic stress-volume paths followed by a porous material during the impact are probably like that shown in Fig. 1a. In most porous materials there is an initial, approximately elastic behavior up to a somewhat ill-defined "yield point." This yield point defines the amplitude of the "elastic" precursor in the material.** For higher stresses, the particles yield or crush, and pores are filled in so that the behavior is largely

* The pressure-volume-energy relations that describe the behavior of porous materials do not actually constitute a true equation of state (this point is discussed in detail later). However, because these relations take the place of an equation of state, they are popularly called an equation of state.

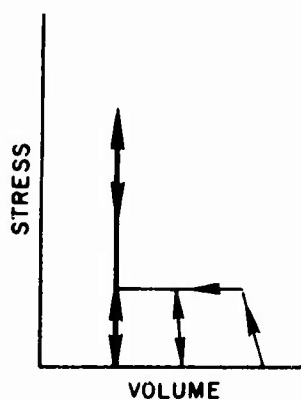
** When a load is applied to a porous material, high stress concentrations occur at contact points of the particles. Thus, even the "elastic" precursor will generally cause a small amount of localized plastic flow that enlarges contact surfaces and relieves the high stress concentrations.



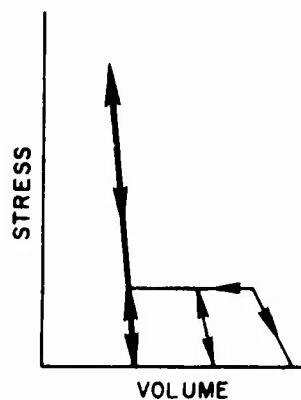
(a) COMPRESSION PATH OF POROUS MATERIAL



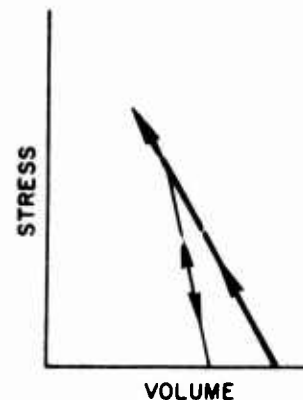
(b) SIMPLE LOCKING OR SNOWPLOW MODEL



(c) ELASTIC/
PERFECTLY PLASTIC
RIGID LOCKING
MODEL



(d) ELASTIC/
PERFECTLY PLASTIC
LOCKING MODEL



(e) ELASTIC-LOCKING
MODEL

GA-6586-40

FIG. 1 COMPRESSION PATH OF A POROUS MATERIAL AND FOUR SIMPLE MODELS FOR POROUS MATERIALS

irreversible. After consolidation (full compaction to the solid state), the compression path for subsequent compressive loadings is taken to coincide with that of the solid material at the same temperature. Simple models that represent this compressive behavior in a porous material are shown in Figs. 1b through 1e.

Various models can be used to define Hugoniot, isentropes, and other stress-strain paths, depending on the experimental conditions. The simple locking or snowplow model specifies compaction at zero stress up to consolidation, and may therefore be used if the elastic compression of the solid is unimportant and material compacts at an essentially constant stress, or if the shock stress is well above the consolidation stress of the material. The elastic/perfectly plastic locking model takes into account the elastic behavior of the solid, but does not allow for any strength of partially compacted material. The elastic-locking model does allow for such strength and is applicable at stresses below consolidation. All of these models lead to fairly straightforward wave-propagation calculations; therefore, they have been used extensively for computations of waves in porous materials. In the following discussion, we mention some of the more complex formulations for porous materials.

In 1965, Thouvenin (Ref. 38) presented his plate-gap model for shock compression of porous materials at high pressures. This model represents a porous material as a series of plates separated by gaps. Wave propagation within the plates, impact of the plates on each other, and consequent removal of gaps were considered in detail to determine the macroscopic behavior of the model. Thouvenin considered particularly the impact of a solid flyer plate on a porous target made of plates of the same material. He determined from wave-propagation calculations, that for the same impact velocity, the free-surface velocity of a porous material should be equal to that of a full-density solid of the same material. He also indicated that a porous solid under the influence of shock reaches an equilibrium state that is on the same pressure-volume Hugoniot as that of the compact solid, that is, that energy, pressure, and volume points coincide after consolidation. But the energy attained in the material while passing from the initial specific volume V_0 at atmospheric pressure

to the final volume V is

$$E = \frac{1}{2} S(V_0 - V) + E_0$$

where S = stress of the shock wave

E_0 = initial specific energy of the material, usually negligible.

The final energies behind a shock of a given stress S must therefore differ if the initial volumes differ. Hence, the coincidence of porous and solid pressure-volume Hugoniot is a violation of the first law of thermodynamics and also contrasts with the findings of experimentalists for strong shocks. In his analysis, Thouvenin does not take into account the difference between the thermodynamic stresses and the mechanical stresses in the wavefront. If this difference were considered and the mechanical stress would follow the Rayleigh line in the P - V plane, then a different Hugoniot would be formed corresponding to each initial density of solid or porous material.

J. F. Heyda (Ref. 39) modified Thouvenin's model slightly to guarantee momentum conservation across the shock front. In this modified model the pressure-volume Hugoniot depends on initial density, unlike Thouvenin's model. Heyda's results correlated well with some experimental data at high pressures. However, this model implicitly assumes an isentropic Hugoniot for the solid plates. This may not be serious at low stresses, but becomes more in error as the shock stress is increased. Furthermore, in a real material, with porosity, one normally expects considerably more entropy production (because of microjetting and other effects) than that provided by a simple plate-gap model even when corrected for noncoincidence of solid Hugoniots and release adiabats.

Prindle (Ref. 40) also presented a theoretical study of shocks in porous materials based on the approach of Thouvenin. He developed a considerably more complex set of equations to explain the response of Thouvenin's model to compaction waves. He included material strength so that a precursor wave could be produced. Low-pressure shocks were assumed to remove voids in the direction of propagation but to leave lateral voids. Stronger shocks were assumed to squeeze the material and remove the voids. The precursor wave was associated with the first

type of void removal, while the main shock produced complete compaction. Prindle obtained analytic solutions for impact problems. However, his model is based on the same isentropic behavior as Thouvenin's model, and therefore suffers from the same theoretical inconsistencies.

Butcher (Ref. 41) discussed the crush-up or consolidation behavior for several models that have been postulated. He discussed in some detail the model that Fritz and Taylor (Ref. 42) developed for adiprene rubber foam. The model is based on the concept of a limiting density and on the static compression curve for the material. The equation of state resulting from the analysis resembles that for a soft solid: it does not show the large permanent deformations that occur with distended metals or plastics. Butcher also discussed the snowplow model and Thouvenin's plate-gap model and made a few calculations with each to illustrate the results obtainable.

Models based directly on Hugoniot measurements have been proposed by Wagner, Brooks, and Bjork (Ref. 43), by Herrmann (Refs. 44, 45); and by Linde and Schmidt (Refs. 3,4), who have discussed phenomenological models that have various degrees of complexity.

None of the models discussed above explicitly allow for external heating, and thus they are not suitable for radiation deposition problems, and therefore fail to account completely for the effects of internal energy. These models may be used for plate impact calculations in which the Hugoniot of the solid matrix material and the Hugoniot of the consolidated porous material essentially coincide, i.e., where thermal effects are negligible. Radiation deposition computations cannot be made with these models. An early model which included external heating was presented by Allen et al. (Ref. 34) in 1964 for a material such as styrofoam. The energy-pressure-volume model was incorporated into FOAM PUFF, a computer program of the PUFF VTS type. The yield, or upper, surface of the equation of state for porous material was similar to the one presented in this report. The variation in the P-V plane was, however, given by a single exponential equation. In the direction of increasing internal energy, the pressure (or strength of the foam) decreased linearly with energy, reaching zero when the internal energy

reached the sublimation energy. Hence, melting was not specifically provided for. The material was allowed to unload and reload in a physically reasonable manner and with a modulus like that of the virgin material. More recent models for porous materials have been formulated by other investigators for very high-pressure work, to emphasize the correspondence between equations of state for porous and solid materials, or to simplify the computations. However, the recent models do not seem to have made important improvements to the FOAM PUFF model and they are less complete.

Herrmann (Ref. 44) presented a formulation for an E-P-V equation of state for crushable distended materials. The equation of state is based essentially upon the Mie-Grüneisen equation of state for solid material with the addition of a parameter alpha, the ratio of the solid to the porous densities. Herrmann also gave an analytical form for the variation of alpha with compaction, thus providing a Hugoniot for any porous material. Herrmann's complete formulation includes analytical formulas for the wave velocity during loading of the virgin material and during unloading and subsequent reloading. His sample calculations showed considerable erosion of the wave fronts. He noted that for computations with porous materials, considerably longer running times than for solids are required, and higher values of the artificial viscosity are needed. Herrmann (Ref. 45) later altered the formulation of the equation of state to provide for arbitrary initial wave velocities of the virgin material.

In his papers, Herrmann has specifically formulated the equation of state only in the P-V plane: he notes that the variation in the energy direction has not yet been defined. However, because the porous equation of state is closely connected with the solid equation of state, the variation in the energy direction is defined by default. In any plane of constant E in the E-P-V space, the P-V curve has the same shape as at $E = 0$ (see Fig. 2). If the porous material were heated at constant volume it would increase in strength, never melting, but becoming solid at some point. Such behavior is not physically reasonable. Therefore, the Herrmann equation of state should be used only for impacts where internal energies less than melting are of interest, or in computations where the stresses are well above the consolidation pressure.

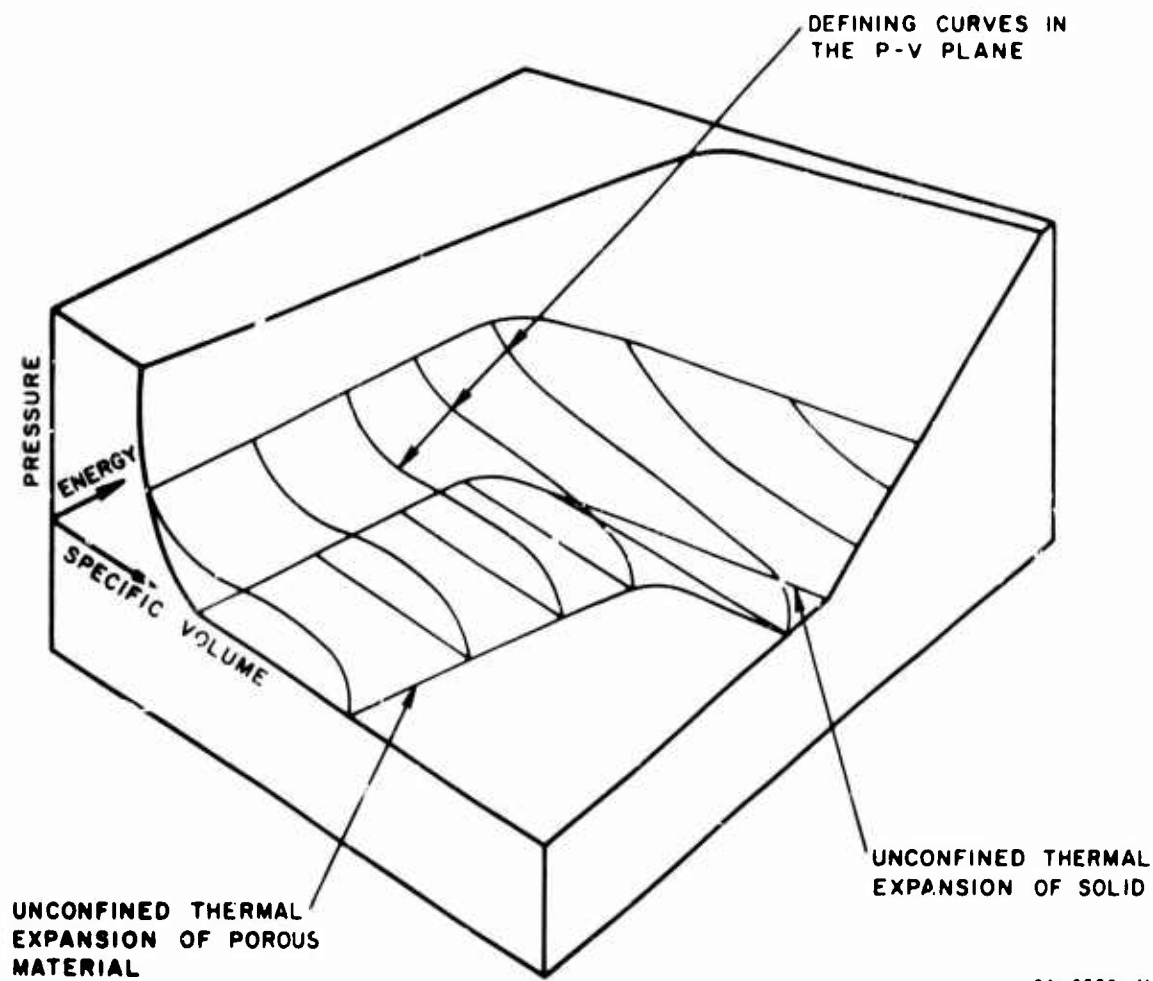


FIG. 2 ENERGY-PRESSURE-VOLUME (E-P-V) DEPICTION OF HERRMANN'S EQUATION OF STATE

As an extension of Herrmann's model, Johnson (Ref. 46) proposed a theory for strain rate-dependent behavior of porous solids. He suggested that the experimentally observed slow rise of the second wave in porous materials results from a significant amount of strain rate dependence. Johnson's formulation starts with the analytical equation of the Hugoniot given by Herrmann. He then presents two possible stress relaxation functions (F_1 and F_2) that are proportional to the plastic strain rate. These two functions are as follows:

$$F_1 = - (K/V_0 T_1) (V - V_{eq}) \quad (1)$$

$$F_2 = - (\sigma/V_0 T_2) (V - V_{eq}) \quad (2)$$

where

K = the bulk modulus

σ = the stress

V_0 = the specific volume of the solid

V = the current volume

V_{eq} = the equilibrium volume for the current stress

T_1 and T_2 = the time constants for the relaxation functions.

Either of these two plastic strain functions can be used in the equation-of-state relations as follows:

$$\frac{d\sigma}{dt} - \frac{M}{V} \frac{dV}{dt} = -F \quad (3)$$

where

t = time

F = a strain rate function

M = the modulus for the usual rate-independent equation of state

$d\sigma = M dV/V$.

Johnson calculates steady-state wave profiles in materials for these two stress relaxation functions. For both functions the thickness of the shock front decreases markedly with increased stress. The profiles are similar for the two formulations but the one that is a function of stress seems to be steeper at high stresses.

Of the many models for quasistatic behavior of porous solids, one empirical equation is worthy of mention here. Kawakita and Tsutsumi (Ref. 47) presented an empirical equation of state for powder compression. The equation is for static work and corresponds to an isotherm rather than to the Hugoniot:

$$K = \frac{V_0 - V}{V_0} = \frac{a b P}{1 + b P} \quad (4)$$

where K is the bulk modulus and a and b are constants. The equation was fitted to data on metal powders, ferrite powders, foodstuffs, and other powders, and appeared, in general, to give a good representation of the data.

Biot (Ref. 48) developed equations of state for elastic and visco-elastic behavior of fluid-filled anisotropic porous media. However, the elastic moduli of the composite material were not given as functions of the known parameters.

MacKenzie (Ref. 49) derived expressions for the elastic constants of a solid containing spherical holes. It was intended that the results would be applicable to sintered material because on sintering the pores usually assume an approximately spherical shape. The analysis was made for static elastic behavior only. The results of the calculations were formulas for bulk and shear moduli, which increase with density of the material, reaching values for the solid when the density is that of a solid. The equations for the moduli are as follows:

$$\frac{1}{K} = \frac{\rho_s}{K_0 \rho} + \frac{3(1 - \rho/\rho_s) \rho_s}{4 G_0 \rho} \quad (5a)$$

$$\frac{G - G_0}{G_0} = 5(1 - \rho/\rho_s) \frac{3 K_0 + 4 G_0}{9 K_0 + 8 G_0} \quad (5b)$$

where

K and G = the bulk and shear moduli of the porous material

K_0 and G_0 = the moduli of the solid material

ρ and ρ_s = densities of the porous and solid materials, respectively.

These formulas show a linear variation of the shear modulus with density.

The bulk modulus increases slowly initially during compaction and then rapidly as the density approaches that of the solid.

2. EXPERIMENTAL

A considerable body of experimental shock propagation data for porous materials has been obtained. Selected important experimental investigations are summarized below.

a. Soil and Rock

Gregson, Ahrens, and Petersen (Ref. 6) studied quartzite, sandstone, basalt, calcite, and plagioclase rocks in the range from 4 to 250 kbar. High values of the Hugoniot elastic limit were observed in solid rocks - 50 to 100 kbar in quartzite, 40 to 50 kbar in feldspar and basalt, and 20 kbar in calcite and marble. Limestone (a porous rock initially at 87 to 95 percent of solid density) showed elastic precursors of 10 to 15 kbar and compaction to the solid (calcite) pressure-volume Hugoniot at 25 to 40 kbar. The sandstones (74 to 88 percent of solid density) tested exhibited precursors of 10 kbar and compaction to the solid (quartz) Hugoniot at 50 to 100 kbar.

Anderson et al. (Ref. 2) conducted a study of equations of state of porous earth media. The study included experiments on wet playa, with initial dry densities of 58 and 73 percent of solid density, a discussion of several forms of the Mie-Grüneisen equation of state, and theoretical studies on shock stability and phase transitions. The stresses in the tests on wet playa ranged from 1 to 400 kbar. The Hugoniot of the wet playa could be synthesized from those of dry playa and water. There appeared to be a phase transition to stishovite at the high pressures. Reversible and irreversible equations of state for materials undergoing phase transitions were constructed. These were applied to the transition between quartz and stishovite. The equations of state were used in wave-propagation calculations. For computations, it was found necessary to employ artificial viscosity during compression and rarefaction both in order to properly damp oscillations.

Petersen, et al. (Ref. 7), reported Hugoniot and release adiabat data on natural and reconstituted tuff, a porous, partially cemented mixture of quartz, feldspar, pumice, and other minerals. No precursor was evident and consolidation appeared to occur at about 100 kbar. The release adiabats (unloading curves) showed recovery to specific volumes larger than the volume of the solid material but less than the initial volume even for stresses well above 100 kbar.

b. Metals

Kormer et al. (Ref. 8) conducted a series of shock compression tests on porous aluminum, copper, lead, and nickel in the megabar pressure range. Initial densities were as low as one-fourth the crystal density. The work was done with bonded metal powders rather than sintered foams. Their test data led them to more complex formulations of the Mie-Grüneisen equation and to determination of the variations of the Grüneisen ratio. The Kormer equation has the form of two simultaneous equations, one for pressure and one for energy, both written as functions of temperature.

Krupnikov et al. (Ref. 9) conducted shock compression tests for porous tungsten (initial densities as low as one-fourth the crystal density) in the megabar range. They were interested in formulating a refined equation of state that would include electronic components. The form of the equation is somewhat simpler than that of Kormer et al. and could be easily programmed for computation. For tungsten, it was found that the effective value of Grüneisen's ratio varied from 1.5 at room conditions to around .17 at 3.5 Mbar.

Boade (Ref. 10) reported the results of 15 experiments with porous tungsten (initially at 19 percent of solid density) up to pressures of 500 kbar. His data gave a good fit to the following equation:

$$U_s = 0.0204 + 1.116 U \quad (6)$$

where U_s and U are shock and particle velocity, respectively, and the units are in cm/ μ sec. The corresponding pressure/particle velocity ($P - U$) plot also gave a smooth fit to the data. However, the pressure-volume plot showed considerable scatter.

Rempel et al. (Ref. 1) conducted shock attenuation experiments on several solid and distended materials. Tests on porous aluminum (0.7 to 1.4 g/cm³), polyurethane (.67 g/cm³), beryllium (1.1 g/cm³), graphite (1.1 and 1.7 g/cm³) and silica (1.0 g/cm³) were made in a pressure range from 0.1 to 6 kbar. The peak stresses and wave shapes were not predictable on the basis of theory available at the time. The fore-runner or precursor wave traveled at a velocity lower than the measured longitudinal sound speed but higher than that computed from the measured elastic moduli. The stress was usually about double that predicted from static compression tests. Some dynamic and static experiments were made with preheated foams. Preheating reduced the elastic modulus, the elastic yield limit and the stress level of the precursor, and it reduced the rate of attenuation of stress in the main wave.

Linde and Schmidt (Ref. 4) reported studies on porous aluminum (initially 1.08 to 2.14 g/cm³) and graphite (0.9 to 1.7 g/cm³). The experimentally determined stress-time profiles were compared with wave-propagation calculations based on an elastic/perfectly plastic locking model (shown in Fig. 1d). It was found necessary to construct a somewhat more complicated Hugoniot model, resulting in the AFOAM computer program for wave propagation calculations. Comparisons between the experiments and calculations for attenuation tests showed that a reasonably accurate procedure for predicting attenuation of stress had been developed. In some cases the entire stress history could be correctly predicted.

Johnson and Wackerle (Ref. 11) conducted a preliminary study of shock compression in porous magnesium and ammonium sulphate as part of a study of granular explosives. The samples were formed by pressing magnesium powder to 75 percent of solid density and sulphate crystals to 74 percent and 98 percent of solid density. Attempts to correlate the experimental results with Thouvenin's model (Ref. 34) were not successful, but the authors thought that the lack of correlation might have been the result of experimental difficulties.

Anderson and Fahrenbruch (Ref. 12) conducted a series of shock wave experiments on porous and solid samples of aluminum and Teflon[®] (E. I. du Pont de Nemours and Co.). Aluminum samples with densities of 1.35, 1.60, and 1.92 g/cm³ were produced by cold pressing atomized aluminum powder. The aluminum data from the Hugoniot experiments, which were conducted with shock stresses of 200 to 700 kbar, were fitted to the equation.

$$S = \frac{\Gamma}{V} E + A(V) \quad (7)$$

where

S = stress

Γ = Grüneisen's ratio

V = specific volume

E = specific internal energy

A = function of volume

The ratio Γ/V , which was found to be a constant, was equal to 5.15 g/cm³. An expression for A was also given.

Boade (Ref. 13) studied shock compression of porous copper (initial densities of 68 and 83 percent of solid) at low stresses and reported the observation of a three-wave shock profile. The first wave had an amplitude of about one-half kbar and traveled at sonic velocity; the second had an amplitude of about 1.1 to 1.3 kbar traveling at about one-half sonic velocity; and the third wave was the main wave. Complete compaction of the material appeared to occur at about 21 kbar. Microscopic examination of the materials showed that the pores were essentially spherical and uniformly distributed with diameters of about 0.1 mm. For the stress levels used it was found that the ratio of Grüneisen's ratio to specific volume was essentially a constant. A Grüneisen ratio of 1.96 was found at the low stress levels. The Hugoniot relation for the porous material was compared with the formulation of Herrmann (Ref. 44), but the fit was not very good. An attempt was made to explain why a three-wave structure might exist.

Butcher and Karnes (Ref. 14) studied shock compression samples of porous iron with initial densities ranging from 1.3 to 7.0 g/cm³. Their materials contained essentially spherical voids 0.1 mm in diameter for the lowest density foams and 0.02 mm for the higher density sintered foams. The data were interpreted on the basis of steady state conditions. For the iron the relation between the yield strength in kilobars and the density was found to be

$$Y = 8.5 (\rho_s / \rho_o)^{-3.9} \quad (8)$$

where

ρ_s = the density of solid material at zero stress

ρ_o = the initial density of the foam.

The relation between the initial wave velocity and density is similar to that between yield and initial density. The compaction appeared to be complete at 26 kbar. For correlation with experimental work, calculations were made using either an elastic/perfectly plastic locking model or a simple locking model (see Fig. 1). The simple locking model was found sufficient for correlation with experiments on the less dense foams. The elastic/perfectly plastic locking model was necessary for correlation with the higher density foams that exhibited a precursor.

Schmidt and Linde (Ref. 5) conducted a series of tests on distended copper, iron, and tungsten, all at about 70 percent of crystal density. Hugoniot and release states for pressures up to about 60 kbar in copper, 50 kbar in iron, and 140 kbar in tungsten were studied. It was found that inclusions such as corrosion products in the pores of the porous materials substantially altered the compaction behavior of the porous copper and iron. Clean samples of the porous copper and iron compacted essentially to solid at pressures of about 20 kbar. The tungsten foam had not fully compacted to the solid state at 140 kbar.

c. Porous Carbon Material

Butcher (Ref. 15) reviewed experiments on three types of porous carbon materials with initial densities of 0.68, 1.14 and 1.30 g/cm³.

The shock wave data on porous carbon materials were compared with the Hugoniot of the solid for tests in which the porous material reached consolidation pressures. Because of the various types of carbon, and because of the phase transformations that occur, even the choice of the correct Hugoniot for the solid was somewhat uncertain. Particle velocities and wave velocities were compared with calculations based on the plate gap model of Thouvenin (Ref. 35). The correlation between experimental data and theoretical calculations was good, especially at the point of complete consolidation. Results on the carbon foams show significant attenuation of peak stress and, hence, inapplicability of the usual shock-front relations, which require the presence of a steady state in the wave front.

Rempel et al. (Ref. 1) and Linde and Schmidt (Ref. 4) conducted combined theoretical and experimental studies of graphites: their general results have been summarized earlier under subsection b.

Boade (Ref. 16) studied the shock compression of foamed graphite with stresses in the range from 8 to 190 kbar. The initial densities were 0.55 and 0.68 g/cm³. Hugoniots were developed for foamed graphite for several initial porosities. The data reduction was done on the assumption of a constant wave form with a single wave structure. However, in some cases a two-wave structure was present. The precursor amplitude appeared to increase with the applied stress level.

d. Miscellaneous Materials

Polyurethane, Beryllium, and silica were among the materials studied by Rempel et al. (Ref. 1). Their results were discussed under subsection b.

Johnson and Wackerle (Ref. 11) made a preliminary study of ammonium sulphate, as mentioned previously under subsection b.

Leibermann (Ref. 18) conducted a series of tests up to about 1 kbar on Celotex, styrofoam, redwood, sugar pine, foam glass, and balsa. The Hugoniots obtained were similar to the isothermal equation of state and the data was reduced by means of simple characteristic plots.

Lee (Ref. 19) studied dynamic compaction of distended boron nitride with an initial density of about half the solid density. The grain size was between 20 and 100 Å. With pressures up to 10 kbar the precursor amplitude was 1.5 kbar. Compaction was not complete at the 10 Kbar pressure level. The experimental data were compared with theoretical calculations based on the simple elastic/perfectly plastic locking model and on Herrmann's model (Ref. 41). Good correlation with the first model was obtained in the P-U plane with the assumption of a yield strength of 2 kbar.

Linde and DeCarli (Ref. 20) studied phase transformations and Hugoniot elastic limits in porous and solid titanium dioxide under shock conditions. For the solid, the elastic limit was 70 or 100 kbar, depending on the orientation of the crystal lattice in the shock wave. Porous samples were formed to densities of 98, 96, 66 and 50 percent of solid density by hot pressing. Hugoniot elastic limits corresponding to these densities--55, 33, 18, 5 kbar--show a marked sensitivity to porosity.

SECTION III

THEORETICAL MODEL FOR A POROUS MATERIAL

1. INTRODUCTION

The major theoretical contributions of this report are:

- A set of constitutive relations for porous materials. These relations provide for compaction to solid, and for loading, unloading, yielding, heating, melting, cooling, and spalling, both before and after full compaction of the material has occurred.
- A modified PUFF-type computer program for calculating the propagation of stress waves through a series of solid or porous materials. This modified code is based on the Lax-Wendroff procedure for integrating the equations of motion.

The SRI PUFF 1 code is a computer program developed for calculating one-dimensional stress-wave propagation through solid or porous materials. The stress waves being computed are initiated either by the deposition of radiated energy in the materials or by the impact of one material on another. Computations are made with the Lagrangian form of the differential equations of motion, so that coordinates move with the materials. The program is termed a Q-code because of the computation of an artificial viscosity stress, or Q, to provide for the propagation of shock waves.

The following features are included in the code:

- Interfaces between different materials are allowed; hence, the stress wave propagation may be followed through a series of materials.
- The equation of state of a solid material is represented by two algebraic equations: the Mie-Grüneisen equation and the expansion equation employed in previous PUFF versions.
- Deviator stress, yield strength, and work hardening are provided for.
- The materials may be distended (porous). Strength of the porous material depends on the internal energy; hence, it is a function of temperature.
- Materials may spall or separate at any coordinate and may subsequently recombine. For porous materials, the spall strength depends on the degree of compaction and on internal energy.

- The radiant energy input is deposited over a period of time so that material may expand during deposition.
- The radiation absorption spectrum for a compound material may be introduced as a series of spectra, one for each component or element of the material.

A complete thermodynamic equation of state for a substance is the locus of all possible equilibrium states for that substance. Each state is a set of values of the five thermodynamic quantities; tensorial stress, specific volume, specific entropy, specific internal energy, and temperature. Very shortly after a shock passes through a homogeneous solid, the material usually reaches thermodynamic equilibrium and the macroscopic thermodynamic quantities vary smoothly in the material. However, the states reached within a porous material are more complex. Stresses initially will be higher at particle contact points, and large strains and distortions will occur as the voids are filled in. Processes such as microjetting and the production of localized "hot spots" will occur. For the scale of homogeneity of most foams, thermodynamic equilibrium generally will not be achieved within the time scale of laboratory experiments. Also, the state reached by a shock is not a unique function of the thermodynamic quantities, but depends on the history of the specimen.

For the above two reasons (lack of equilibrium and lack of uniqueness) no true equation of state can be applied to the porous material as a whole. However, we can, and have, developed constitutive relations that will serve the same function as an equation of state. In the remainder of the report we will employ the popular terminology and loosely refer to the constitutive relations as "porous equations of state." In the present formulation we have accounted for the history of the material. We will also assume that average thermodynamic quantities are equilibrium values and that when the material is fully compacted to a solid, the average quantities lie on the true equation-of-state surface of the solid.

For convenience in formulating the equations of state for both solid and porous materials, the stress tensor will be defined as the sum of a pressure and a deviator stress tensor. The pressure is defined as

$$P = \frac{1}{3} (S_{11} + S_{22} + S_{33}) \quad (9)$$

where the S's are stresses on any three mutually orthogonal planes. The deviator stress is the variation of any normal stress from the average:

$$SD_{ii} = S_{ii} - P \quad (i = 1, 2, 3) \quad (10)$$

For the one-dimensional strain case to be treated here, the stresses can be conveniently taken in the directions of principal stresses so that only normal stresses occur. Furthermore, the deviator stresses are simply related,

$$SD_{22} = SD_{33} = -\frac{1}{2} SD_{11} \quad (11)$$

so that the only stress quantities to be computed are SD_{11} and P. The pressure is computed as a function of two or more of the other thermodynamic quantities. The deviatoric stress is computed from a stress-strain relation. The stress is then found as a simple sum of SD_{11} and P. With this separation of stress into two components, the development of an equation of state requires the construction of two relationships, one for pressure and one for deviator stress. This component approach has been used in the earlier development of PUFF and is continued here for building the model for distended materials.

2. EQUATION OF STATE OF A SOLID

We consider first an equation of state of a solid (i.e., nonporous) material. The substance is termed solid because it is solid at the initial pressure and internal energy; however, the equation of state describes the material behavior in solid, liquid, and gaseous phases. The equation used here for pressure is of the form

$$P = P(E, V) \quad (12)$$

which says that pressure is a function of only specific internal energy and specific volume. The thermodynamic quantities entropy and temperature are not considered explicitly. Equation 12 defines a surface in E-P-V space.

An equation of state represents equilibrium states. Therefore, as a material undergoes gradual changes, such as heating, compression, etc., the successive states describe a path on the equation-of-state surface if there is no heat conduction or other nonequilibrium process occurring. If the material is compressed by passing through a steady-state shock front and the initial and final states are equilibrium states, then these states lie on the equation-of-state surface. These initial and final states are connected by a straight line, the Rayleigh line, which lies on or above the surface, for the usual, concave-upward, surfaces. The states of transition within a shock front are not states of thermodynamic equilibrium and hence do not necessarily lie on the surface.

Shock experiments lead to the determination of a Hugoniot or Rankine-Hugoniot equation of state which is not a complete equation of state, but represents one curve on the equation-of-state surface. This line is the locus of final states that can be obtained by a steady-state shock transition from a given initial state. A common form for a pressure-volume Hugoniot is shown in Fig. 3.

This same curve is redrawn in Fig. 4 on the E-P-V equation-of-state surface for the material. During compression there is some increase in internal energy, so that the Hugoniot does not lie in a single P-V plane.

As a reminder of the role of stress in the compression of the solid, consider the stress-volume Hugoniot of Fig. 3. During compression the stress is greater than the pressure; on unloading, the stress decreases rapidly to yielding and then follows a stress adiabat below the pressure adiabat. The unloading (pressure) adiabat is also depicted in Fig. 4. The unloading adiabat lies to the right of the Hugoniot for materials that expand during heating. For such materials less internal energy

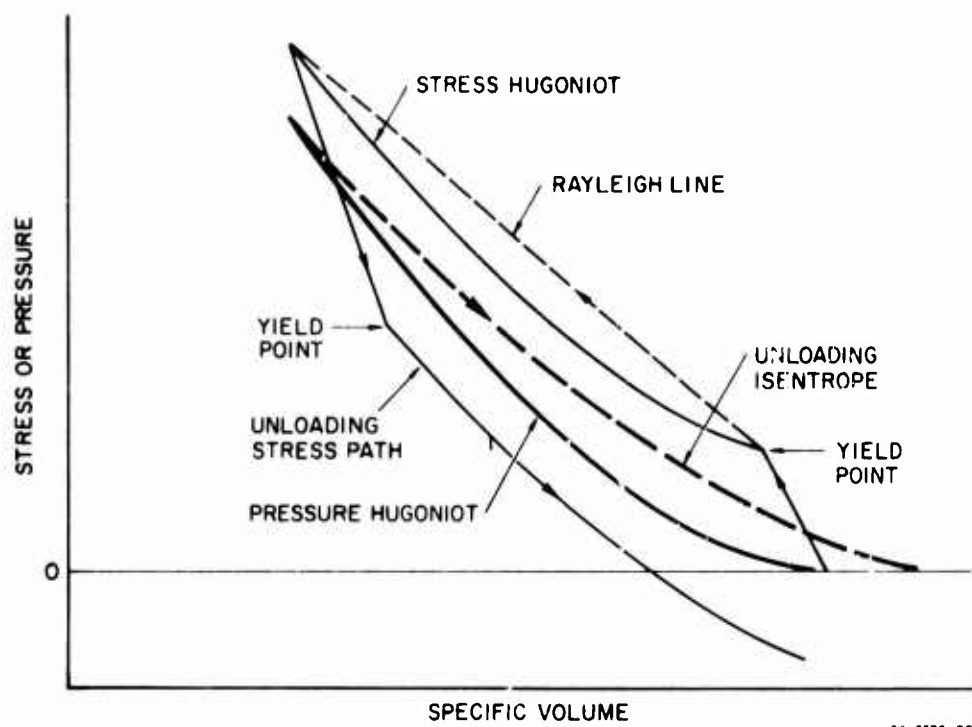


FIG. 3 COMMON FORMS OF PRESSURE AND STRESS HUGONIOTS

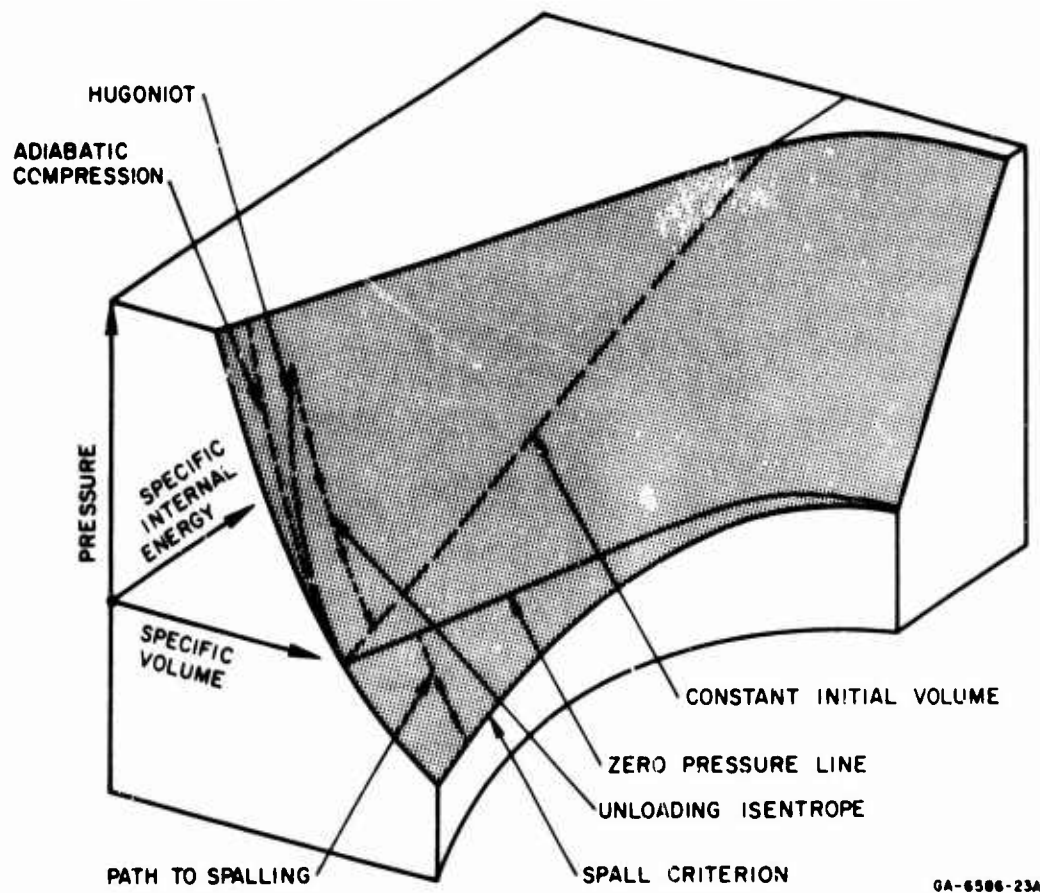


FIG. 4 ENERGY-PRESSURE-VOLUME (E-P-V) SURFACE FOR A SOLID MATERIAL

is recovered by the adiabatic decompression than was inserted to produce the shock compression. A line illustrating a path of adiabatic, gradual compression is also shown in Fig. 4.

Several other lines of interest are shown in Fig. 4. The zero (or atmospheric) pressure line is the locus of points obtained by simply heating the material without external mechanical confinement. Heating increases the internal energy, and thermal expansion occurs. For small increases in internal energy, the zero pressure curve describes the usual expression for volumetric thermal expansion

$$V = V_0 (1 + \alpha \Delta \theta)$$

or

$$V = V_0 \left(1 + \frac{\Gamma \Delta E}{VK} \right) \quad (13)$$

where

α = the volumetric thermal expansion coefficient

Γ = the Grüneisen ratio

K = the bulk modulus

$\Delta \theta$ = the change in temperature

ΔE = the change in internal energy

V_0 = the initial specific volume

If we take the usual assumption that Γ/V and K are constant at zero pressure, then ΔE is proportional to $\Delta \theta$ while the material is solid. As the material is further heated it melts and then vaporizes. The $P = 0$ curve becomes asymptotic to the line described by

$$\begin{cases} E = \text{sublimation energy} \\ P = 0 \end{cases}$$

for large V .

The region of spalling is not well-defined at present, so that the depicted surface below zero pressure is conjectural. Spalling, or mechanical separation of the material, occurs if the solid material is

subjected to a sufficiently large tensile stress. The occurrence of spalling depends on the magnitude of the applied stress and, in general, on all three principal stresses at a point. (Hence, there is considerable ambiguity in depicting spalling on a pressure coordinate as in Fig. 4.) Because of the time required to form and propagate cracks and to move masses of material so that separation can occur, the duration of loading is also significant. The spall resistance will also depend on temperature or internal energy. If the material is liquid at the time of separation and the separation is accompanied by the production of bubbles rather than the growth of cracks, the phenomenon is termed cavitation. Bull (Ref. 50) has pointed out that the occurrence of cavitation is governed by the size of cavitation nuclei (bubbles or foreign particles), surface tension, viscosity and inertia forces, and the amplitude and duration of the applied stress. Of these, the viscosity and stress amplitude will probably dominate under shock loading. When the material reaches the point of vaporization, it ceases to have any resistance to cavitation. For the SRI PUFF 1 code a single tensile stress value is used for the spallation criterion at present.

When spalling occurs, the stress on the spall surface immediately returns to zero. The material some distance from the spall surface is relieved gradually by rarefaction waves from the spall surface. This deeper material then returns to higher compression stresses upward along a path similar to the original spall path, recovering internal energy as it recompresses. The region to the right of the spall criterion cannot be reached. It may be noted that specific volume is taken to mean the total volume of solid particles on both sides of the spall (but not including the volume of the space between the spall surfaces) divided by the mass of the particles.

When material is held at a particular volume and heated (internal energy is added), it goes through states that are straight lines on the equation-of-state surface. This is indicative of the fact that for constant $V (= V_1)$ the analytical equations for the surface have the form

$$E = A(V_1) \cdot PV_1 \quad (14)$$

where $A(V_1)$ is a function of V_1 only.

The equation-of-state surface depicted in Fig. 4 is an idealized form applicable to a material that does not experience phase changes or other phenomena that lead to regions of negative curvature in the P-V plane. While this surface represents the material behavior qualitatively, only certain regions of the surface are well understood quantitatively. The best understood region is in the vicinity of the Hugoniot because of the availability of experimental data along that curve. The least understood regions are those near spalling and just to the right of the curve $V = V_0$.

The equation of state for a solid and the subroutine for calculating it in SRI PUFF 1 are essentially the same as those in PUFF 66. The equation of state is described by two analytical equations (one for compression and one for expansion) and is bounded for negative stresses by a spall criterion.

The equation used to describe compression is the Mie-Grüneisen equation

$$P - P_{REF} = \frac{\Gamma(V)}{V} (E - E_{REF}) \quad (15)$$

where

P_{REF} and E_{REF} = a point on some reference curve at the same specific volume V

$\Gamma(V)$ = the Grüneisen ratio.

Equation (15) has been derived on the assumption that Γ is a function of V only. Equation (15) provides a means for extending the information of a known P-V relation (such as a Hugoniot) to other values of internal energy. Because the Hugoniot is the P-V relation that is most likely to be known, the computations are constructed so that the Hugoniot is the reference curve used. The Hugoniot P-V equation is presumed to be in the form

$$P_H = C\mu + D\mu^2 + S\mu^3 \quad (16)$$

where

$$\mu = \frac{\rho}{\rho_0} - 1 = \frac{V_0}{V} - 1$$

The internal energy along the Hugoniot is

$$E_H = \frac{1}{2} P_H (V_0 - V_H) \quad (17)$$

Equation (17) is based on the assumption that the initial internal energy is zero and that the Hugoniot is everywhere concave upward. In general, the latter assumption excludes consideration of phase changes. Also, the relation is strictly true only if the stress Hugoniot coincides with the pressure Hugoniot; however, at high pressures there is usually little inaccuracy introduced by this approximation. With the aid of Equations (16) and (17) the Mie-Grüneisen equation takes the following form in the program:

$$P = (C\mu + D\mu^2 + S\mu^3) * \left(1 - \frac{\Gamma\mu}{2}\right) + \Gamma\rho E \quad (18)$$

In the computer program the Grüneisen ratio Γ_0 at initial density is taken as a constant, EQSTG. Then Γ is treated as a function of density such that $\Gamma\rho$ is constant.

At a constant volume, Equation (18) has the form of Equation (14); hence, constant volume lines on the equation-of-state surface are straight lines. The Mie-Grüneisen equation of state is used for densities greater than the initial density. Thus on the equation-of-state surface the straight line $V = V_0$ is the boundary between the Mie-Grüneisen equation and an expansion equation.

The expansion equation, which is unchanged from PUFF 66, meets four requirements:

- It joins smoothly to the Mie-Grüneisen equation along $V = V_0$.
- It expands like $PV = (\gamma - 1)E$ at large expansions (like a gas).
- It provides a linear relation between P and E for constant V .

- It accounts for the partition of internal energy into components for kinetic energy and for intermolecular bond disintegration (sublimation).

An equation which satisfies these requirements is

$$P = \rho \left[H + (\Gamma - H) \frac{\rho}{\rho_0} \right] * \left\{ E - E_S \left[1 - \exp \left(N (1 - \rho_0 \rho) \rho_0 \rho \right) \right] \right\} \quad (19)$$

where

ρ = density

ρ_0 = initial density

Γ = Grüneisen ratio

$H = \gamma - 1 = C_P/C_V - 1$ for expansion at low densities

$N = C/(\Gamma E_S \rho_0)$

E_S = sublimation energy

C = coefficient in Equation (18), the bulk modulus at low pressures

In the PUFF 66 manual (Ref. 35), a value of 0.25 is suggested for H . The sublimation energy as defined there is the difference between the internal energy of the solid material at ambient conditions and the internal energy of the fully expanded vapor at a temperature of absolute zero.

The form of the equation-of-state surface generated by the two equations and the spall criterion is shown in Fig. 4. When the spall criterion is omitted, cuts through the surface at constant energy produce the curves shown in Fig. 5 (for aluminum). For internal energy less than the sublimation energy, these curves indicate that as the material is expanded the pressure decreases to some minimum and then increases again to zero. In many cases this uniform expansion of continuous material will be interrupted by spalling or cavitation.

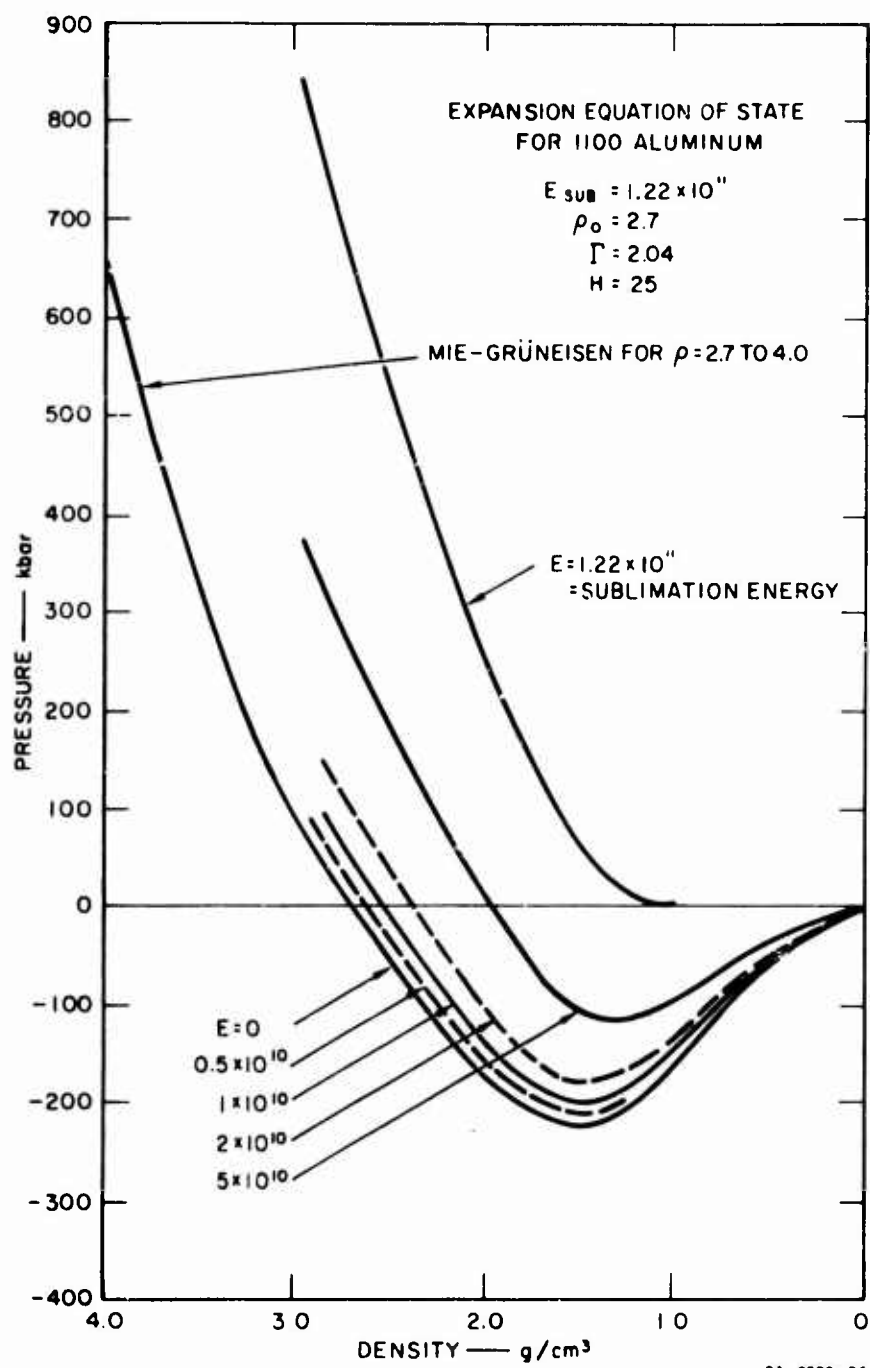


FIG. 5 P-V RELATIONS AT CONSTANT INTERNAL ENERGY FOR 1100 ALUMINUM

If the material is heated without external confinement, the path is on the intersection of the $P = 0$ surface and the equation-of-state surface (see Fig. 6). The initial expansion follows the usual law of thermal expansion, Equation (13).

The deviator stress equation takes a much simpler form in the PUFF formulation than does the pressure equation. The deviatoric stress is

$$SD = \frac{4}{3} \int_{\rho_0}^{\rho} G \frac{d\rho}{\rho} \quad \text{for } |SD| < \frac{2}{3} Y \quad (20)$$

otherwise

$$|SD| = \frac{2}{3} Y \quad (21)$$

where

- G = the shear modulus
- ρ = the density
- Y = the yield strength

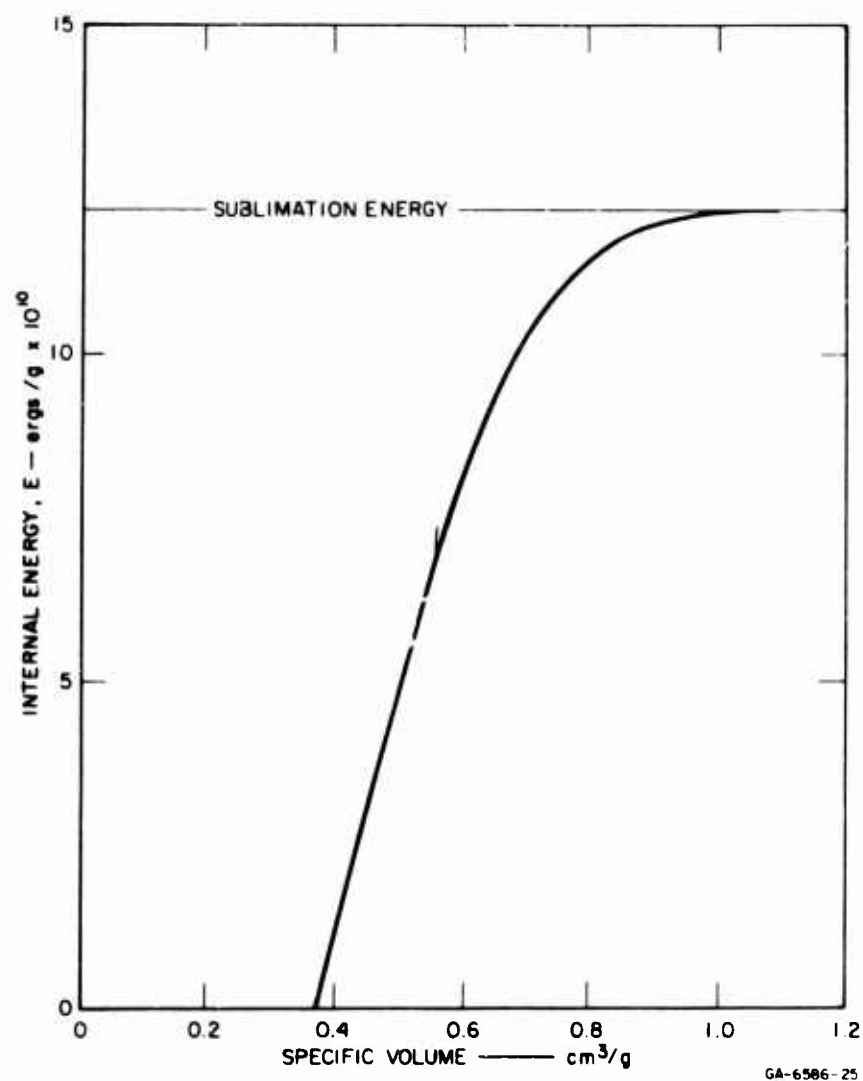


FIG. 6 RELATION BETWEEN ENERGY AND VOLUME FOR UNCONFINED EXPANSION OF SOLID

3. CONSTITUTIVE RELATIONS FOR A DISTENDED MATERIAL

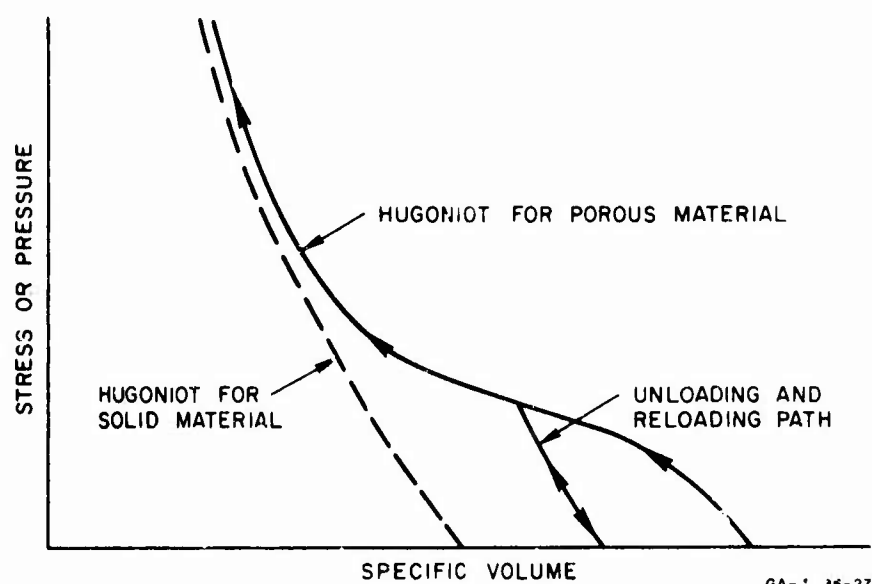
a. Introduction

The model proposed here for the description of the state of a distended material consists of a set of constitutive relations to define behavior while the material is porous, plus an equation of state for the solid substance to be used in describing behavior after consolidation. As discussed above, the model for behavior of porous material is not, strictly speaking, an equation of state because not only is thermodynamic equilibrium generally not achieved, but there is no unique relation among E , P , and V .^{*} Instead, the pressure depends not only on E and V , but also on the previous E - P - V states.

A Hugoniot for a porous material is shown in Fig. 7. This Hugoniot plus a Hugoniot for the same material starting at the normal solid density, are traced on the equation-of-state surface of Fig. 8. A comparison of these two Hugoniots illustrates that for the same pressure or volume, points on the Hugoniot for the porous material are at higher energy states because a greater amount of compressional work ($\int P dV$) is expended to reach a given pressure or volume. The individual rounded particles undergoing shock compression are loaded by a highly nonuniform stress field, are caused by yield and flow to fill the voids, and are locally heated by the energy of deformation and other processes (e.g., microjetting and adiabatic compression of any gas in the pores).

The portion of the constitutive relations that describes the behavior of the unconsolidated material with solid particles is the main feature to be developed (see Fig. 9). Any point in this three-dimensional region represents a possible state for the material.

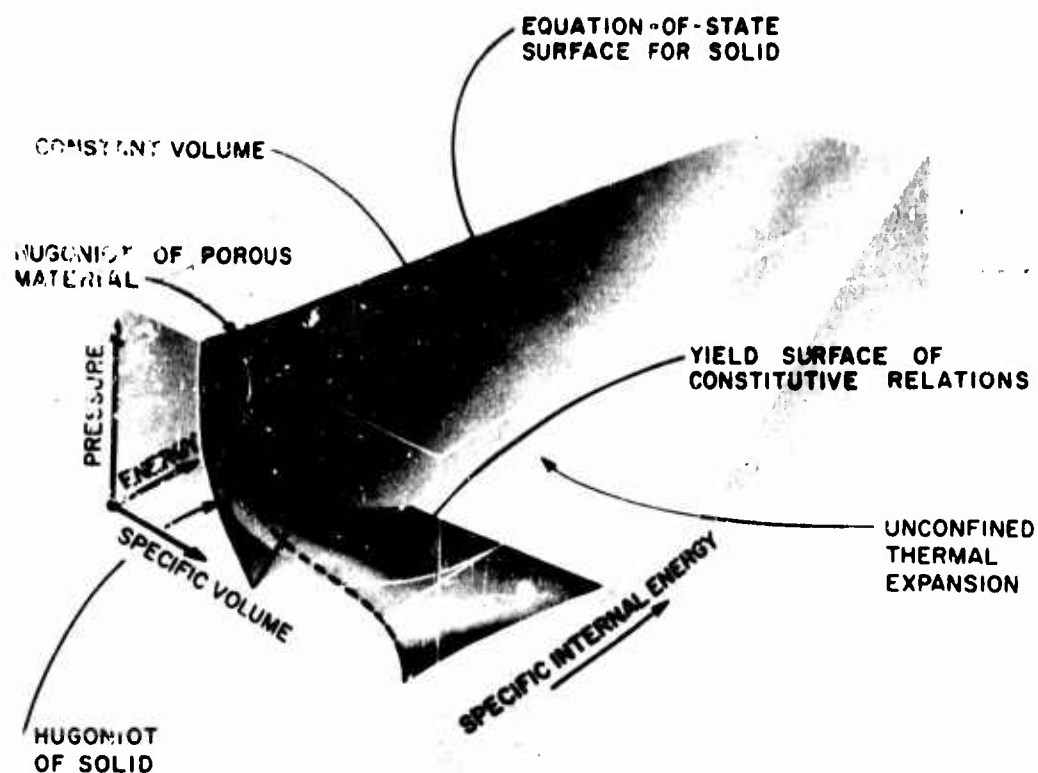
^{*} This point is discussed further in subsection c below.



GA- 36-27

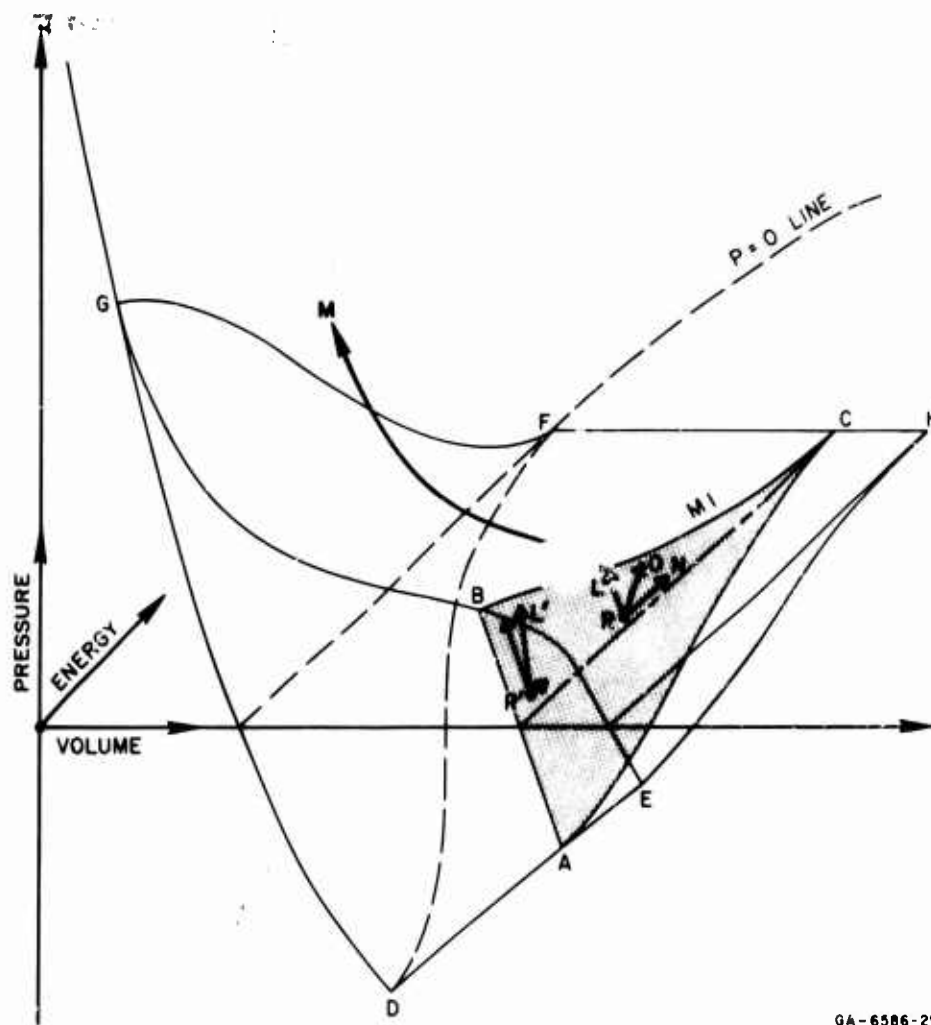
FIG. 7 HUGONIOT FOR A POROUS MATERIAL

NOT REPRODUCIBLE



GP-6886-28

FIG. 8 DEPICTION IN E-P-V SPACE OF THE CONSTITUTIVE RELATIONS FOR A POROUS MATERIAL



GA-6586-29

FIG. 9 CONSTITUTIVE RELATIONS OF A POROUS MATERIAL, EMPHASIZING THE INTERMEDIATE SURFACE FOR ELASTIC RESPONSE TO LOADING AND HEATING

The region is bounded above by a surface prescribed by the yielding of the particles (surface EBGFCH), below by spalling or separation of the particles (surface EADFCH), and to the left by consolidation to a solid material (surface DFG). When the state point (R, as an example) is within this region, the state point is constrained to move on an intermediate surface (ABC) which is approximately parallel to the equation-of-state surface for a solid at the same E and P values. The detailed character of the intermediate and bounding surfaces is developed in the

following paragraphs, based on a consideration of various processes that material may undergo: loading, unloading, and reloading; heating and cooling; and spalling.

The behavior of the porous material under heating at zero pressure can be estimated by considering the behavior of the solid particles. If the material is heated from an arbitrary initial point at zero pressure, such as point R in Fig. 9, the expansion path is along the curve^{*} RN defined by

$$\begin{cases} P = 0 \\ V = V_1 (1 + \alpha \Delta \theta) \end{cases}$$

where $\Delta \theta$ is a change in temperature. Note that this expression for the path holds for $V_1 = V_0$, the initial specific volume, and $V_1 = V_s$, the solid volume. Because this path represents no mechanical yielding, particle rearrangement, melting, or spalling, it is presumed to lie on an intermediate surface ABC of Fig. 9.

Unloading from a partially consolidated state will occur along a different path than that along which the loading (including nonshock loadings) has occurred; i.e., the load-unload process is irreversible (nonisentropic). A possible loading-unloading path is shown in Fig. 7. This unloading path serves to further define the intermediate surface ABC of Fig. 9. The unloading path is not in a single P-V plane (see lines R'L' and RL in Fig. 9), but slopes in the E direction to indicate a decrease in internal energy with unloading. The fact that unloading does not return the material to its initial state is anticipated from a consideration of the deformed particles of the material. During loading, they have been deformed to fill voids. On unloading, they will exhibit a rebound that will usually be much smaller than the initial

* For the computations, the change in temperature is assumed to be proportional to the change in internal energy while the particles are in the solid phase. Hence RN is a straight line in the computations.

loading deformation.* Hence the much steeper slope of the unloading than the loading P-V relation of Fig. 7. Reloading will occur mainly through elastic deformation of the particles again and will proceed along a path similar to the unloading curve until gross plastic flow begins when the virgin loading curve is reached.

Shear and bulk moduli along the unloading and reloading paths are assumed to be a function of density. The moduli are assumed to vary in the same manner as the pressure along the porous Hugoniot. Hence, normally the moduli will be small initially, and correspond to the precursor velocity. The moduli will then increase with compaction, reaching the value of the solid moduli at complete consolidation. The unloading moduli govern the arrival time of small reflected waves that reach the gage later than the precursor but earlier than the main wave. Hence, by comparing experimental records with computed histories it is possible to determine the variation of the moduli.

The behavior of the porous material under combined loading and heating determines the upper-bound surface on the constitutive relations of Fig. 9. Assume that by some combination of heating and loading the state is some point on the $P = 0$ surface, on the curve $V = V_1 (1 + \alpha \Delta \theta)$. Then let the material be loaded adiabatically. The paths RL and R'L' on the intermediate surface ABC of Fig. 9 represent such loadings. When yielding occurs, the particles flow, changing the configuration, and the state point moves out of the plane ABC along the path LM. Yielding of the aggregate depends on the stresses and the yield strengths of the individual particles. In turn, yield strength depends on the temperature. Available data on the variation of yield strength with temperature are used to construct the yield locus BC. Fig. 10 presents yield strengths of some aluminum alloys as a function of temperature. The assumption is made here that the pressure along curve BC in Fig. 9 is proportional to the thermal strength reduction curve of Fig. 10.

* This is true at early times even for materials like ATJ graphite, which recover their initial distention at some later time (Ref. 4).

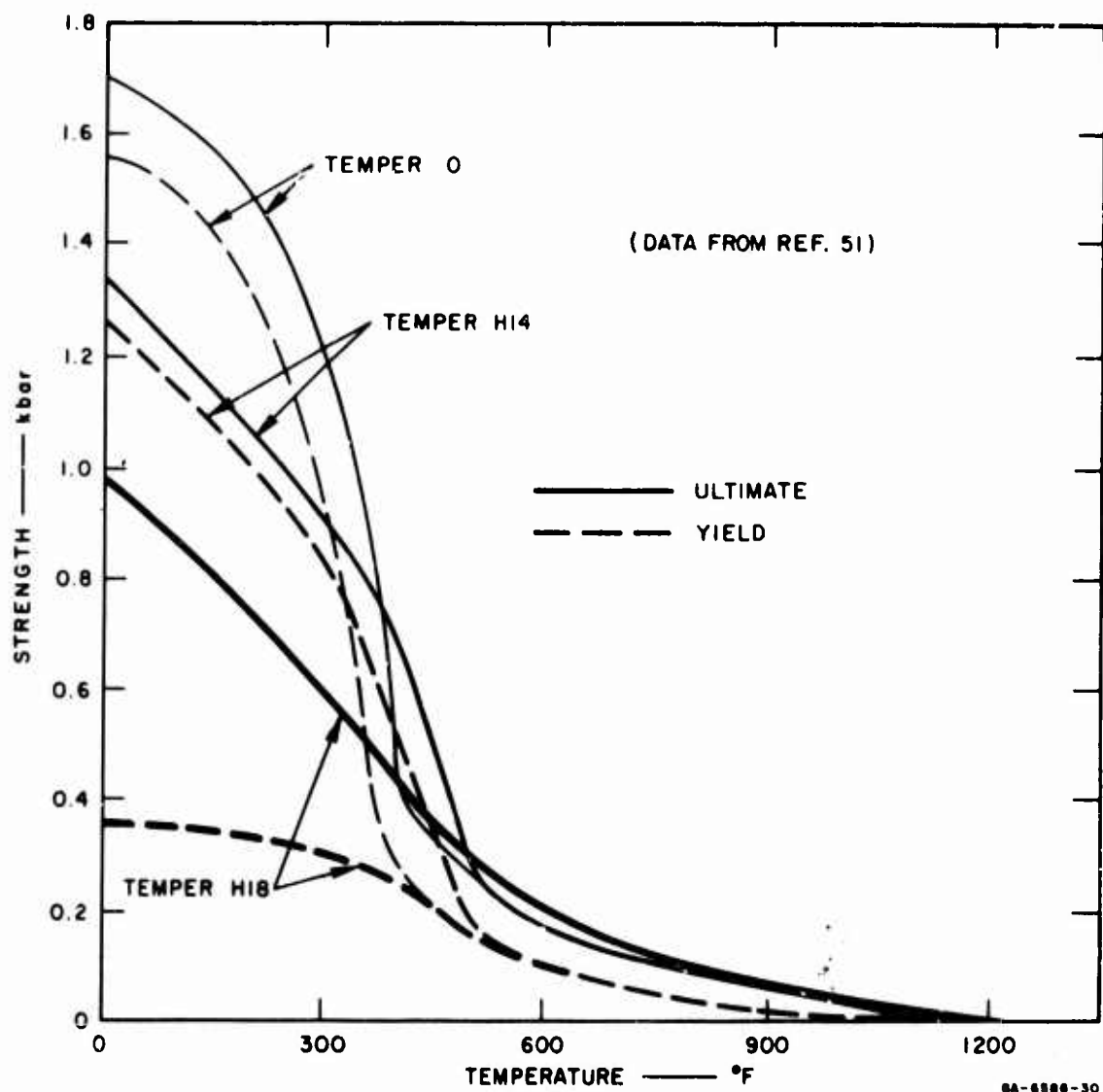


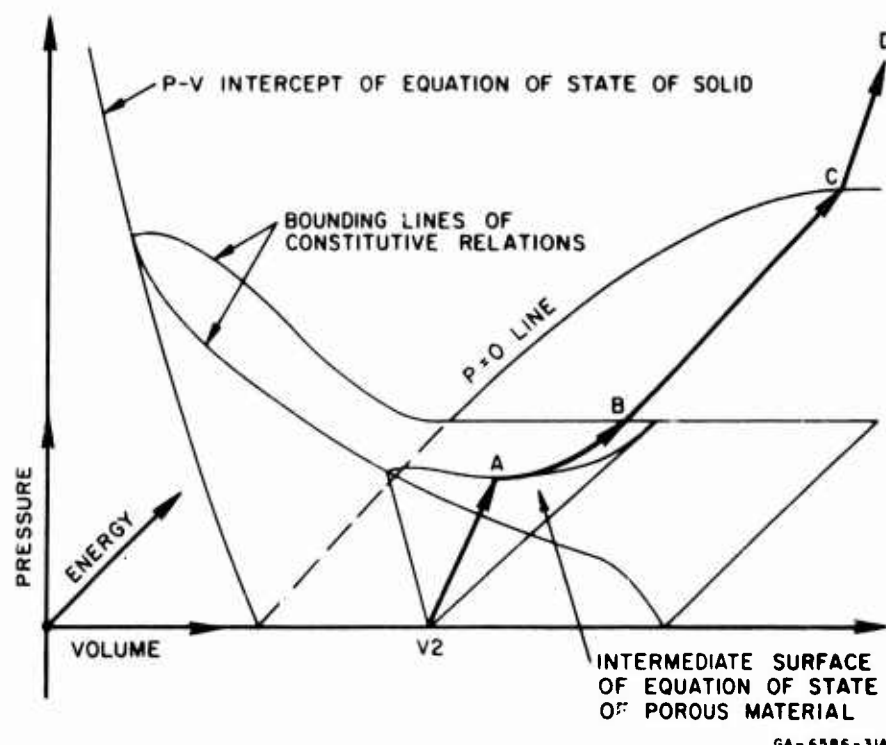
FIG. 10 VARIATION OF STRENGTH WITH TEMPERATURE FOR 1100 ALUMINUM

If unloading proceeds below the $P = 0$ surface, spalling may occur. The strength of the interparticle bonds will probably depend on the amount of precompression and heating. Hence, spall strength should be a function of porosity, particle size and shape, degree to which interparticle welding has occurred, as well as on the usual quantities such as strain rate, temperature, maximum stress and deviatoric stress, and the loading history. Then the spall strength forms a surface (or family of surfaces if all factors are considered) in the E-P-V space. A possible spall criterion surface is shown in Fig. 9. Direct tests of

spall strength of porous materials are not available. However, estimates of such strength may be made by considering the extent to which interparticle welding has occurred and by estimates from photomicrographs of the areas of interparticle bonds. The spall criterion surface is defined for the purposes of the computer program by a linear relation in the P-V plane from D to E in Fig. 9. The remainder of the surface is defined by its intersection with an intermediate surface ABC. The thermal strength reduction function of Fig. 10 is presumed to govern tensile as well as compressive strength. With this definition of the spall surface, the behavior of the porous material with particles in a solid phase is defined.

The behavior of porous material comprised of melted or gaseous particles will now be examined by using the surfaces shown in Fig. 11. Consider a porous sample held at a constant volume V_2 and initially at $E = 0, P = 0$. If the material is heated (in some type of instantaneous flash-heating process), the pressure increases as the material tries to expand. Simultaneously, the yield strength decreases with heating. With further heating, yielding occurs (point A in Fig. 11), the supported external pressure decreases, and the thermal expansion of the particles partially fills the voids. When the particles melt (point B), no external pressure is supported and the molten particles are in an unconsolidated state like water vapor in the air. As heating continues, the particles expand and flow at interparticle contact points until all the voids are filled (point C). Under further heating (following the filling of all voids) at the constant volume V_2 , pressure increases to some point D in proportion to the increase in internal energy in accordance with the linear relation

$$E = A(V_2) \cdot PV_2 \quad (22)$$



GA-6586-31A

FIG. 1 LOCUS OF STATES CAUSED BY HEATING POROUS MATERIAL WITHOUT EXPANSION

Note that at state point D, the material is now on the equation-of-state surface for the solid. The joint actually occurs over the whole surface DFG and along the $P = 0$ line in Fig. 9 because material may pass from a porous to a solid state at any point on the surface or line. However, the most commonly used consolidation paths will include points on the $P = 0$ line and on the line FG joining the yield surface and the solid equation-of-state surface. For use in the program, the joint line FG is required to pass through the points at $E = 0$ and at $E = \text{energy of melting}$. The joint provides continuity of the two surfaces being joined and does not require a local distortion of either surface.

b. Hugoniot Functions

There are provisions in the code for both P-V and SD-V relations for a porous material. These relations are not inserted as a single function but as a series of functions, each pertaining to an interval on the abscissa (specific volume). Figure 12 exhibits some possible variations of pressure and yield strength. The pressure is taken as a series of parabolic segments, and the yield strength is taken to vary linearly within each specific volume interval.

The pressure function is not a Hugoniot, as it lies entirely in the $E = 0$ plane. For impacts that just produce consolidation, the internal energy is fairly small, so that the Hugoniot and the pressure function will not differ greatly.

The yield strength information is provided as a series of linear segments (see Fig. 12), each segment corresponding to one of the porous regions defined for the pressure Hugoniot. Both the yield strength and the shear modulus decrease with increasing internal energy. Hence, for the porous material, the deviator stress is also treated as a function of internal energy.

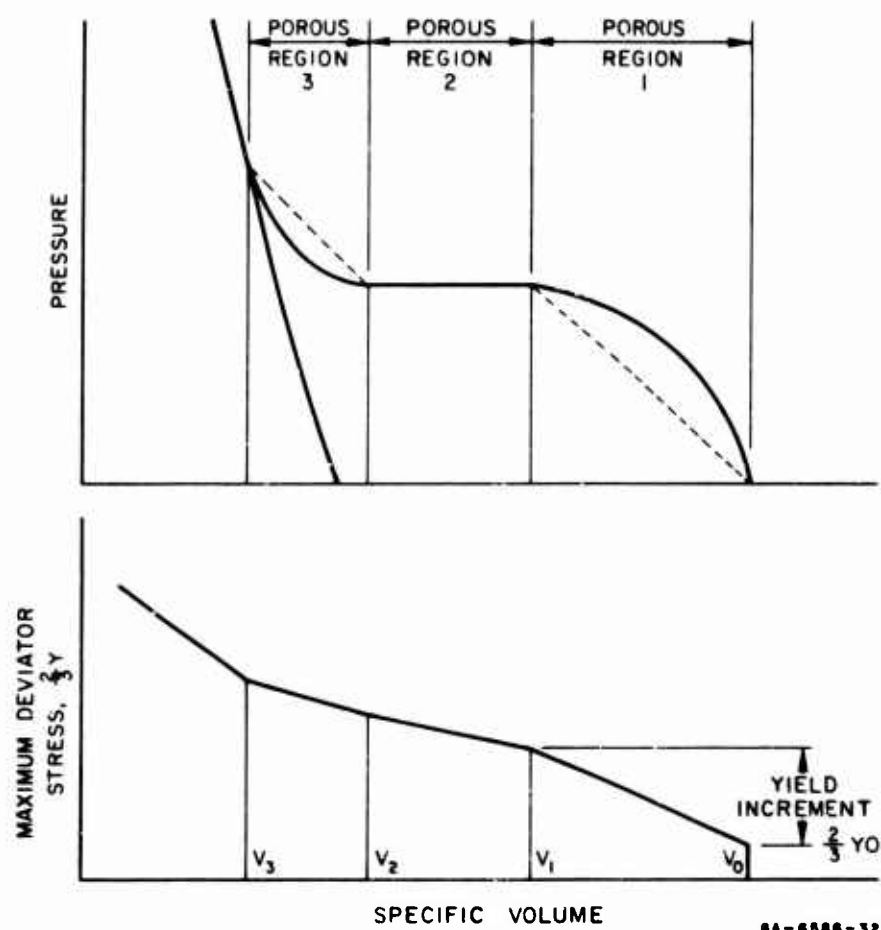


FIG. 12 POSSIBLE PRESSURE HUGONIOT AND VARIATION OF YIELD STRENGTH FOR A POROUS MATERIAL

c. Intermediate Surface Computations

The intermediate surfaces are generated in such a way that loading and unloading, heating, and cooling are provided for in a way similar to that for the solid equation-of-state. The requisite E-P-V equation is

$$P = P_0 - \frac{K * \Delta V}{V} + \frac{K * \Gamma * \Delta E}{V_s * K_0} \quad (23)$$

where

- P_0 = the pressure at the previous cycle
- V = the specific volume at the previous cycle
- K = the bulk modulus on the intermediate surface, generally a function of E and V
- ΔV = the change in specific volume
- Γ = the Grüneisen ratio
- ΔE = the change in internal energy from the previous cycle
- V_s = the specific volume of the solid particles
- K_0 = the bulk modulus of the solid material

The second term on the right side of Equation (23) provides for loading or unloading. The third term provides for expansion or contraction under heating and cooling. If P is held constant in Equation (23) and the material is heated, then

$$\Delta V = \frac{V \Gamma}{V_s K_0} \Delta E \quad (24)$$

For the solid material at low stresses the corresponding relation is

$$\Delta V = \frac{\Gamma}{K_0} \Delta E \quad (25)$$

Hence, for the same amount of energy deposition the thermal expansion of the porous material is larger than that of the solid by the factor V_0/V_s , as expected.

d. Strength Reduction

As a material is heated, it loses strength, reaching approximately zero strength at melting. (Curves showing this strength reduction are shown in Fig. 10 for three tempers of 1100 Aluminum.)

For computational purposes, the strength reduction function is assumed to consist of two parabolas, as shown in Fig. 13.

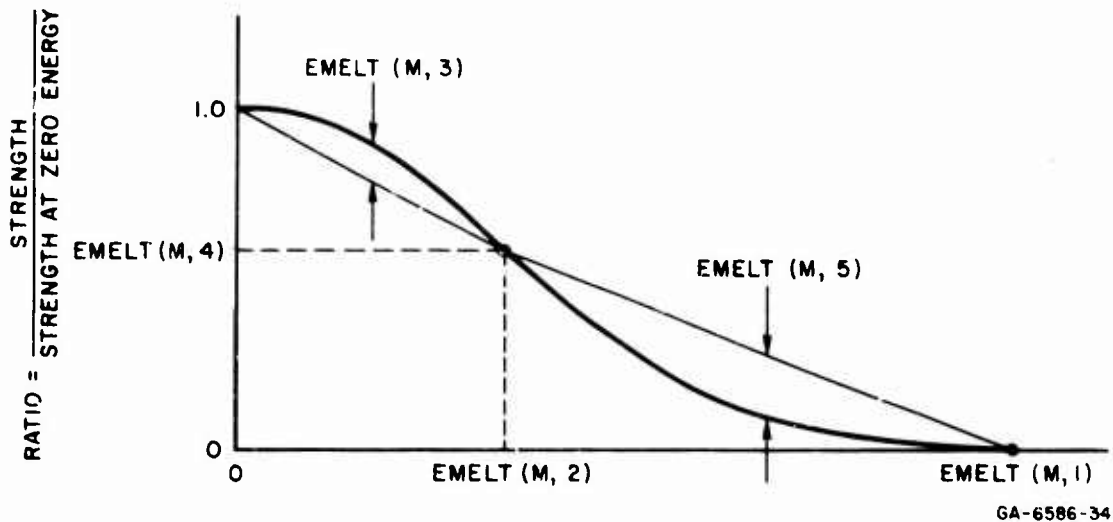


FIG. 13 THERMAL STRENGTH REDUCTION FUNCTIONS EMPLOYED IN COMPUTER CODE

e. Discussion of the Postulated Constitutive Relations

As mentioned above, it is not strictly legitimate to call the postulated E-P-V surfaces for a porous material an equation-of-state and it does not appear that a "true" equation-of-state for the porous materials is applicable. In the porous material, pressure is not a unique function of energy and volume, but depends on the previous history of the material. The stresses and temperature vary throughout the porous material so that the constitutive relations do not represent equilibrium states for the material, but, rather, averages of the thermodynamic variables. This nonequilibrium condition will persist for some time after the shock has

consolidated the material,* so that the "equation of state" used for the solid will really represent only "effective average" states. Such averages of the thermodynamic variables do not determine points that lie on the equation-of-state for the solid particles. However, the average thermodynamic quantities should lie very near the surface. The strongest variation of any variable within particles is in E , the weakest variation is in V . The equation-of-state surface is linear in E and P for constant V , and hence all of the states of the particles at any instant lie near a surface that is approximately planar. Thus a reasonable approximation is that the average values of the thermodynamic variables lie near the surface.

Uniqueness of the bounding surfaces (yield, spall, solidification) of the constitutive relations has been assumed for the construction of the constitutive relations. For the actual material these surfaces might be different if they were reached by different processes (for example, loading and heating, instead of heating and loading).

The intermediate surfaces for porous material (such as ABC in Fig. 9) have been somewhat arbitrarily constructed with a bulk modulus that varies with temperature in the same manner as the yield strength, and with a constant expansion coefficient. The warped intermediate surface thus defined has not been verified experimentally. The path across this surface on loading (path LM in Fig. 9) is like that of an ideally plastic material with work hardening. The actual path (and hence the actual intermediate surface) would be rounded near yielding and might not even contain a linearly elastic region. These questions on the legitimacy of the E - P - V surface for a porous substance indicate that calculations made by using the surface are not rigorously justifiable on thermodynamic grounds. The surface may be used for computations with the realization of its approximate nature. The equation-of-state surface for a porous material is somewhat idealized but is intended to account approximately for all of the important phenomena. Because the surface was generated from considerations of temperature (although energy was used as a variable rather than temperature), volume, and pressure, those quantities are probably represented

* The time required for equilibration will be a function of the particle size.

best. No attempt has been made to indicate the variation of entropy in the porous media.

SECTION IV

EXPERIMENTAL MEASUREMENTS

1. QUASI-STATIC MEASUREMENTS OF PRESSURE-VOLUME

Quasi-static one-dimensional compression tests were performed on samples of the porous (70 percent of solid density) copper, iron, and tungsten studied previously by Schmidt and Linde (Ref. 5). The purpose of these tests was to measure a loading isotherm and unloading and re-loading curves for the three materials. It was hoped that these measured curves would then aid in the formation of constitutive relations to describe the behavior of the porous materials in the "partially compacted region," particularly just above the "elastic" limit, where accurate dynamic measurements are difficult to obtain. A major question of interest was whether the quasi-static P-V data could be used to approximate the dynamic data in the "partial compaction" region, despite the drastic differences in loading rate.

The testing apparatus, shown schematically in Fig. 14, was made of high-strength steel. The capacity was limited to about 10 kbar. The porous samples used were about 1 inch long. They were inserted in the die inside a 1-mil-thick sleeve of indium--the indium being required for lubrication to reduce wall friction. Pressure was applied with a hydraulic jack acting on the plunger above the sample. Tests were performed by loading to a certain pressure and reading the length of the plungers and sample with a gage recording to 0.0001 inch. Then the pressure was released until the gage reading began to change. The "true" pressure was then taken as the average of the upper and lower pressures. This double-reading procedure was employed to reduce errors associated with friction between the sample and the body of the die.

To determine both the loading isotherm and the unload-reload behavior, two testing plans were adopted. In the first, the loading was increased monotonically to 10 kbar. In the second plan, the loading proceeded only to some fraction of 10 kbar and then the sample was unloaded and reloaded to a higher pressure. This load-unload cycle was repeated until 10 kbar was reached.

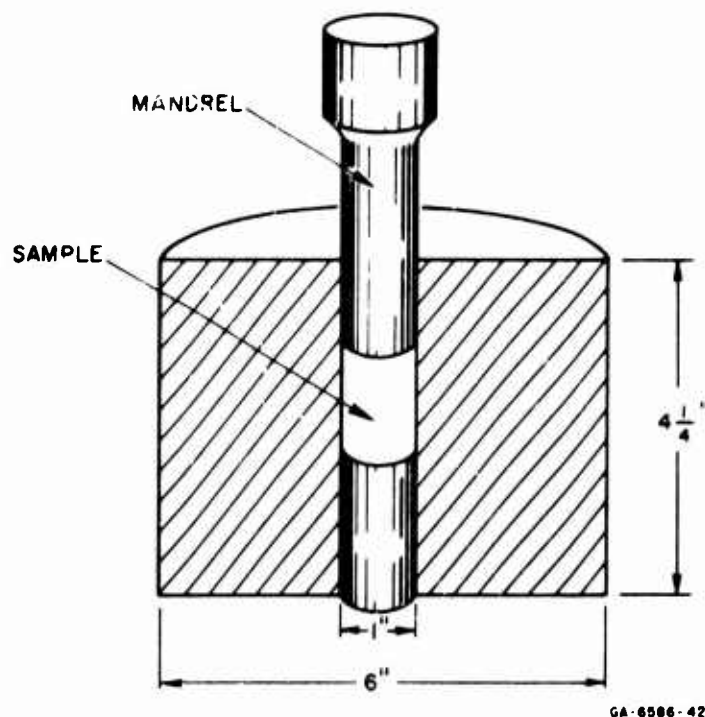


FIG. 14 CUTAWAY VIEW OF QUASI-STATIC COMPRESSION DEVICE

Compression of the sample was deduced from the recorded overall shortening of the combination of the sample and two plungers. In determining the total volume change of the sample, an allowance was also made for the lateral expansion of the die. This lateral expansion (which necessitated a small correction to the longitudinal volume change) was deduced from calibration tests with sodium chloride as a sample with a known compression isotherm.

A comparison of the results from the first and second test plans indicated that the isotherm of the porous sample was not altered significantly by the unload-reload cycle. Unloading and reloading curves had slopes similar to that of nonporous material; the accuracy of the measurements was not sufficient to determine the variation of modulus with density. The loading isotherms developed in three tests are shown in

Figs. 15 through 17. The irregularities in the curves shown are associated with errors introduced in the load-unload cycles and are not significant features of the data. Hugoniot data from Schmidt and Linde (Ref. 5), Boade (Ref. 7, 8) and Butcher and Karnes (Ref. 11) are also shown in these figures. It is noted that there is rather good correlation between the static and dynamic data.

The main results of the quasi-static study were:

- The loading isotherm may be taken as unique, independent of intermediate unload-reload cycles.
- Unloading and reloading occur along P-V lines with moduli similar to those of the solid material.
- The isotherms show an initial steep loading to a yield point and then a more gradual loading up toward consolidation. Complete consolidation appears to be approached asymptotically.
- The static plain-strain yield point is between 50 and 100 percent of the Hugoniot elastic limit and the correspondence between static and dynamic data is very close at higher stress levels.

2. DYNAMIC MEASUREMENTS OF SHOCK ATTENUATION

To aid in development and verification of the prediction capability, several shock-attenuation experiments were performed on samples of porous copper, iron, and tungsten of the same type and from the same supplier as specimens used by Schmidt and Linde (Ref. 5). Specimens were cleaned of pore contaminants, and dynamic experiments were performed as described in Ref. 5. Manganin transducers of the nominally 10-ohm design were used in all experiments, with the gage element located nominally 0.25 mm from the foam specimen surface. The precise gage position and planarity were measured optically after potting of the gages in C-7 epoxy.

Longitudinal acoustic velocities were measured for each specimen prior to shock loading. These measured velocities exhibited sample-to-sample variations of several percent and were generally a few percent lower than the velocities measured for specimens used by Schmidt and Linde (Ref. 5)

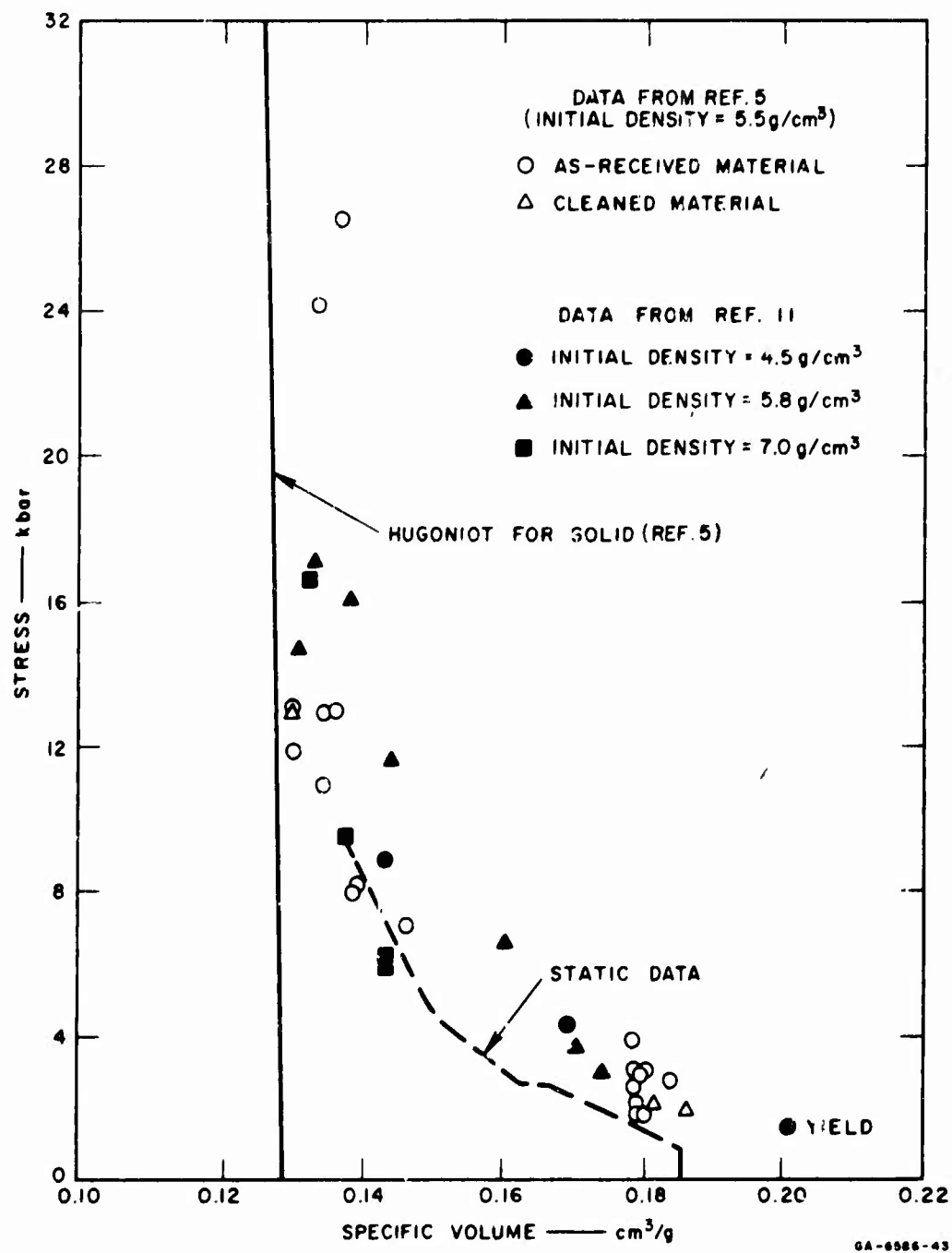


FIG. 15 STATIC AND DYNAMIC COMPRESSION DATA FOR POROUS IRON

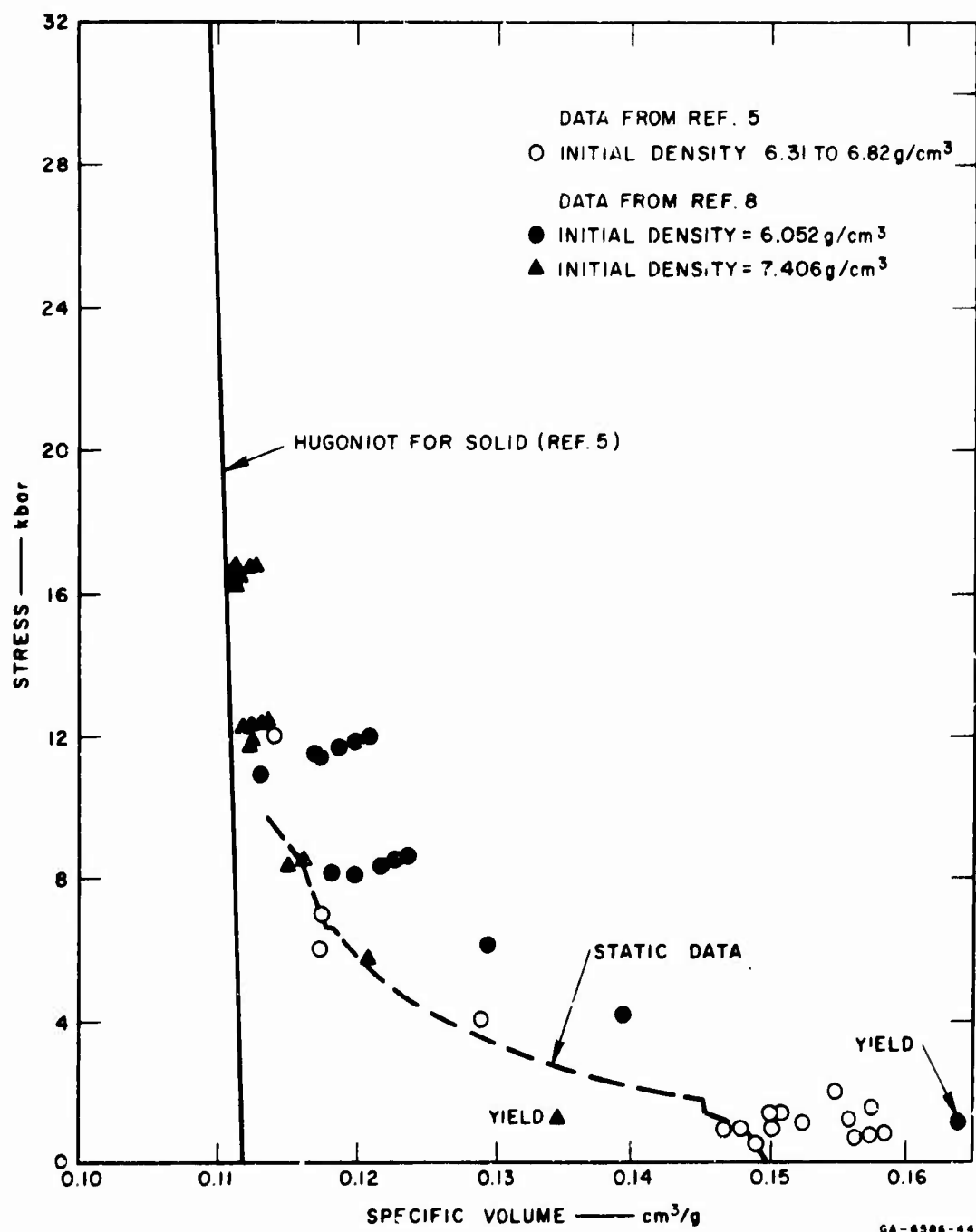


FIG. 16 STATIC AND DYNAMIC COMPRESSION DATA FOR POROUS COPPER

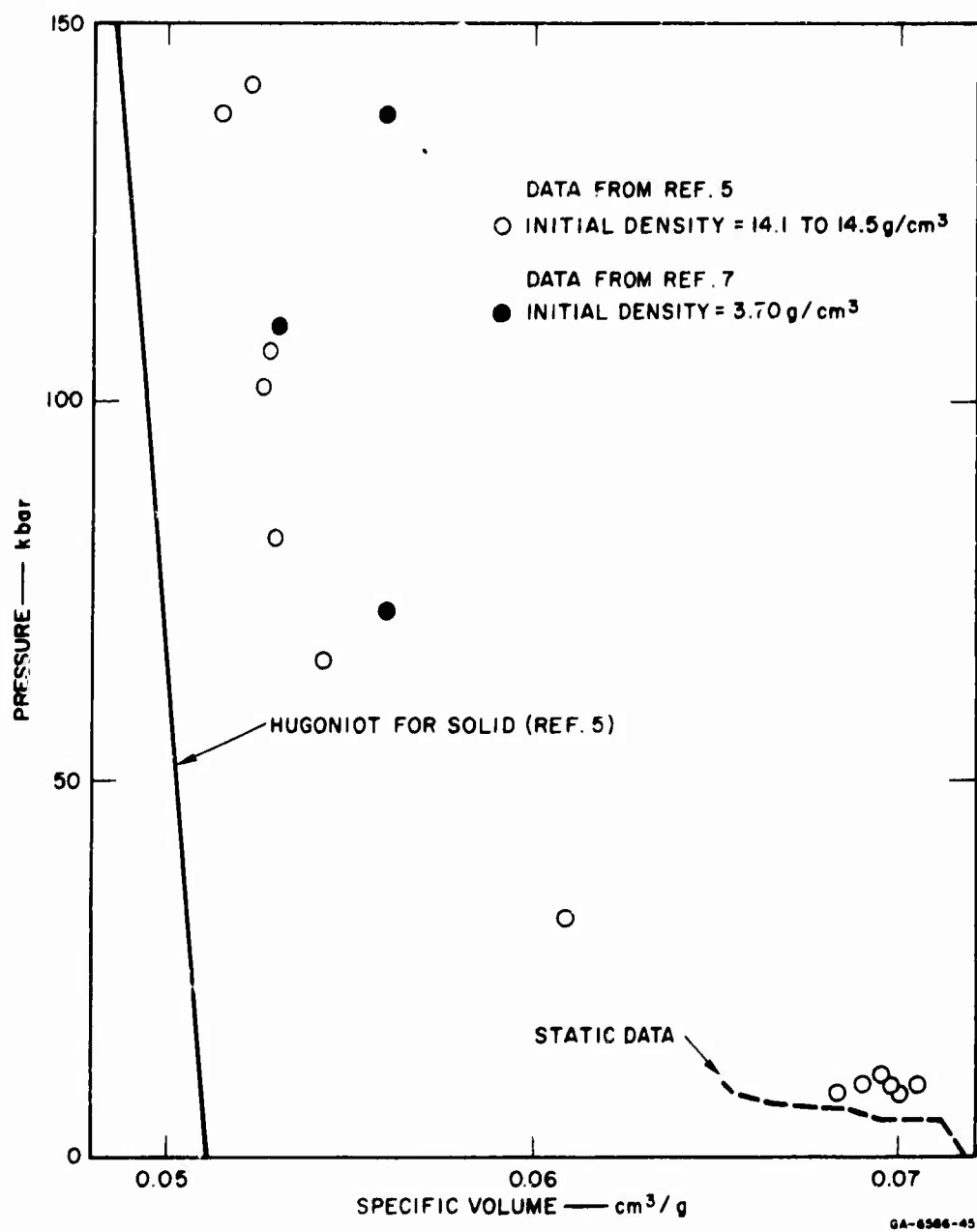


FIG. 17 STATIC AND DYNAMIC COMPRESSION FOR POROUS TUNGSTEN

A summary of the shock attenuation experiments is given in Table 1.*

3. STATIC AND DYNAMIC COMPRESSION OF POLYURETHANE FOAM

The backing material for the flyer plate in most of the shock attenuation tests was a polyurethane foam with a density of about 0.185 g/cm^3 . The Hugoniot of this foam was estimated through a series of quasi-static compression tests and two dynamic experiments. The quasi-static compression tests were performed in a manner similar to that used for the porous metals except that the engirdling die was much lighter. The Hugoniot measurements (summarized in Table II) were made with a copper-polyurethane impact and a polyurethane-polyurethane impact. Two gages were used at different thicknesses in the foam on one Hugoniot shot to ascertain that a steady state shock front had been established. The results of both static and dynamic experiments are shown in Fig. 18. For comparison, the solid polyurethane data of Butcher (Ref. 52) is also exhibited.

* Actual profiles and wave arrival times obtained are given in Figs. 19 through 24 of Section V.

Table I

CONDITIONS OF ATTENUATION EXPERIMENTS

Porous Target				Solid Flyer				Tilt Across Gage (μ sec)	Shot No.
Material	Thickness (cm)	Density (g/cm^3)	Acoustic Velocity cm/sec ($\times 10^5$)	Material	Thickness (cm)	Density (g/cm^3)	Velocity cm/sec ($\times 10^4$)		
Iron	0.297	5.51	3.10	Iron	0.0445	7.81	7.33	< 0.114	13,347
	0.158	5.42	3.31		0.0465	7.81	7.42	0.048	13,403
	0.158	5.29	3.50		0.165	7.81	7.38	0.068	13,418
Copper	0.314	6.53	3.41	Copper	0.0325	8.94	7.35	0.014	13,349
	0.191	6.43	3.48		0.0376	8.94	7.43	0.054	13,404
	0.159	6.54	3.32		0.1651	8.94	7.43	0.140	13,417
Tungsten	0.162	14.56	3.90	Tungsten	0.0505	19.6	7.38	----	13,402
	0.310	14.26	3.79		0.114	19.6	7.35	0.034	13,473

Notes

1. Backing material was polyurethane foam ($\rho_0 = 0.185$) for all flyers except the last. In that test the backing material was Plexiglas[®] (Rohm and Haas Co.) with an initial density of $1.189 \text{ g}/\text{cm}^3$.
2. Records were obtained with manganin wire gages embedded 1 mil into C-7 epoxy. Gages were immediately behind the target.

Table II

HUGONIOT DATA FOR POLYURETHANE FOAM

Shot No.	Target			Flyer				Tilt Across Gage (μ sec)	Results			
	Thick. (mm)	Density (g/cm^3)	Longit. Acoustic Velocity (mm/ μ sec)	Mat'l.	Thick. (mm)	Density (g/cm^3)	Impact Velocity (mm/ μ sec)		Stress (kbar)	Particle Velocity (mm/ μ sec)	Density* (g/cm^3)	Shock Velocity (mm/ μ sec)
13405	6.14	0.186	1.36	PF**	10.62	0.187	0.744	0.031	2.15	0.366	0.70	0.50
13420	3.12	0.188	1.55	Cu	6.30	8.94	0.719	--	7.2	0.702	0.96	0.87
	6.52								7.2	0.702		

* Assuming single shock.

** Polyurethane foam.

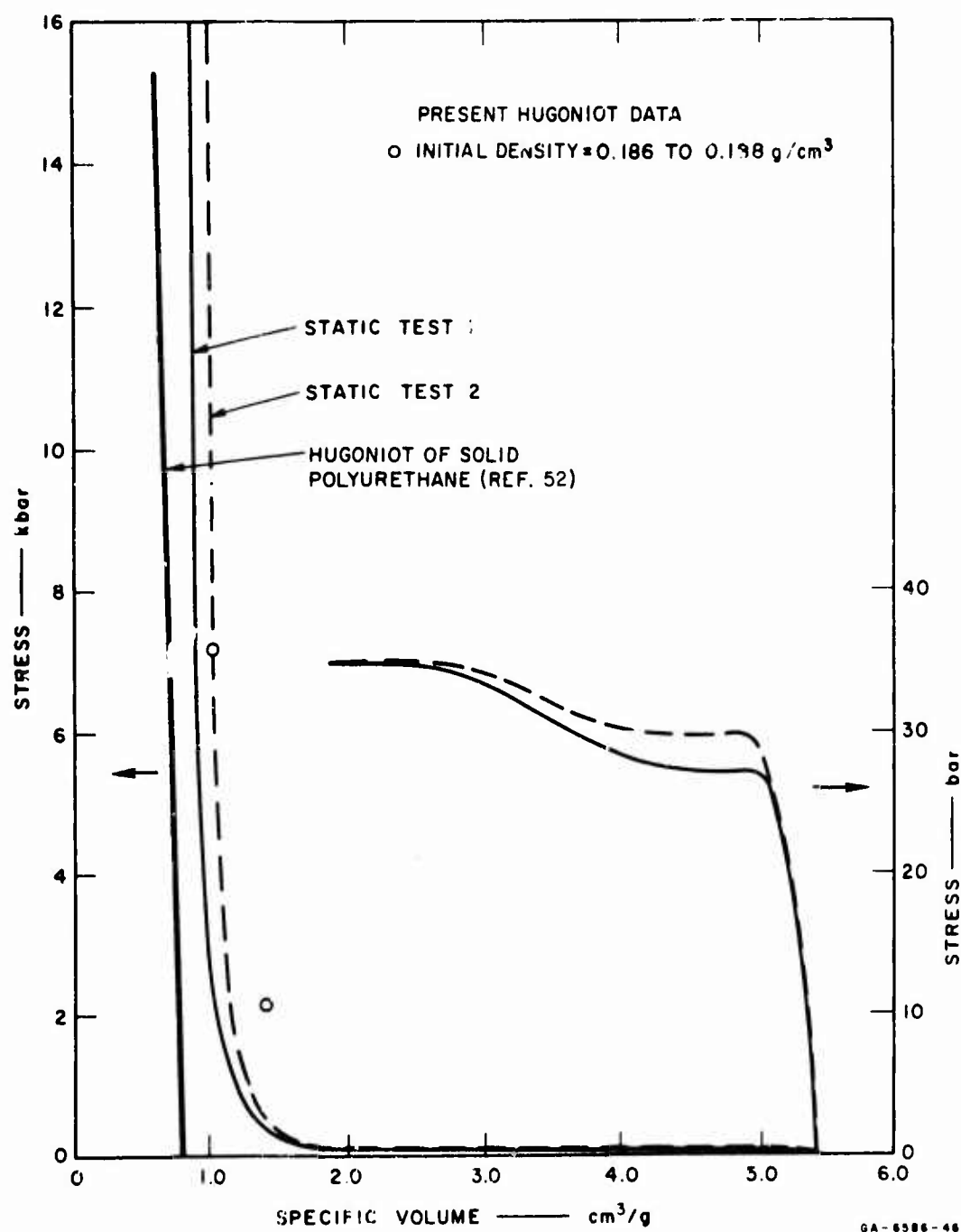


FIG. 18 STATIC AND DYNAMIC COMPRESSION DATA FOR POLYURETHANE FOAM

SECTION V

COMPARISON OF THEORY AND EXPERIMENT

1. DISCUSSION OF WAVE-PROPAGATION PHENOMENA

Experimental data obtained from either mechanical impact or radiation deposition experiments generally are in the form of stress or particle velocity histories at some distance from the impact or irradiated surface. From such records, we can estimate or assume the sequence of events that resulted in the record. If an adequate "equation of state" and wave-propagation code are available for porous materials, such histories will be predictable.

For impact experiments, it is desirable to use a solid flyer plate of the same material as that of the matrix of the porous target. For attenuation studies, the flyer is considerably thinner than the target. According to our computations, the result of the impact is often a series of impacts and rebounds. In some cases, the flyer and target actually separate; but in others, the stress history at the impact interface shows only a series of stress oscillations, each oscillation being smaller than the one preceding it. This process is repeated throughout the time of interest. To follow such a phenomenon reliably the computer code should allow for spalling and recombination.

In the case where the porous material is irradiated, the surface material is vaporized, an inner section is melted, and the deeper material is left in the porous state. The vapor is under high pressure and attempts to expand both forward and backward. The forward moving vapor is termed the blowoff. The molten porous material is like a mist and has no significant pressure associated with it. The cooler porous material is under some pressure because of the tendency to expand under heating. The backward-moving vapor extends rapidly in the direction of the molten material, consolidating it. The cooler material on the other side of the molten region expands much more slowly toward the molten material. After some time, the pressure pulse caused by vapor expansion meets the expanding cooler material, thus completing consolidation of the molten material. The waves that travel deep into the porous material and

reflect from the rear surface are the initial compression stress (caused by radiative heating), then an expansion wave associated with the motion of the cooler material toward the molten material, and finally a compressive wave resulting from impact of the vapor (or consolidated molten material) with the cooler material. This third wave is also the one that might be associated with the blowoff of vaporized material from the front surface. Because of the dissipative nature of the porous material, the third wave will usually be greatly attenuated before it reaches the rear surface.

2. COMPUTED STRESS HISTORIES

The main test of the validity of both the computer code and the equation of state for porous materials is a comparison of computed stress histories with those recorded by a stress gage. The experimental situation of most interest is one in which stresses are attenuated. This situation is of interest both because of the intended use of porous materials as a stress-attenuating medium and because in such a case both loading and unloading occur so that virtually all aspects of the theoretical equation of state are exercised.

The numerical parameters in the constitutive relations of the porous materials were selected on the basis of experimental Hugoniot data (Ref. 5) and the results of static compression tests. These basic data and the selected theoretical isotherms are shown in Figs. 19 through 22. The same equation of state, approximate cell sizes, and amounts of artificial viscosity were used for all computations for a material, except that minor adjustments (motion of the curve to the right or left) were made in the low-pressure region of the equation of state to account for the slightly different initial density of each sample.

Computed stress histories at the Manganin gage locations and corresponding experimental gage records are shown in Figs. 23 through 30. Stress levels are those attained in C-7 epoxy about 0.25 mm from the specimen-epoxy interface. It may be noted that the most detail is present in the records in which a great deal of attenuation has occurred and there is significant separation of precursor and main wave. These records are most instructive for verifying the constitutive relations of the porous material.

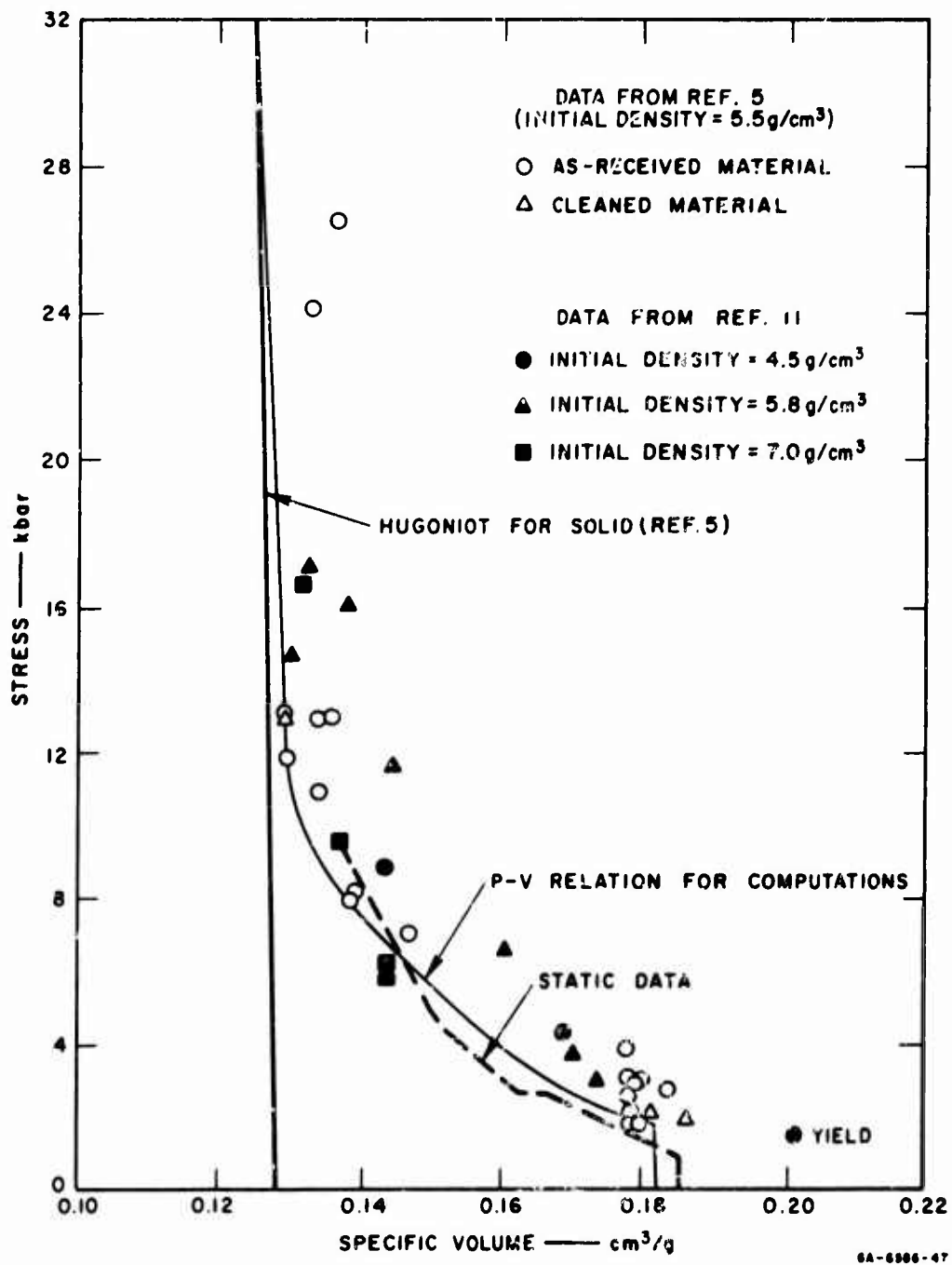


FIG. 19 COMPARISON OF THEORETICAL ISOTHERM WITH DATA FOR POROUS IRON

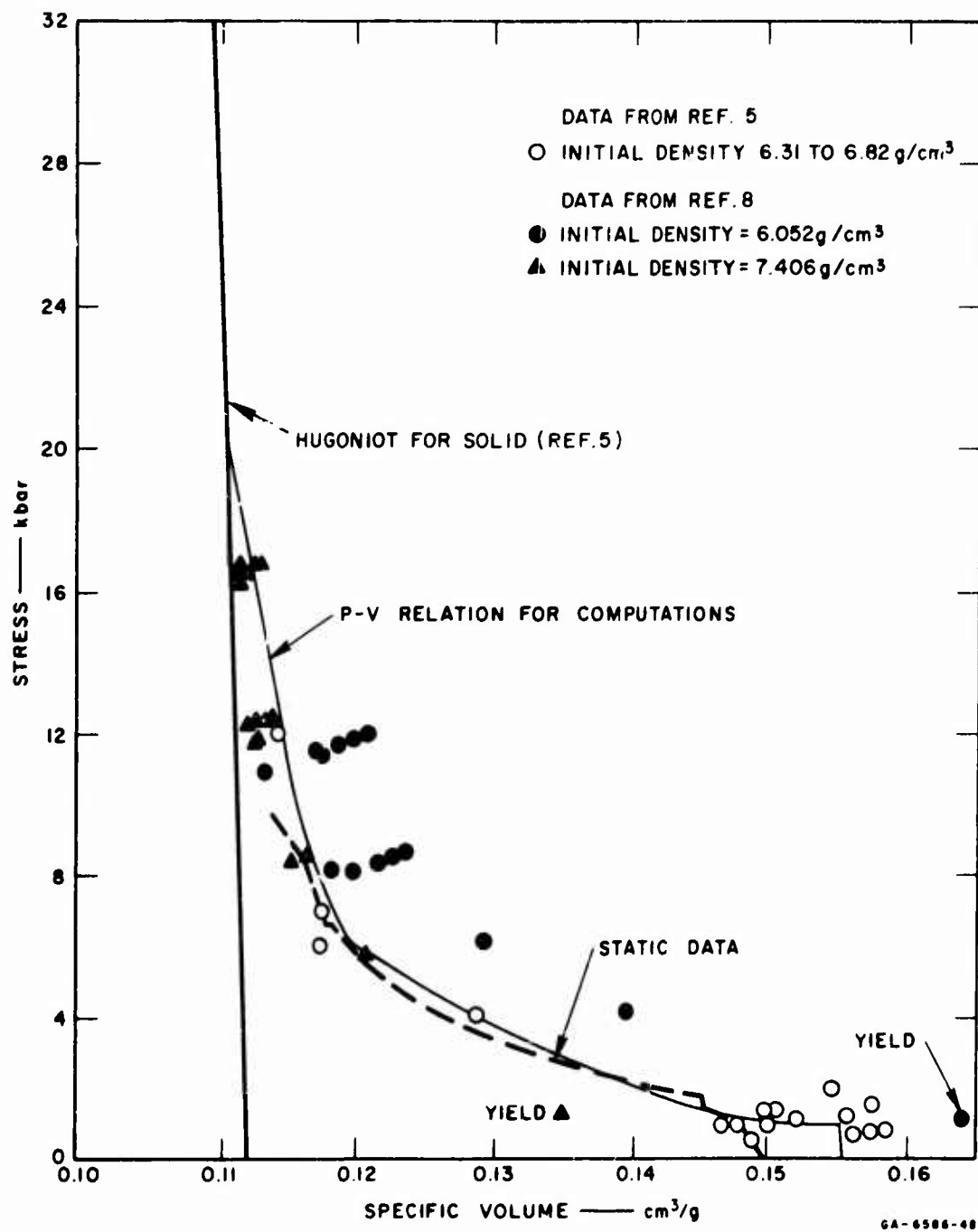


FIG. 20 COMPARISON OF THEORETICAL ISOTHERM WITH DATA FOR POROUS COPPER

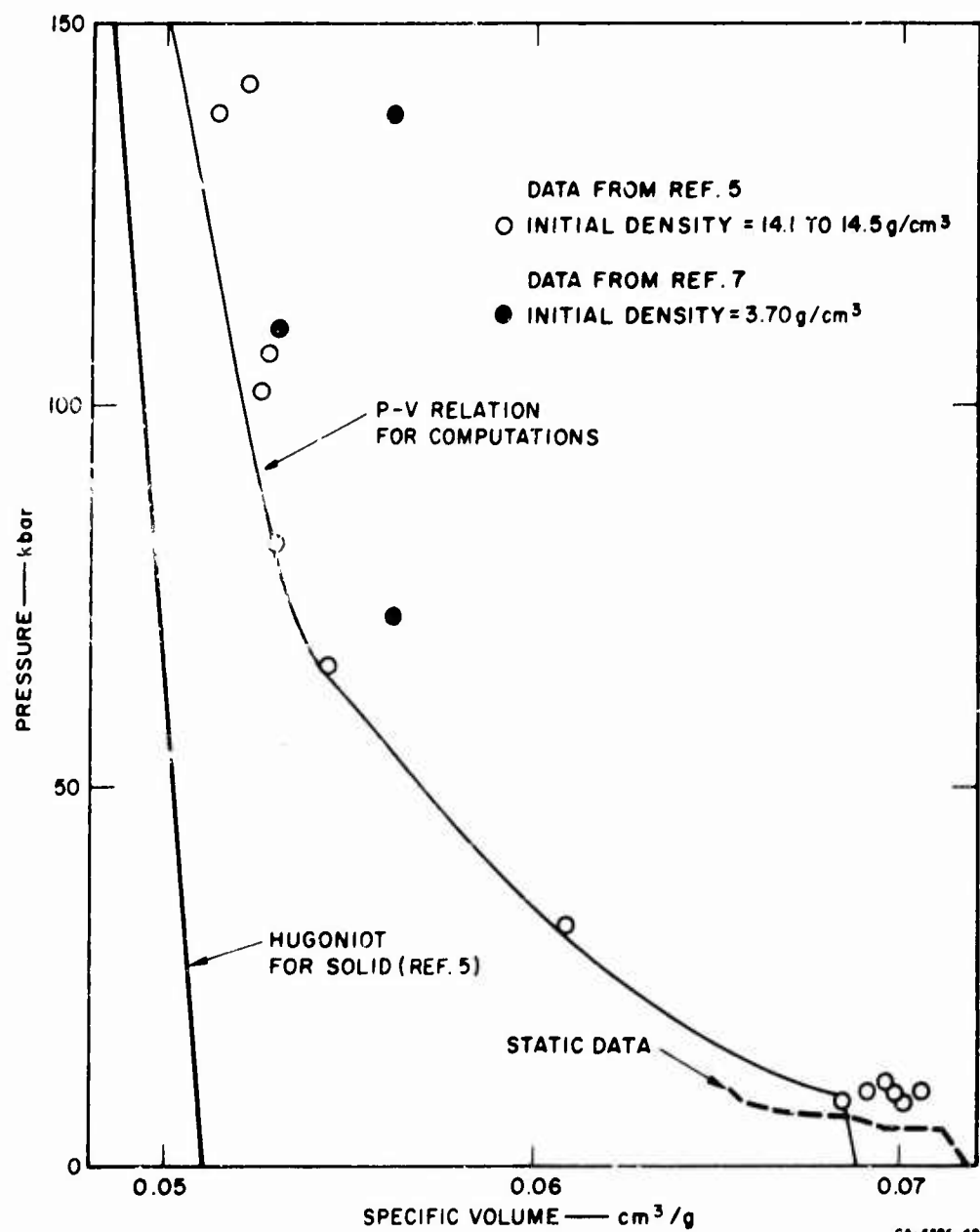


FIG. 21 COMPARISON OF THEORETICAL ISOTHERM WITH DATA FOR POROUS TUNGSTEN

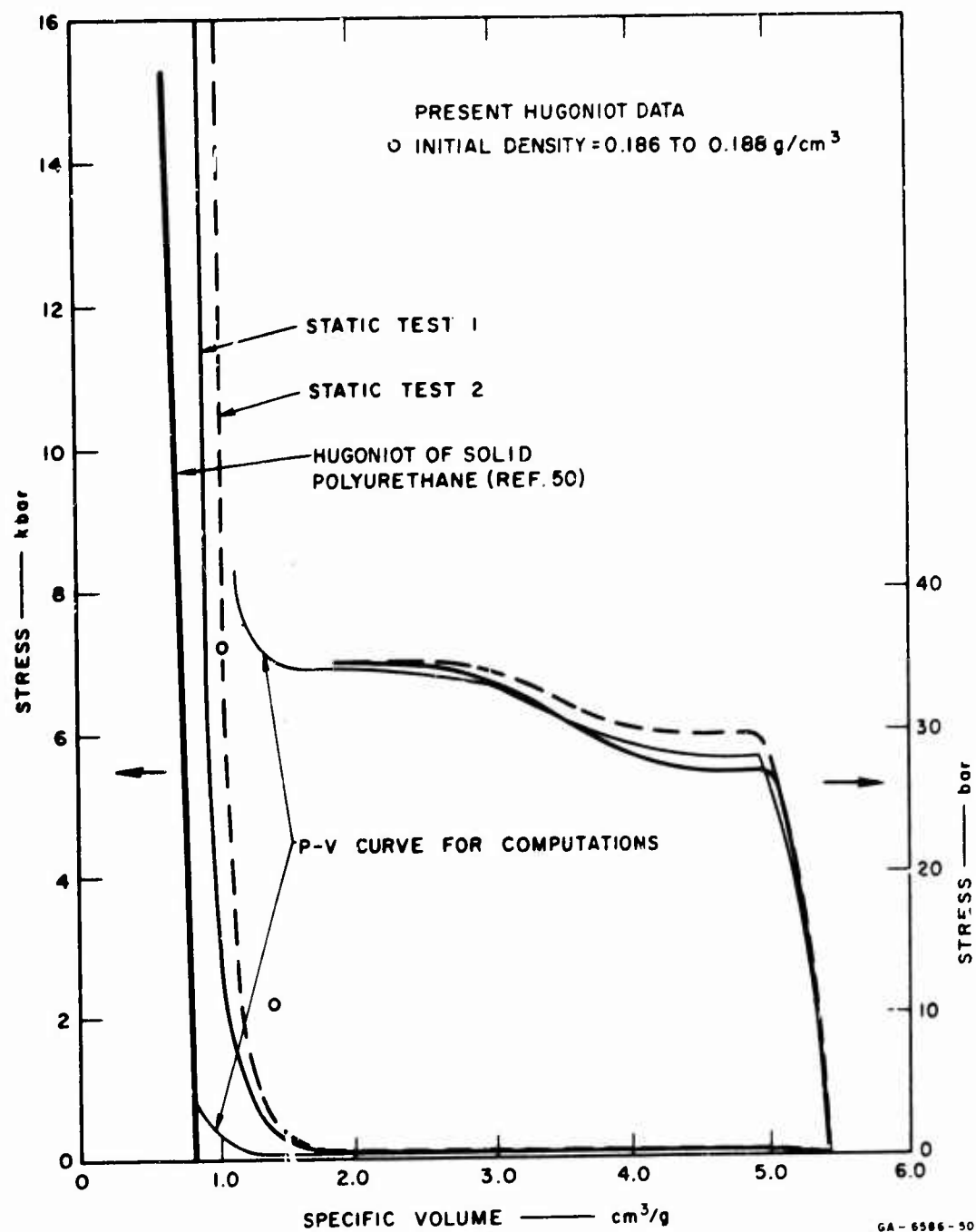


FIG. 22 COMPARISON OF THEORETICAL ISOTHERM WITH DATA FOR POLYURETHANE FOAM

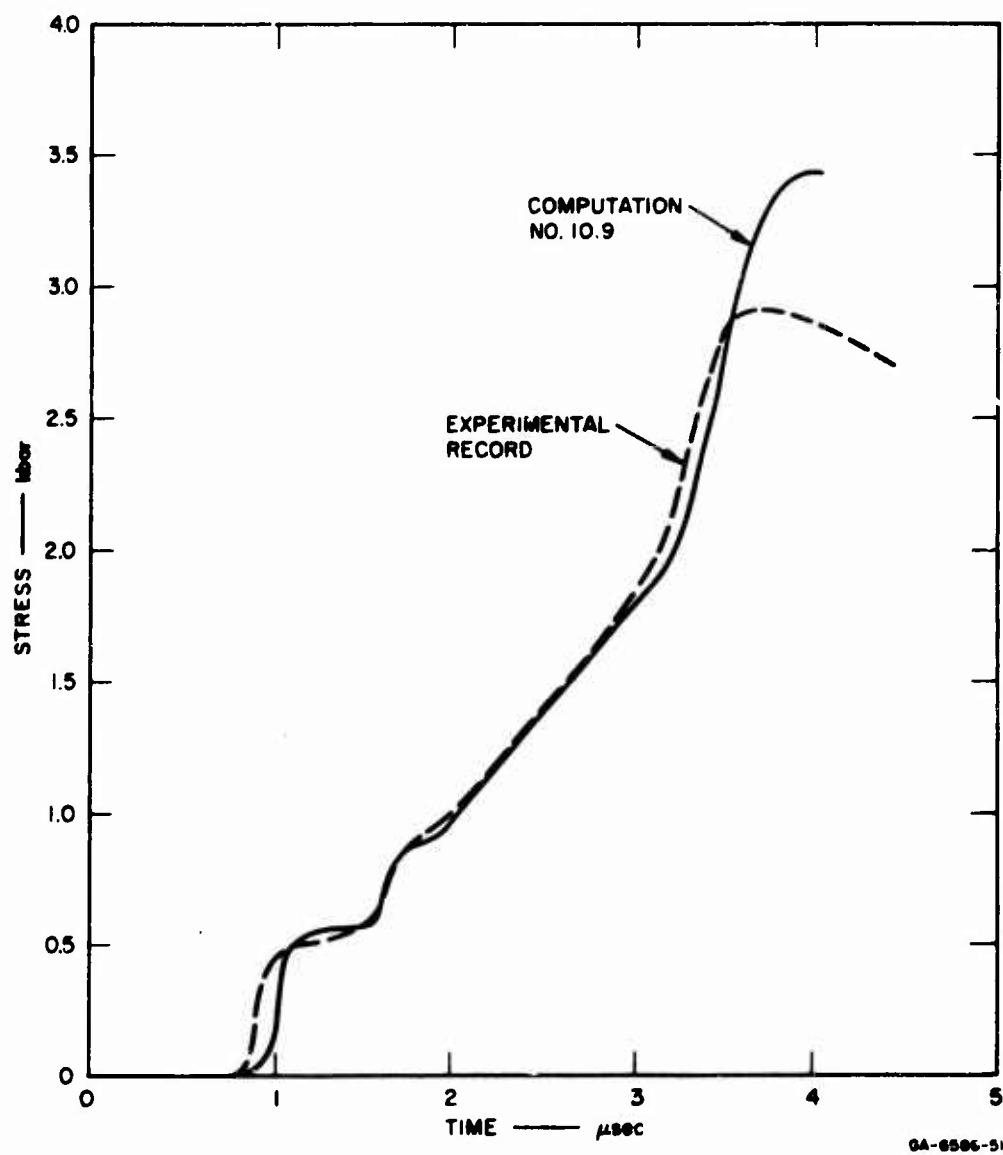


FIG. 23 IRON/POROUS IRON IMPACT, SHOT 13347

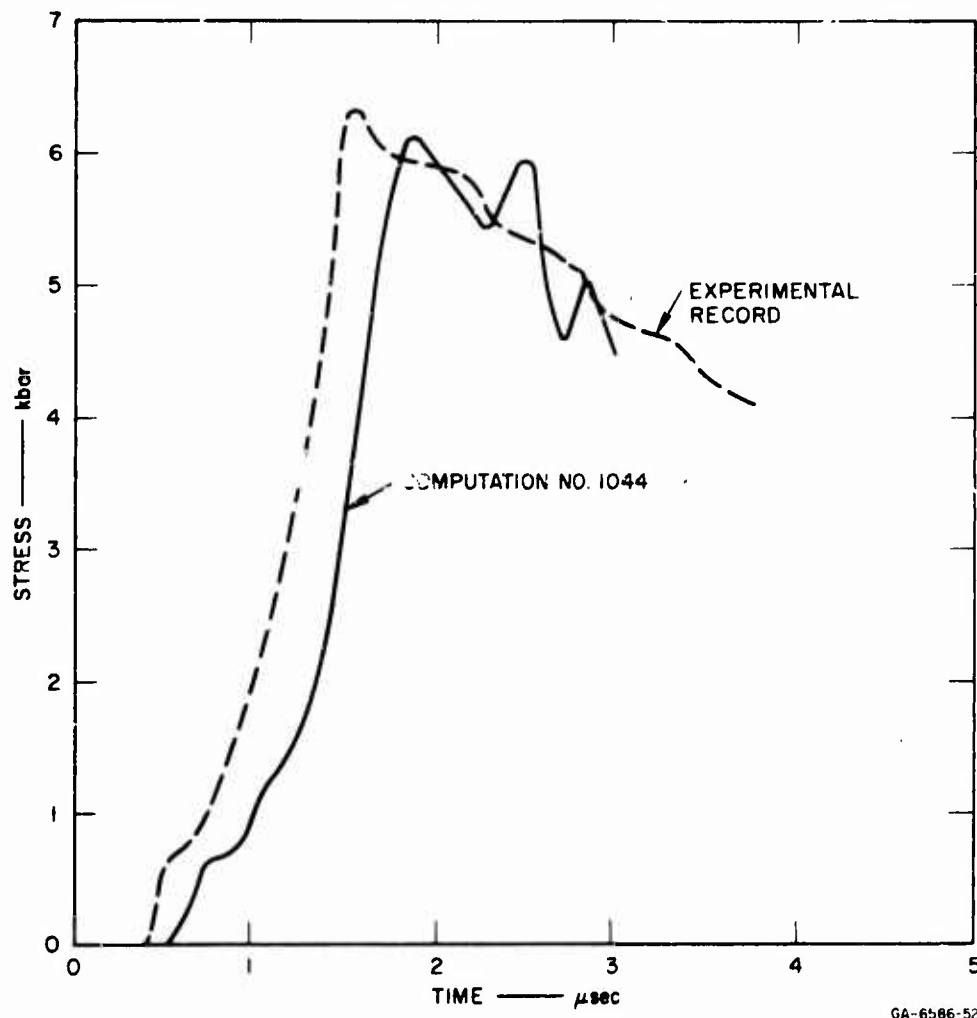


FIG. 24 IRON/POROUS IRON IMPACT, SHOT 13403

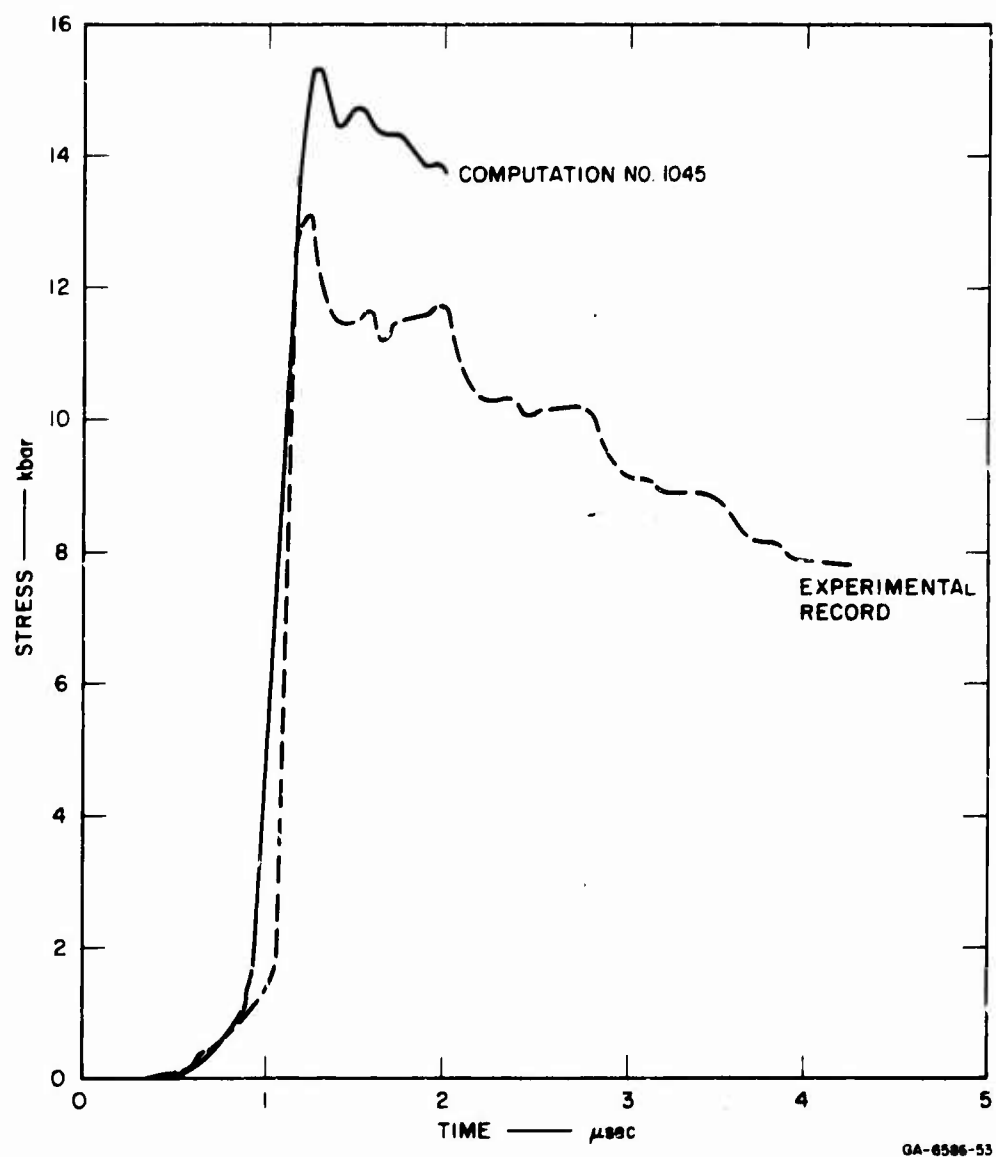


FIG. 25 IRON/POROUS IRON IMPACT, SHOT 13418

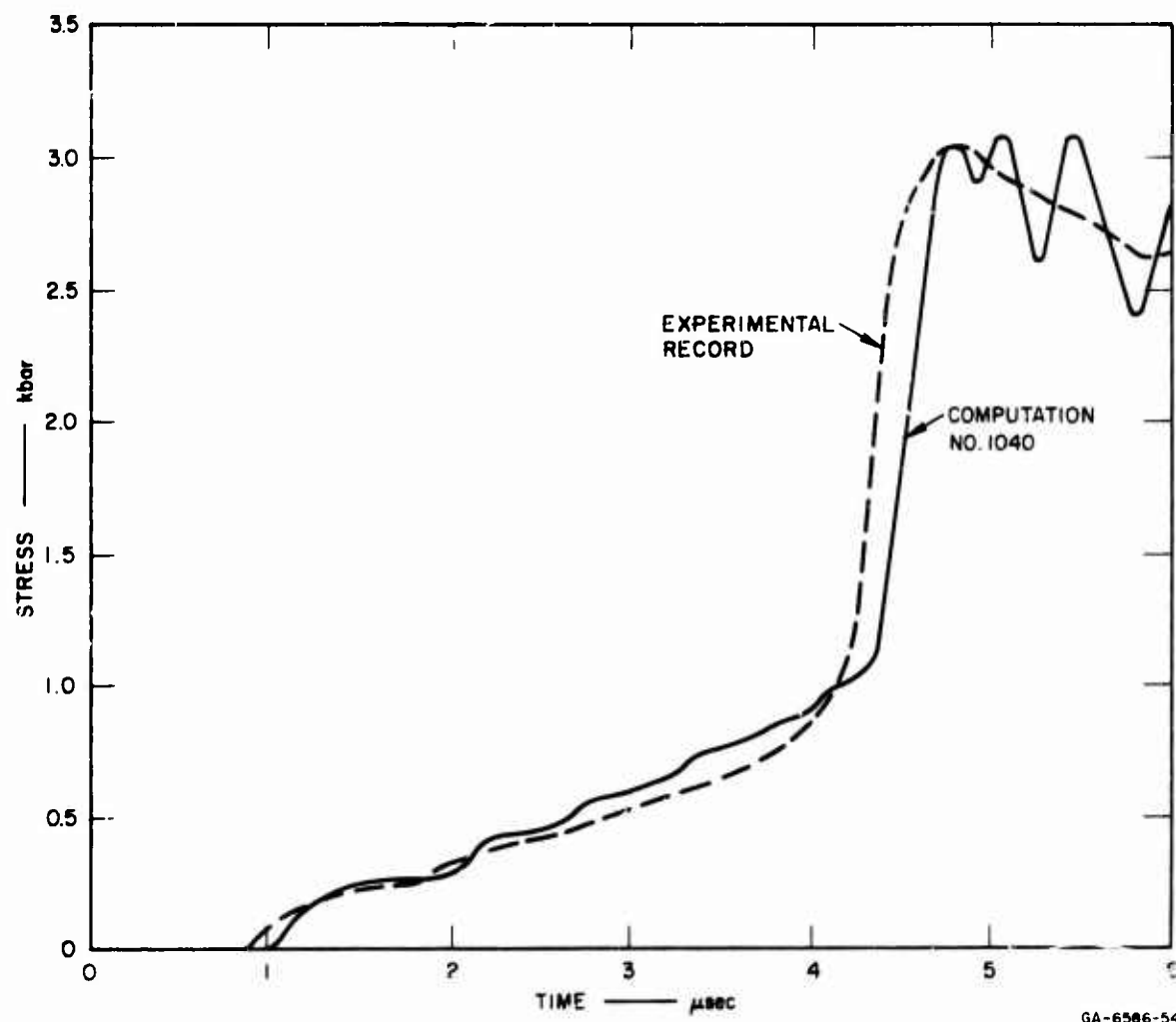


FIG. 26 CUPPER/POROUS CUPPER IMPACT, SHOT 13349

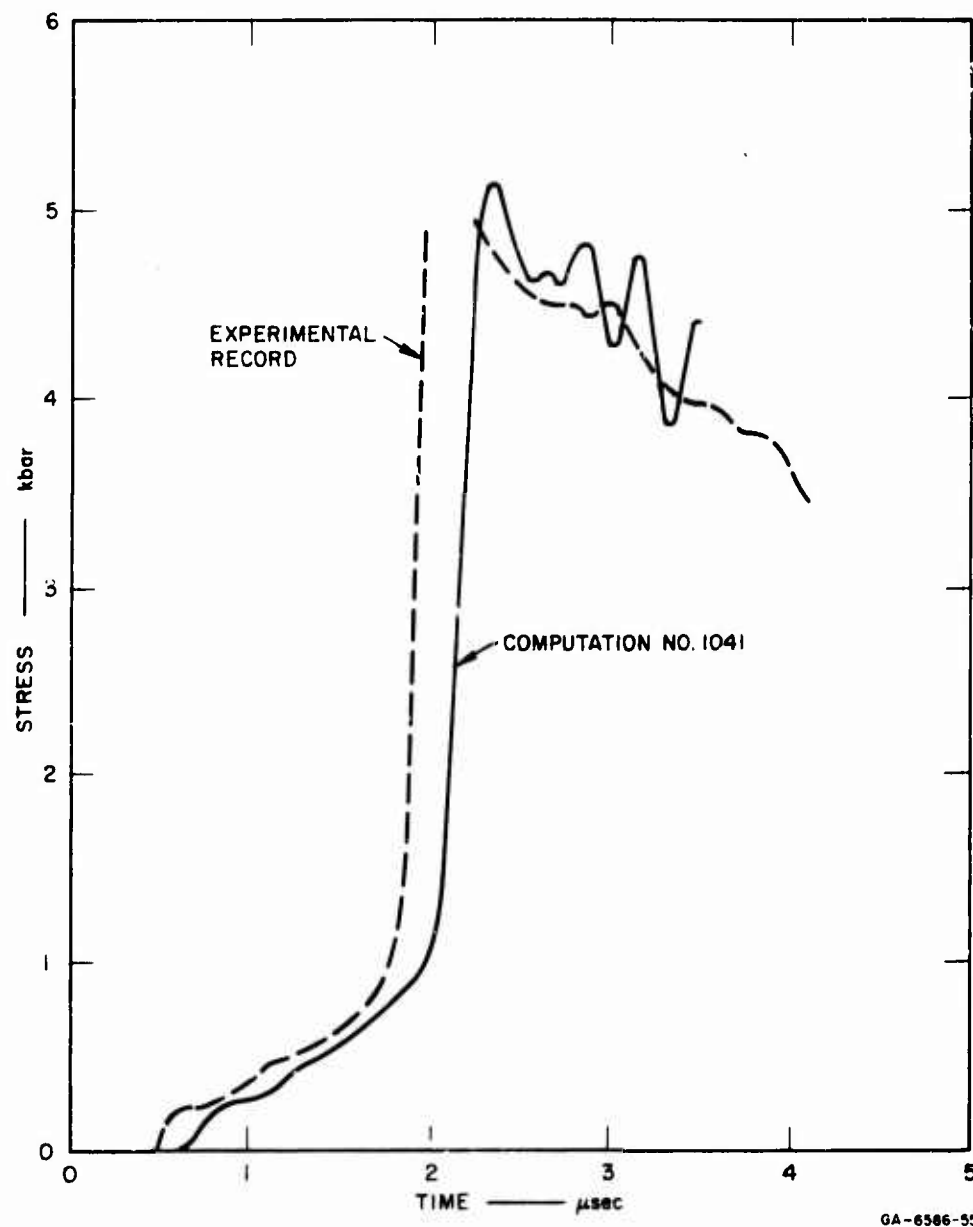


FIG. 27 COPPER/POROUS COPPER IMPACT, SHOT 13404

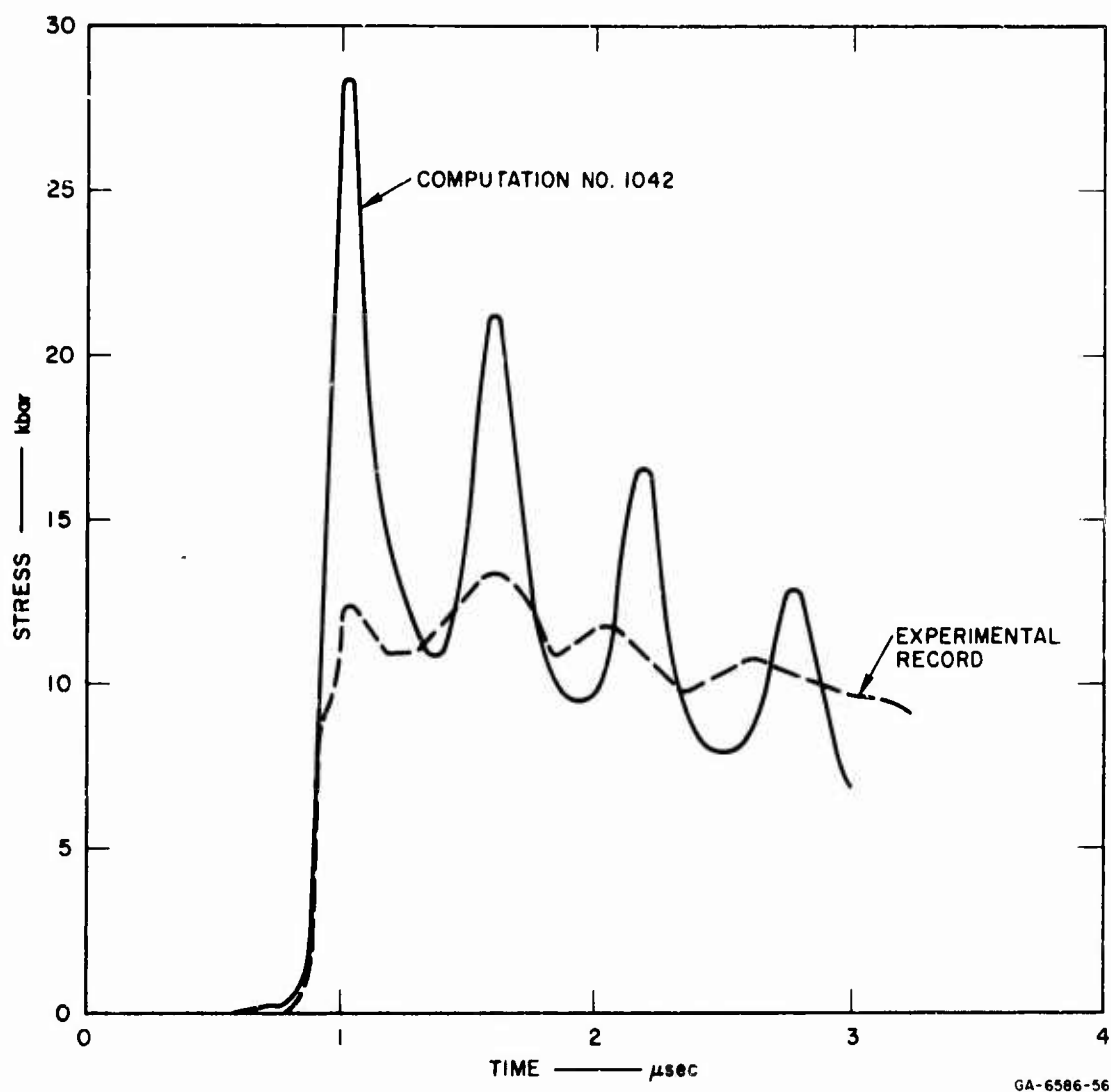


FIG. 28 COPPER/POROUS COPPER IMPACT, SHOT 13417

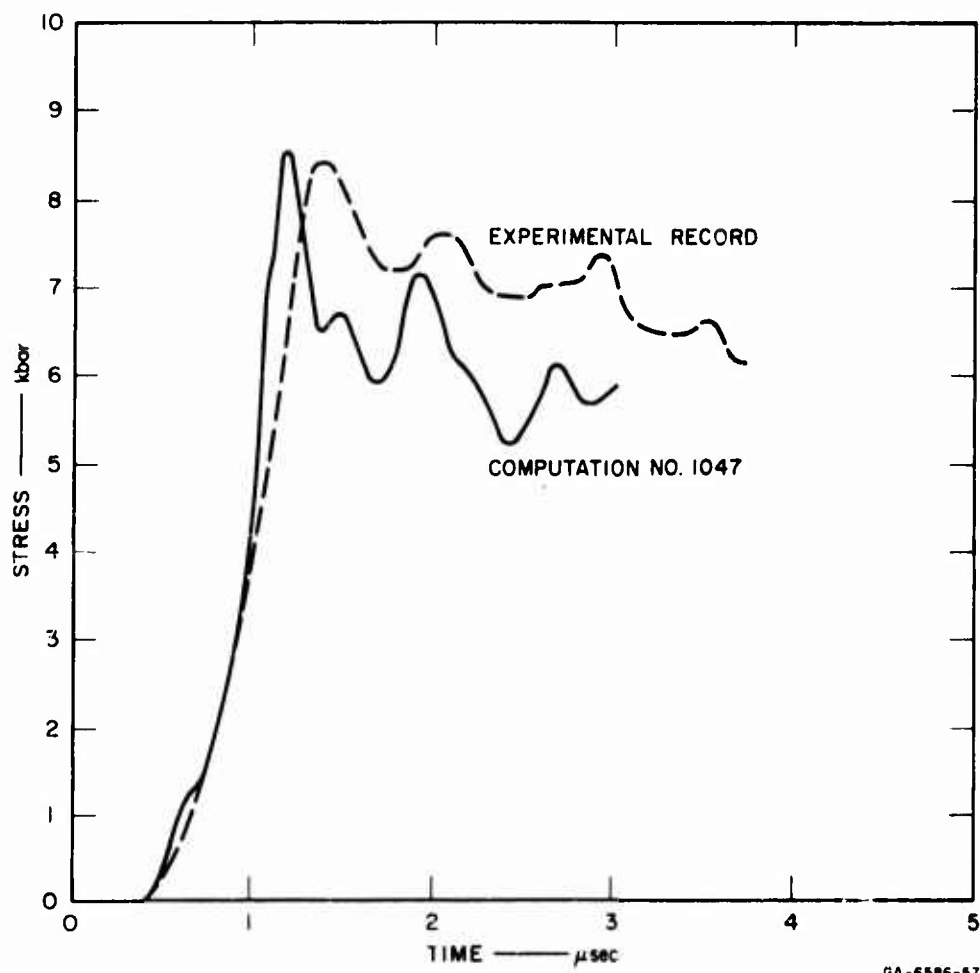


FIG. 29 TUNGSTEN/POROUS TUNGSTEN IMPACT, SHOT 13402

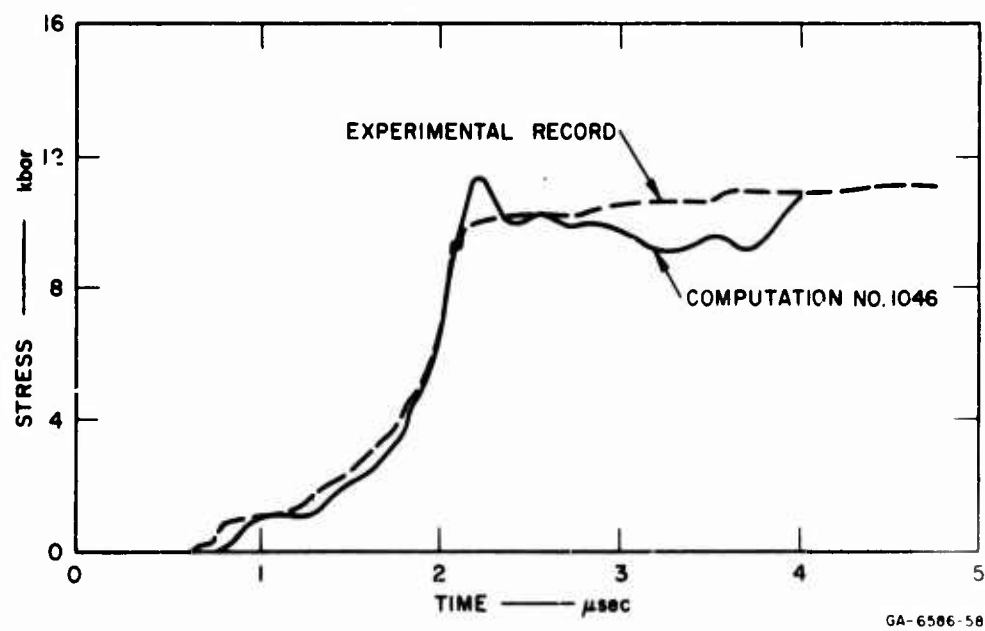


FIG. 30 TUNGSTEN/POROUS TUNGSTEN IMPACT, SHOT 10473

The comparisons for porous iron, Figs. 23 through 25 show fairly good correlation of wave front shapes: the precursors have the right amplitudes and even the precursor reverberations (small jumps in stress between the precursor and main wave) are apparent in Fig. 23. The computed magnitude of the main wave is an overestimate in Figs. 23 and 25, but is correct in Fig. 24. The arrival times coincide satisfactorily in Figs. 23 and 25, but not in Fig. 24. The variability of the correlation is interesting because the same equation of state was used for all of the computations. The most probable causes for the unevenness in the correlation are:

- Dominance of different features of the equation of state in the three cases; e.g., the high-pressure portion of the Hugoniot and the unloading modulus are most important for a thin target under high-velocity impact, while the low-pressure portion of the Hugoniot is most important if the stress at the gage is low. However, this reason is probably not important for the iron impacts; the test conditions of Figs. 23 and 25 bracket those for Fig. 24.
- Material variability among the three samples tested. For example, even though samples were "cleaned" (Ref. 5), the measured acoustic velocities (see Table I) are somewhat more variable than those obtained earlier on similar material (see Ref. 5), and even the earlier specimens showed appreciable sample-to-sample variation.

The comparison of stress histories for the porous copper impacts are shown in Figs. 26 through 28. The computed arrivals are a little late in Figs. 26 and 27, but the peak stresses compare satisfactorily with the experimental records. The arrival time is satisfactory in Fig. 28 but the computed peak stress is much higher than the measured peak stress. The marked peaks in both experimental and computed records correspond to actual reverberations through the flyer plate. The computed results for this case are strongly dependent on the thickness of the flyer plate and on the unloading wave velocity. The stress at the point of impact was 70 kbar. This high stress persists almost to the gage. Then the first unloading wave arrives and reduces the stress at the gage. With a 5 percent increase in flyer plate thickness or 5 percent reduction in unloading velocity, the peak stress at the gage would have been 70 kbar. In addition to the possible sources of discrepancy discussed above for

iron, possible causes for the disagreement between computed and measured stress histories of Fig. 28 are as follows:

- The high tilt that occurred in the experiment (see Table I) would lead to an apparent damping of measured peaks.
- An error may have occurred in measuring the flyer thickness.
- The solid equation of state may be too "soft," hence velocities are too low. A higher velocity would not significantly alter the results of Figs. 26 and 27 but could drastically alter the correlation in Fig. 28.

Clearly, a repeat of Shot 13,417 should be performed.

Two tungsten records are shown in Figs. 29 and 30. The correlation between measured record and computed history for both stress amplitudes and arrival times appears to be acceptable.

The computed results are primarily a function of the experimental conditions and the theoretical Hugoniot but are also modified to some extent by the cell size, amount of artificial viscosity, the time and extent of rezoning, and other discretionary factors. Therefore, for the convenience of those wishing to reproduce these records, the complete data input for each of the eight computations is given in the Appendix.

The results depicted in the previous eight figures and the calculations that lead to these as a final result have brought the authors to the following two main conclusions:

1. The constitutive relations (or equation of state) and the computational scheme developed for porous materials are adequate for predicting stress wave magnitudes and profiles in a porous material as a function of time. The precursor, small reflected waves, and other details of wave propagation in a porous material are adequately represented; hence, the model may be used to study stress wave interactions, including details of a compressive wave front and subsequent rarefactions. The major uncertainty is the numerical values of parameters for a given material having specimen-to-specimen variations.

2. The uncertainty in the results obtained from discretionary factors in the present computation scheme can be as great as the difference between the experimental and computed records. This uncertainty can be examined by doubling or halving the cell size and artificial viscosity values that were used. Such changes will modify peak stresses by 5 to 10 percent and alter arrival times by smaller percentages. Although neither cell size nor artificial viscosity has an intended physical significance, its effect on the computed results is as real as are changes in the theoretical Hugoniot. The ideal value of cell size is the minimum that can be afforded (computation times increase as the inverse square of cell size). Appropriate values of artificial viscosity are suggested in the next section.

3. CONSTRUCTION OF INPUT DATA

The details of writing the input for the computer program are given in the manual for the SRI PUFF 1 code (Ref. 50). In this section some guidance for developing input quantities is presented, based on our experience with the program.

The first step is to select a realistic Hugoniot (actually a "dynamic isotherm" is used in the code) for the material. As evidenced in Figs. 15 through 18 both static and dynamic data are useful in constructing this theoretical Hugoniot. The Hugoniot need not be smooth: even severe joints lead to only minor oscillations in the stress records at early times in the computation. The EMELT variables, which define the variation of strength with internal energy, have been selected by using published melting point and enthalpy data plus information on the variation of yield or ultimate strength with temperature.

The initial bulk and shear moduli are selected based on the known or expected precursor velocity. The slope of the initial section of Hugoniot is also constructed to correspond with the precursor velocity. The strain hardening parameter, YADDP, is varied through the porous regions to provide for an increase of yield strength so that the yield is that of the solid when the material is compacted to solid.

The layout of cells for an impact problem is made with small cells near the point of impact and large cells farther away. It was found that to achieve fidelity to detail for the impact problems, at least 10 cells should be used for a thin solid flyer. If the wave front is of paramount importance, then more cells should be used throughout. For impact conditions similar to those studied here, the cells in the porous target at the impact point should be about half the size of the cells in the flyer. This is in accord with the common practice of matching travel time through cells at interfaces.

These small cells are necessary because the peak stress at the interface usually is not reached until the first porous cell is compacted to solid. Because of the motions required to produce compaction, some time is needed to consolidate the first cell and this time appears as the initial rise of the stress wave. If the initial rise is comparable to the duration of the stress wave (twice the travel time through the flyer), then the interface stress will not resemble the "true" stress wave.

Even if the impact is instantaneous, the resulting stress wave will broaden after it has propagated some distance into the porous material. Hence, at later times and greater depths into the material the cells need not be so small. Our practice has been to initiate the problem with small cells at the impact point in the target, varying up to cells 5 to 10 times as large at the rear of the target. Then at the conclusion of the main impact with the flyer (one reverberation of stress through the flyer), the REZONE subroutine is called and the small cells near the impact point are increased several fold so that all cells in the target are about the same size.

For radiation deposition problems the cells should be small at the irradiated surface and may increase in size in the cooler region. At least 4 or 5 cells should be in the region that is vaporized. If possible economically, small cells should be used also throughout the molten zone to minimize oscillations in the calculated stress. The cells may be rezoned following completion of deposition, but only a small

increase (e.g., doubling) in cell sizes should be permitted at that time. Later, after the molten material has been compacted and the vapor is well expanded, the cells may be rezoned to several times their original size.

For both impact and radiation problems the artificial viscosity may be set at $COSQ = 4.0$ and $C1 = 0.1$ for the first try.* Then a computation should be run and the results examined. The results may indicate that changes in the input data are desirable. The following are guidelines in deciding which data to change:

- If your Hugoniot is not well established, then note that increases in the concavity of the Hugoniot will increase stress attenuation and will usually cause the main wave to arrive a little later (because lower stresses will be associated with lower wave velocities).
- A decrease in the cell dimensions makes a sharper delineation of the wave front, showing yield point and reflected waves more clearly. Smaller cells also reduce the stress attenuation, steepen wave fronts, and may augment oscillations in the wave front.
- A decrease in the artificial viscosity may induce instability but will usually only allow an increase in oscillations. However, the decrease may also decrease oscillations if there had been too much viscosity before. The decrease in viscosity will also decrease the attenuation, steepen wave fronts, sharpen the definition of features in the wave front, and retard arrival times (viscosity slightly augments wave velocity).

* For steady-state wave propagation, the physically correct amount of viscosity is that which causes the total stress state to follow a straight line from yield to the peak stress on a stress-volume plot (Rayleigh line). The correctness can only be judged after a computation by plotting successive values of R (total stress) versus $1/\rho$ (ρ = density) for a few cells. (Cells near an impact interface should not be considered in the comparison because their stress-volume paths will not follow the Rayleigh line.)

4. AREAS REQUIRING FURTHER EFFORT

During the construction of the equation of state and the computer program we discovered some problem areas outside the scope of the present work. The most notable problem was the lack of a complete spall criterion. Only a rudimentary one has been inserted during the project but this is not satisfactory for several reasons. The criterion is independent of time although it is known that spall strength is a function of the tensile stress duration. The rudimentary criterion is also independent of internal energy so that a vapor has the same spall strength as the solid. Some of these more glaring deficiencies could be easily remedied in the program but it was felt that such changes should await the results to be obtained under a current project at SRI on fracturing.

In code computations of radiation deposition in solid materials, there are often violent nonphysical oscillations of pressure in the vaporized region. When the material is initially porous, these oscillations also occur, possibly with even more violence. For porous materials one cause of the oscillations may be the discontinuities in the theoretical formulation of the equation of state surface. Such discontinuity occurs between the zero pressure plane of the molten mist and the surface for the expanding vapor. When a cell passes through this discontinuity (when the material is consolidated from a distended mist to a poreless liquid or gas), large stress oscillations are induced in the consolidated material. Such oscillations are nonphysical and corrections should be made in the program to remove them. The oscillations are of such a magnitude that they make nonsense of spalling calculations in the molten and vaporized material. Because the motion of the molten and vaporized material has an important effect on the blow-off momentum, and therefore on the momentum transmitted through the porous material to the backing material, stress oscillations are of great concern. The consolidation that induces the oscillations is similar to the situation occurring during an impact and could be handled with similar steps.

- Use a special iterative interface computation at the boundary between vapor and molten material.

- Employ very short time steps for 20 cycles just following consolidation.
- Increase the viscosity of the interface between vapor and molten material.
- Use smaller cells in the consolidating region.

Another change that would reduce the severity of the impact and thus reduce the magnitude of the oscillations is to provide for the partial pressure of the molten material, i.e., make an adjustment in the expansion equation of state. Some combination of these approaches should be used to improve the calculation of the motion of the vapor.

In experimental studies of porous materials, a large number of repetitive tests should be included. There appears to be much more scatter in experimental data from distended material than from the corresponding solids. This scatter is to be expected because the constitutive relations may depend on the pore size, previous stress history of the particles, interparticle bonding, inclusions, and other factors that may accidentally vary from sample to sample. Therefore, instead of expecting single values for data points, we should obtain mean values and standard deviations from the values. Then our mathematical model can be constructed to represent the average behavior of the material. As a basis for such an average model, it is necessary to repeat experiments under apparently identical conditions. For basic studies on porous materials great care should be taken to acquire samples with uniform properties. For Hugoniot and attenuation experiments, a minimum of three identical shots should be conducted. We should start by repeating the shock attenuation experiments reported above (particularly Shot 13,417).

The constitutive relations developed on the project have been shown to represent the response of a room-temperature porous material undergoing a low-velocity impact. Such an impact exercises the constitutive relations only in the vicinity of the Hugoniot. To more completely verify these relations, it is necessary to study high-pressure (megabar) impacts, externally heated specimens, and the case of radiation deposition. Sparse experimental data of both types are

available. More data should be obtained and compared with shock-wave computations, using the present constitutive relations to further verify or modify the relations.

A great deal of intuition and very little experimental evidence has been employed to define the detailed behavior of the porous material during loading and unloading, heating, cooling, yielding, and spalling. As a consequence, there are many small uncertainties in the formulations. Some questions that have not yet been treated in detail but could readily be further investigated are:

- How long does it take for the porous material to come to thermal equilibrium? To what degree of accuracy can the "consolidated" material be represented by the usual equation of state for a solid? Are some characteristics of the uncompact material retained?
- What are the microscopic details of the collapse of the pores. How great are the thermal gradients within the yielding particles? How can we theoretically derive appropriate values for the "effective" Grüneisen ratio?
- What is the effect of solid, liquid, or gaseous inclusions in the pores? Such inclusions may have importance in allowing foams to operate effectively as countermeasure materials in "shine-through" situations where premature collapse of the foams would render them ineffective.

Some of these problems, such as stress oscillations in the vapor, temperature effects and off-Hugoniot behavior, and the spalling criterion, should be handled immediately; the other problems may involve refinements that are not economically justifiable for present applications.

APPENDIX

INPUT DATA FOR COMPUTED STRESS RECORDS

The SRI PUFF 1 computer code was employed to calculate the stress records shown in Figs. 23 through 30. The input data on which the calculations were based are given in the following pages.

NDATE= 8/27/68 IDENT=1019 IRON-IRON FOAM IMPACT. 13347

STRESS HISTORY AT INTERFACES BETWEEN MATERIALS 1 AND 2 IS FOR COMPARISON WITH GAGE RECORD OF DAVE SCHMIDT FROM SHOT 13347
COMPUTATIONS WERE MADE WITH SRI PUFF 1 ON THE CDC 3200 AT SRI. THE VERSION OF SRI PUFF 1 IS EQUIVALENT TO THAT SUPPLIED TO AFWL WITH FINAL REPORT ON DISTENDED MATERIAL MODEL DEVELOPMENT.

*** IRON-IRON FOAM IMPACT ***

1 NTEDT = 10 NJEDIT = 6 NREZON = 1 NSEPRAT = 0
2 TEDIT = 3.000E-07 5.000E-07 1.000E-06 1.500E-06 2.000E-06 2.500E-06 3.000E-06
3.500E-06 4.000E-06 4.500E-06
3 JEDITS = 47 54 61 68 75 82
4 NTR = 1
5 JREZON = 60
6 NEDTM = 10000 NEDIT = 10000 NPERN = 1
7 STOPS JCYCS = 1000 CKS = 3.000E 00 TS = 5.000E-06
8 NMTRLS = 4 MATFL = 2 UZERO = 7.330E 04
POLYURETHANE FM RHOS = 1.19 NEQST = 1 NPOR = 4 NYO = 1 NCON = 0
EQSTC = 7.816E+10 EQSTD = 1.956E+11 EQSTE = 3.000E+10 EQSTG = 2.000E+00
EQSTH = 0.250E+00 EQSTS = 2.214E+11
YOS = 1.000E+00 MU = 1.000E+09 YADD = 0.
COSQ = 2.000E+00 C1 = 0.050E 00 C2 = 0
TENS(1) = -1.000E+10 TENS(2) = -1.000E+10 TENS(3) = -1.000E+10
RHOP = 0.184 0.202 0.333 0.625 1.205 1.250
COSQ = 2.0 2.0 2.0 2.0 2.0
C1 = 0.05 0.05 0.05 0.05 0.05
1 P2 = 2.800E+07 DELP = 6.000E+06 YADD = 0.
2 P2 = 3.350E+07 DELP = -1.400E+06 YADD = 0.
3 P2 = 3.450E+07 DELP = 2.500E+05 YADD = 0.
4 P2 = 8.000E+08 DELP = -1.900E+08 YADD = 0.
EMELT = 3.000E+09 9.000E+08 0. 0.5 0.
AK = 1.000E+09 MUP = 1.000E+09 YO = 0.
NZONES = 1, 10 CELLS IN 6.000E-01 CM, DELFIN = 4.000E-02
IRON RHO = 7.810E+00 NEQST = 1 NPOR = 0 NYO = 1 NCON = 0
EQSTC = 1.568E+12 EQSTD = 5.644E+12 EQSTE = 8.400E+10 EQSTG = 1.600
EQSTH = 0.250E+00 EQSTS = 1.216E+13
YO = 5.741E+09 MU = 6.000E+11 YADD = 0.
COSQ = 2.000E+00 C1 = 0.050E 00 C2 = 0
TENS(1) = -1.000E+11 TENS(2) = 0. TENS(3) = -1.000E+10
NZONES = 1, 10 CELLS IN 4.450E-02 CM
IRON FOAM RHOS = 7.81 NEQST = 1 NPOR = 4 NYO = 1 NCON =
EQSTC = 1.568E+12 EQSTD = 5.644E+12 EQSTE = 8.400E+10 EQSTG = 1.600
EQSTH = 0.250E+00 EQSTS = 1.216E+13
YO = 5.700E+09 MU = 6.000E+11 YADD = 0.
COSQ = 4.000E+00 C1 = 0.5 C2 = 0
TENS(1) = -1.000E+11 TENS(2) = -1.000E+10 TENS(3) = -3.000E+09
RHOP = 5.51 5.532 7.23 7.73 7.95 8.0
COSQ = 4.0 4.0 4.0 4.0 4.0
C1 = 0.1 0.1 0.1 0.1 0.1
1 P2 = 1.800E+09 DELP = 0. YADD = 0.
2 P2 = 8.000E 09 DELP = -1.000E 09 YADD = 0.
3 P2 = 1.200E 10 DELP = -1.000E+09 YADD = 0
4 P2 = 3.500E 10 DELP = -2.000E 09 YADD = 3.800E 09
EMELT = 4.750E+09 2.000E+09 0. 0.5 0.
AK = 6.000E+11 MUP = 2.000E+11 YO = 0.
NZONES = 1, 50 CELLS IN 0.287 CM, DELX = 2.200E-03
C7 (MN GAGE) RHO = 1.190E+00 NEQST = 1 NPOR = 0 NYO = 0 NCON = 0
EQSTC = 7.816E+10 EQSTD = 1.956E+10 EQSTE = 3.000E+10 EQSTG = 2.000E+00
EQSTH = 2.500E-01 EQSTS = 2.214E+11
COSQ = 2.000E+00 C1 = 0.050E 00 C2 = 0
TENS(1) = -3.000E+09 TENS(2) = 0. TENS(3) = 0.
NZONES = 1, 50 CELLS IN 1.500E+00 CM, DELX = 1.200E-02

END

NDATE= 10/22/68 IOENT=1044 IRON-IRON FOAM IMPACT 13403

STRESS HISTORY AT INTERFACES BETWEEN MATERIALS 1 AND 2 IS FOR COMPARISON WITH
GAGE RECORD OF DAVE SCHMIDT FROM SHOT 13403
COMPUTATIONS WERE MADE WITH SRI PUFF 1 ON THE CDC 3200 AT SRI. THE VERSION
OF SRI PUFF 1 IS EQUIVALENT TO THAT SUPPLIED TO AFWL WITH FINAL REPORT ON
DISTENDED MATERIAL MODEL DEVELOPMENT.

*** IRON-IRON FOAM IMPACT ***

```
1 NTEDT =      6 NJEDIT =      6 NREZON =      1 NSEPRAT =      0
2 TEDITS= 3.000E-07 5.000E-07 1.000E-06 1.500E-06 2.000E-06 2.500E-06 3.000E-06
3 JEDITS= 28 33 38 43 48 56
4 NTR =      1
5 JREZON= 48
6 NEDTM =      10000 NEDIT =      10000 NPERN =      3
7 STOPS      JCYS =      1000 CKS = 3.000E 00 TS = 3.000E-06
8 NMTRLS=      4 MATFL =      2 UZERO = 7.420E 04
POLYURETHANE FM RHOS = 1.19 NEQST = 1 NPOR = 4 NYO = 1 NCON = 0
EQSTC = 7.816E+10 EQSTD = 1.956E+11 EQSTE = 3.000E+10 EQSTG = 2.000E+00
EQSTH = 0.250E+00 EQSTS = 2.214E+11
YOS = 1.000E+00 MU = 1.000E+09 YADD = 0.
COSQ = 2.000E+00 C1 = 0.050E 00 C2 = 0
TENS(1)= -1.000E+10 TENS(2)= -1.000E+10 TENS(3)= -1.000E+10
RHOP = 0.187 0.202 0.333 0.625 1.205 1.250
COSQ= 2.0 2.0 2.0 2.0 2.0
C1= 0.05 0.05 0.05 0.05 0.05
1 P2 = 2.800E+07 DELP = 6.000E+06 YADD = 0.
2 P2 = 3.350E+07 DELP = -1.400E+06 YADD = 0.
3 P2 = 3.450E+07 DELP = 2.500E+05 YADD = 0.
4 P2 = 8.000E+08 DELP = -1.900E+08 YADD = 0.
EMELT = 3.000E+09 9.000E+08 0. 0.5 0.
AK = 1.000E+09 MUP = 1.000E+09 YO = 0.
NZONES= 1, 10 CELLS IN 6.000E-01 CM, DELFIN= 4.000E-02
IRON RHO = 7.810E+00 NEQST = 1 NPOR = 0 NYO = 1 NCON = 0
EQSTC = 1.568E+12 EQSTD = 5.644E+12 EQSTE = 8.400E+10 EQSTG = 1.600
EQSTH = 0.250E+00 EQSTS = 1.216E+13
YO = 5.741E+09 MU = 6.000E+11 YADD = 0.
COSQ = 2.000E+00 C1 = 0.050E 00 C2 = 0
TENS(1)= -1.000E+11 TENS(2)= 0. TENS(3)= -1.000E+10
NZONES= 1, 10 CELLS IN 4.650E-02 CM
IRON FOAM RHOS = 7.81 NEQST = 1 NPOR = 4 NYO = 1 NCON = 0
EQSTC = 1.568E+12 EQSTD = 5.644E+12 EQSTE = 8.400E+10 EQSTG = 1.600
EQSTH = 0.250E+00 EQSTS = 1.216E+13
YO = 5.700E+09 MU = 6.000E+11 YADD = 0.
COSQ = 4.000E+00 C1 = 0.100E 00 C2 = 0
TENS(1)= -1.000E+11 TENS(2)= -1.000E+10 TENS(3)= -3.000E+09
RHUP = 5.42 5.442 7.23 7.73 7.95 8.0
COSQ= 4.0 4.0 4.0 4.0 4.0
C1= 0.1 0.1 0.1 0.1 0.1
1 P2 = 1.800E+09 DELP = 0. YADD = 0.
2 P2 = 8.000E+09 DELP = -1.000E 09 YADD = 0.
3 P2 = 1.200E 10 DELP = -1.000E+09 YADD = 0
4 P2 = 3.500E+10 DELP = -2.000E+09 YADD = 3.800E+09
EMELT = 4.750E+09 2.000E+09 0. 0.5 0.
AK = 6.000E+11 MUP = 2.000E+11 YO = 0.
NZONES= 1, 30 CELLS IN 1.580E-01 CM, DELX= 2.300E-03
C7 (MN GAGE) RHO = 1.190E+00 NEQST = 1 NPOR = 0 NYO = 0 NCON = 0
EQSTC = 7.816E+10 EQSTD = 1.956E+10 EQSTE = 3.000E+10 EQSTG = 2.000E+00
EQSTH = 2.500E-01 EQSTS = 2.214E+11
COSQ = 2.000E+00 C1 = 0.050E 00 C2 = 0
TENS(1)= -3.000E+09 TENS(2)= 0. TENS(3)= 0.
NZONES= 1, 30 CELLS IN 7.500E-01 CM, DELX= 1.200E-02
```

END

NDATE= 10/22/68 IDENT=1045 IRON-IRON FOAM IMPACT 13418

STRESS HISTORY AT INTERFACES BETWEEN MATERIALS 1 AND 2 IS FOR COMPARISON WITH
GAGE RECORD OF DAVE SCHMIDT FROM SHOT 13418
COMPUTATIONS WERE MADE WITH SRI PUFF 1 ON THE CDC 3200 AT SRI. THE VERSION
OF SRI PUFF 1 IS EQUIVALENT TO THAT SUPPLIED TO AFWL WITH FINAL REPORT ON
DISTENDED MATERIAL MODEL DEVELOPMENT.

```

      * * * IRON-IRON FOAM IMPACT * * *
1 NTEDT =      4 NJEDIT =      6 NREZON =      1 NSFPRAT =      0
2 TEDITS= 1.000E-06 1.500E-06 2.000E-06 2.500E-06
3 JEDITS=  58  63  68  73  78  86
4 NTR =      1
5 JREZON=  78
6 NEDTM = 10000 NEDIT = 10000 NPERN =      3
7 STOPS      JCYCS = 1000 CKS = 3.000F 00 TS = 2.000E-06
8 NMTRLS=      4 MATFL =      2 UZERO = 7.380E 04
POLYURETHANE FM RHOS = 1.19 NEQST = 1 NPOR = 4 NYO = 1 NCON = 0
EQSTC = 7.816E+10 EQSTD = 1.956E+11 EQSTE = 3.000E+10 EOSTG = 2.000E+00
EQSTH = 0.250E+00 EQSTS = 2.214E+11
YOS = 1.000E+00 MU = 1.000E+09 YADD = 0.
COSQ = 2.000E+00 C1 = 0.050E 00 C2 = 0
TENS(1)= -1.000E+10 TENS(2)= -1.000E+10 TENS(3)= -1.000F+10
RHOP = 0.187 0.202 0.333 0.625 1.205 1.250
COSQ= 2.0 2.0 2.0 2.0 2.0
C1= 0.05 0.05 0.05 0.05 0.05
1 P2 = 2.800E+07 DELP = 6.000E+06 YADD = 0.
2 P2 = 3.350E+07 DELP = -1.400E+06 YADD = 0.
3 P2 = 3.450E+07 DELP = 2.500E+05 YADD = 0.
4 P2 = 8.000E+08 DELP = -1.900E+08 YADD = 0.
EMELT = 3.000E+09 9.000E+08 0. 0.5 0.
AK = 1.000E+09 MUP = 1.000E+09 YO = 0.
NZONES= 1, 10 CELLS IN 6.000E-01 CM, DELFIN= 4.000E-02
IRON RHO = 7.810E+00 NEQST = 1 NPOR = 0 NYO = 1 NCON = 0
EQSTC = 1.568E+12 EQSTD = 5.644E+12 EQSTE = 8.400F+10 EOSTG = 1.600
EQSTH = 0.250E+00 EQSTS = 1.216E+13
YO = 5.741E+09 MU = 6.000E+11 YADD = 0.
COSQ = 2.000E+00 C1 = 0.050E 00 C2 = 0
TENS(1)= -1.000E+11 TENS(2)= 0. TENS(3)= -1.000E+10
NZONES= 1, 40 CELLS IN 1.650E-01 CM
IRON FOAM RHOS = 7.81 NEQST = 1 NPOR = 4 NYO = 1 NCON =
EQSTC = 1.568E+12 EQSTD = 5.644E+12 EQSTE = 8.400E+10 EOSTG = 1.600
EQSTH = 0.250E+00 EQSTS = 1.216E+13
YO = 5.700E+09 MU = 6.000E+11 YADD = 0.
COSQ = 4.000E+00 C1 = 0.100E 00 C2 = 0
TENS(1)= -1.000E+11 TENS(2)= -1.000E+10 TENS(3)= -3.000E+09
RHOP = 5.29 5.312 7.23 7.73 7.95 8.0
COSQ= 4.0 4.0 4.0 4.0 4.0
C1= 0.1 0.1 0.1 0.1 0.1
1 P2 = 1.800E+09 DELP = 0. YADD = 0.
2 P2 = 8.000E+09 DELP = -1.000E 09 YADD = 0.
3 P2 = 1.200E 10 DELP = -1.000E+09 YADD = 0
4 P2 = 3.500E+10 DELP = -2.000E+09 YADD = 3.800F+09
EMELT = 4.750E+09 2.000E+09 0. 0.5 0.
AK = 6.000E+11 MUP = 2.000E+11 YO = 0.
NZONES= 1, 30 CELLS IN 1.580E-01 CM, DELX= 2.300E-03
C7 (MN GAGE) RHO = 1.190E+00 NEQST = 1 NPOR = 0 NYO = 0 NCON = 0
EQSTC = 7.816E+10 EQSTD = 1.956E+10 EQSTE = 3.000E+10 EOSTG = 2.000E+00
EQSTH = 2.500E-01 EQSTS = 2.214E+11
COSQ = 2.000E+00 C1 = 0.050E 00 C2 = 0
TENS(1)= -3.000E+09 TENS(2)= 0. TENS(3)= 0.
NZONES= 1, 30 CELLS IN 7.500E-01 CM, DELX= 1.200E-02

```

END

NDATE= 10/17/68 IDENT=1040 COPPER-COPPER FOAM IMPACT 13349

STRESS HISTORY AT INTERFACES BETWEEN MATERIALS 1 AND 2 IS FOR COMPARISON WITH GAGE RECORD OF DAVE SCHMIDT FROM SHOT 13349
COMPUTATIONS WERE MADE WITH SRI PUFF 1 ON THE CDC 3700 AT SRI. THE VERSION OF SRI PUFF 1 IS EQUIVALENT TO THAT SUPPLIED TO AFWL WITH FINAL REPORT ON DISTENDED MATERIAL MODEL DEVELOPMENT.

* * * COPPER-COPPER FOAM IMPACT * * *

1 NTEDT = 11 NJEDIT = 6 NREZON = 1 NSEPRAT = 0
2 TEDITS= 5.000E-07 1.000E-06 1.500E-06 2.000E-06 2.500E-06 3.000E-06 3.500E-06
4.000E-06 4.500E-06 5.000E-06 5.500E-06
3 JEDITS= 31 44 57 70 83 106
4 NTR = 1
5 JREZCN= 64
6 NEDTM = 10000 NEDIT = 10000 NPERN = 3
7 STOPS JCYS = 1000 CKS = 3-0 TS = 6.000E-06
8 NMTRLS= 4 MATFL = 2 UZERO = 7.350E 04
POLYURETHANE FM RHOS = 1.19 NEQST = 1 NPOR = 4 NYO = 1 NCON = 0
EQSTC = 7.816E+10 EQSTD = 1.956E+11 EQSTE = 3.000E+10 EQSTG = 2.000E+00
EQSTH = 0.250E+00 EQSTS = 2.214E+11
YOS = 1.000E+00 MU = 1.000E+09 YADD = 0.
COSQ = 2.000E+00 C1 = 0.050E 00 C2 = 0
TENS(1)= -1.000E+10 TENS(2)= -1.000E+10 TENS(3)= -1.000E+10
RHOP = 0.186 0.202 0.333 0.625 1.205 1.250
COSQ= 2.0 2.0 2.0 2.0 2.0
C1= 0.05 0.05 0.05 0.05 0.05
1 P2 = 2.800E+07 DELP = 6.000E+06 YADD = 0.
2 P2 = 3.350E+07 DELP = -1.400E+06 YADD = 0.
3 P2 = 3.450E+07 DELP = 2.500E+05 YADD = 0.
4 P2 = 8.000E+08 DELP = -1.900E+08 YADD = 0.
EMELT = 3.000E+09 9.000E+08 0. 0.5 0.
AK = 1.000E+09 MUP = 1.000E+09 YO = 0.
NZONES= 1, 10 CELLS IN 6.000E-01 CM, DELFIN= 4.000E-02
COPPER FLYER RHO = 8.94 NEQST= 1 NPOR = 0 NYO = 1 NCON= 0
EQSTC= 1.432E 12 EQSTD = 2.463E 12 EQSTE = 5.310E 10 EQSTG = 2.04
EQSTH= 0.25 EQSTS = 1.593E 12
YO = 1.060E 09 MU = 4.570E 11 YADD = 0.
COSQ = 4.0 C1 = 0.1 C2 = 0.
TENS(1)= -1.000E+11 TENS(2)= 0. TENS(3)= -1.000E+10
NZONES= 1, 10 CELLS IN 3.250E-02 CM
COPPER FOAM RHOS = 8.940 NEQST= 1 NPOR= 4 NYO = 1 NCON= 0
EQSTC= 1.432E 12 EQSTD = 2.463E 12 EQSTE = 5.310E 10 EQSTG = 2.04
EQSTH= 0.25 EQSTS = 1.593E 12
YOS = 1.060E+09 MU = 4.570E 11 YADD = 0.
COSQ = 4.0 C1 = 0.1 C2 = 0.
TENS(1)= -1.000E 11 TENS(2)= -1.000E 10 TENS(3)= -1.000E 10
RHOP = 6.530 6.539 8.333 8.75 9.0634 9.2
COSQ = 4.0 4.0 4.0 4.0 4.0
C1 = 0.1 0.1 0.1 0.1 0.1
1 P2 = 1.000E 09 DELP = 0. YADD = 0.
2 P2 = 6.000E09 DELP = -1.000E09 YADD = 0.
3 P2 = 1.200E 10 DELP = -5.000E 08 YADD= 0.
4 P2 = 2.000E 10 DELP = -5.000E 08 YADD = 7.000E 08
EMELT = 4.500E 09 2.000E 09 0. 0.3 0.
AK = 7.440E+11 MUP = 3.000E+11 YO = 0.
NZONES= 1, 80 CELLS IN 3.140E-01 CM, DELX= 2.200E-03
C7 (MN GAGE) RHO = 1.190E+00 NEQST = 1 NPOR = 0 NYO = 0 NCON = 0
EQSTC = 7.816E+10 EQSTD = 1.956E+10 EQSTE = 3.000E+10 EQSTG = 2.000E+00
EQSTH = 2.500E-01 EQSTS = 2.214E+11
COSQ = 2.000E+00 C1 = 0.050E 00 C2 = 0
TENS(1)= -3.000E+09 TENS(2)= 0. TENS(3)= 0.
NZONES= 1, 30 CELLS IN 7.500E-01 CM, DELX= 1.200E-02

END

NDATE= 10/21/68 IDENT=1041 COPPER-COPPER FOAM IMPACT 13404

COMPUTATIONS WERE MADE WITH SRI PUFF 1 ON THE CDC 3200 AT SRI. THE VERSION
STRESS HISTORY AT INTERFACES BETWEEN MATERIALS 1 AND 2 IS FOR COMPARISON WITH
GAGE RECORD OF DAVE SCHMIDT FROM SHOT 13404
OF SRI PUFF 1 IS EQUIVALENT TO THAT SUPPLIED TO AFWL WITH FINAL REPORT ON
DISTENDED MATERIAL MODEL DEVELOPMENT.

*** COPPER-COPPER FOAM IMPACT ***

1 NTEDT = 5 NJEDIT = 6 NREZON = 1 NSEPRAT = 0
2 TEDIT= 5.000E-07 1.000E-06 1.500E-06 2.000E-06 2.500E-06
3 JEDIT= 30 40 50 60 70 82
4 NTR = 1
5 JREZON= 64
6 NEDTH = 10000 NEDIT = 10000 NPERN = 3
7 STOPS JCYCS = 1000 CKS = 3.0 TS = 3.500E-06
8 NMTRLS= 4 MATFL = 2 UZERO = 7.430E 04
POLYURETHANE FM RHOS = 1.19 NEQST = 1 NPOR = 4 NYO = 1 NCON = 0
EQSTC = 7.816E+10 EQSTD = 1.956E+11 EQSTE = 3.000E+10 EQSTG = 2.000E+00
EQSTH = 0.250E+00 EQSTS = 2.214E+11
YOS = 1.000E+00 MU = 1.000E+09 YADD = 0.
COSQ = 2.000E+00 C1 = 0.050E 00 C2 = 0
TENS(1)= -1.000E+10 TENS(2)= -1.000E+10 TENS(3)= -1.000E+10
RHOP = 0.185 0.202 0.333 0.625 1.205 1.250
COSQ = 2.0 2.0 2.0 2.0 2.0
C1 = 0.05 0.05 0.05 0.05 0.05
1 P2 = 2.800E+07 DELP = 6.000E+06 YADD = 0.
2 P2 = 3.350E+07 DELP = -1.400E+06 YADD = 0.
3 P2 = 3.450E+07 DELP = 2.500E+05 YADD = 0.
4 P2 = 8.000E+08 DELP = -1.900E+08 YADD = 0.
EMELT = 3.000E+09 9.000E+08 0. 0.5 0.
AK = 1.000E+09 MUP = 1.000E+09 YO = 0.
NZONES= 1, 10 CELLS IN 6.000E-01 CM, DELFIN= 4.000E-02
COPPER FLYER RHO = 8.94 NEQST= 1 NPOR = 0 NYO = 1 NCON= 0
EQSTC= 1.432E 12 EQSTD = 2.463E 12 EQSTE = 5.310E 10 EQSTG = 2.04
EQSTH= 0.25 EQSTS = 1.593E 12
YO = 1.060E 0 MU = 4.570E 11 YADD = 0.
COSQ = 4.0 C1 = 0.1 C2 = 0.
TENS(1)= -1.000E+11 TENS(2)= 0. TENS(3)= -1.000E+10
NZONES= 1, 10 CELLS IN 3.760E-02 CM
COPPER FOAM RHOS = 8.940 NEQST= 1 NPOR= 4 NYO = 1 NCON= 0
EQSTC= 1.432E 12 EQSTD = 2.463E 12 EQSTE = 5.310E 10 EQSTG = 2.04
EQSTH= 0.25 EQSTS = 1.593E 12
YOS = 1.06E+09 MU = 4.570E 11 YADD = 0.
COSQ = 4.0 C1 = 0.1 C2 = 0.
TENS(1)= -1.000E 11 TENS(2)= -1.000E 10 TENS(3)= -1.000E 10
RHOP = 6.430 6.445 8.333 8.75 9.0634 9.2
COSQ = 4.0 4.0 4.0 4.0 4.0
C1 = 0. 0. 0. 0. 0.
1 P2 = 1.000E 09 DELP = 1.667E 08 YADD = 0.
2 P2 = 6.000E 09 DELP = -1.000E 09 YADD = 0.
3 P2 = 1.200E 10 DELP = -5.000E 08 YADD= 0.
4 P2 = 2.000E 10 DELP = 0. YADD = 7.000E 08
EMELT = 4.500E 09 2.000E 09 0.03 0.65 0.
AK = 7.440E+11 MUP = 3.000E+11 YO = 0.
NZONES= 1, 56 CELLS IN 1.910E-01 CM, DELX= 2.200E-03
C7 (MN GAGE) RHO = 1.190E+00 NEQST = 1 NPOR = 0 NYO = 0 NCON = 0
EQSTC = 7.816E+10 EQSTD = 1.956E+10 EQSTE = 3.000E+10 EQSTG = 2.000E+00
EQSTH = 2.500E-01 EQSTS = 2.214E+11
COSQ = 2.000E+00 C1 = 0.050E 00 C2 = 0
TENS(1)= -3.000E+09 TENS(2)= 0. TENS(3)= 0.
NZONES= 1, 30 CELLS IN 7.500E-01 CM, DELX= 1.200E-02

END

NDATE= 10/21/68 IDENT=1042 COPPER-COPPER FOAM IMPACT 13417

STRESS HISTORY AT INTERFACES BETWEEN MATERIALS 1 AND 2 IS FOR COMPARISON WITH
GAGE RECORD OF DAVE SCHMIDT FROM SHOT 13417
COMPUTATIONS WERE MADE WITH SRI PUFF 1 ON THE CDC 3200 AT SRI. THE VERSION
OF SRI PUFF 1 IS EQUIVALENT TO THAT SUPPLIED TO AFML WITH FINAL REPORT ON
DISTENDED MATERIAL MODEL DEVELOPMENT.

*** COPPER-COPPER FOAM IMPACT ***

```
1 NTEDT = 5 NJEDIT = 6 NREZON = 1 NSEPRAT = 0
2 TEDIT= 5.000E-07 1.000E-06 1.500E-06 2.000E-06 2.500E-06
3 JEDIT= 60 70 80 90 100 106
4 NTR = 1
5 JREZON= 94
6 NEDTM = 10000 NEDIT = 10000 NPERN = 3
7 STOPS JCYCS = 1000 CKS = 3.0 TS = 3.000E-06
8 NMTRL= 4 MATFL = 2 UZERO = 7.420E 04
POLYURETHANE FM RHOS = 1.19 NEQST = 1 NPOR = 4 NYO = 1 NCON = 0
EQSTC = 7.816E+10 EQSTD = 1.956E+11 EQSTE = 3.000E+10 EQSTG = 2.000E+00
EQSTH = 0.250E+00 EQSTS = 2.214E+11
YOS = 1.000E+00 MU = 1.000E+09 YADD = 0.
COSQ = 2.000E+00 C1 = 0.050E 00 C2 = 0
TENS(1)= -1.000E+10 TENS(2)= -1.000E+10 TENS(3)= -1.000E+10
RHOP = 0.186 0.202 0.333 0.625 1.205 1.250
COSQ= 2.0 2.0 2.0 2.0 2.0
C1= 0.05 0.05 0.05 0.05 0.05
1 P2 = 2.800E+07 DELP = 6.000E+06 YADD = 0.
2 P2 = 3.350E+07 DELP = -1.400E+06 YADD = 0.
3 P2 = 3.450E+07 DELP = 2.500E+05 YADD = 0.
4 P2 = 8.000E+08 DELP = -1.900E+08 YADD = 0.
EMELT = 3.000E+09 9.000E+08 0. 0.5
AK = 1.000E+09 MUP = 1.000E+09 YO = 0.
NZONES= 1, 10 CELLS IN 6.000E-01 CM, DELFIN= 4.000E-02
COPPER FLYER RHO = 8.94 NEQST= 1 NPOR = 0 NYO = 1 NCON= 0
EQSTC= 1.432E 12 EQSTD = 2.463E 12 EQSTE = 5.310E 10 EQSTG = 2.04
EQSTH= 0.25 EQSTS = 1.593E 12
YO = 1.060E 09 MU = 4.570E 11 YADD = 0.
COSQ = 4.0 C1 = 0.1 C2 = 0.
TENS(1)= -1.000E+11 TENS(2)= 0. TENS(3)= -1.000E+10
NZONES= 1, 40 CELLS IN 1.651E-01
COPPER FOAM RHOS = 8.940 NEQST= 1 NPOR= 4 NYO = 1 NCON= 0
EQSTC= 1.432E 12 EQSTD = 2.463E 12 EQSTE = 5.310E 10 EQSTG = 2.04
EQSTH= 0.25 EQSTS = 1.593E 12
YOS = 1.06E+09 MU = 4.570E 11 YADD = 0.
COSQ = 4.0 C1 = 0.5 C2 = 0.
TENS(1)= -1.000E 11 TENS(2)= -1.000E 10 TENS(3)= -1.000E 10
RHOP = 6.543 6.558 8.333 8.75 9.0634 9.2
COSQ = 4.0 8.0 8.0 16.0 16.0
C1 = 0.5 0.5 0.5 0.5 0.5
1 P2 = 1.000E 09 DELP = 1.667E 08 YADD = 0.
2 P2 = 6.000E 09 DELP = -1.000E 09 YADD = 0.
3 P2 = 1.200E 10 DELP = -5.000E 08 YADD= 0.
4 P2 = 2.000E 10 DELP = 0. YADD = 7.000E 08
EMELT = 4.500E 09 2.000E 09 0.08 0.65
AK = 7.440E+11 MUP = 3.000E+11 YO = 0.
NZONES= 1, 50 CELLS IN 1.590E-01 CM, DELX= 2.000E-03
C7 (MN GAGE) RHO = 1.190E+00 NEQST = 1 NPOR = 0 NYO = 0 NCON = 0
EQSTC = 7.816E+10 EQSTD = 1.956E+10 EQSTE = 3.000E+10 EQSTG = 2.000E+00
EQSTH = 2.500E-01 EQSTS = 2.214E+11
COSQ = 2.000E+00 C1 = 0.050E 00 C2 = 0
TENS(1)= -3.000E+09 TENS(2)= 0. TENS(3)= 0.
NZONES= 1, 30 CELLS IN 7.500E-01 CM, DELX= 1.200E-02
```

END

NOATE= 10/25/68 IDENT=1047 TUNGSTEN-TUNGSTEN FOAM IMPACT 13402

STRESS HISTORY AT INTERFACES BETWEEN MATERIALS 1 AND 2 IS FOR COMPARISON WITH
GAGE RECORD OF DAVE SCHMIDT FROM SHOT 13402
COMPUTATIONS WERE MADE WITH SRI PUFF 1 ON THE CDC 3200 AT SRI. THE VERSION
OF SRI PUFF 1 IS EQUIVALENT TO THAT SUPPLIED TO AFWL WITH FINAL REPORT ON
DISTENDED MATERIAL MODEL DEVELOPMENT.

```

* * * TUNGSTEN-TUNGSTEN FOAM IMPACT * * *
1 NTEDT = 7 NJEDIT = 6 NREZON = 1 NSEPRAT = 0
2 TEDITS= 5.000E-07 1.000E-06 1.500E-06 2.000E-06 2.500E-06 3.000E-06 3.500E-06
3 JEDITS= 28 34 40 45 50 56
4 NTR = 1
5 JREZON= 50
6 NEDTM = 10000 NEDIT = 10000 NPERN = 1
7 STOPS JCYCS= 2000 CKS= 3.0 TS = 3.000E-06
8 NMTRLS= 4 MATFL= 2 UZERO = 7.300E 04
POLYURETHANE FM RHOS = 1.19 NEQST = 1 NPOR = 4 NYO = 1 NCON = 0
EQSTC = 7.816E+10 EQSTD = 1.956E+11 EQSTE = 3.000E+10 EQSTG = 2.000E+00
EQSTM = 0.250E+00 EQSYS = 2.214E+11
YOS = 1.000E+00 MU = 1.000E+09 YADD = 0.
COSQ = 2.000E+00 C1 = 0.050E 00 C2 = 0.
TENS(1)= -1.000E+10 TENS(2)= -1.000E+10 TENS(3)= -1.000E+10
RHOP = 0.202 0.333 0.625 1.205 1.250
COSQ= 2.0 2.0 2.0 2.0 2.0
C1= 0.05 0.05 0.05 0.05 0.05
1 P2 = 2.800E+07 DELP = 6.000E+06 YADD = 0.
2 P2 = 3.350E+07 DELP = -1.400E+06 YADD = 0.
3 P2 = 3.450E+07 DELP = 2.500E+05 YADD = 0.
4 P2 = 8.000E+08 DELP = -1.900E+08 YADD = 0.
EMELT = 3.000E+09 9.000E+08 0. 0.5 0.
AK = 1.000E+09 MUP = 1.000E+09 YO = 0.
NZONES= 1, 10 CELLS IN 6.000E-01 CM, DELFIN= 4.000E-02
TUNGSTEN FLYER RHO= 1.960E 01 NEQST= 1 NPOR = 0 NYO = 1 NCON= 0
EQSTC= 3.101E 12 EQSTD = 3.487E 12 EQSTE = 4.620E 10 EQSTG = 1.62
EQSTM = 0.25 EQSTS = 4.265E 11
YO = 1.812E 10 MU = 1.550E 12 YADD = 0.
COSQ= 2.0 C1 = 0.1 C2 = 0.
TENS(1)= -2.000E 11 TENS(2)= 0. TENS(3)= 0.
NZONES= 1, 10 CELLS IN 5.050E-02
TUNGSTEN FOAM RHOS = 19.6 NEQST= 1 NPOR= 4 NYO= 1 NCON= 0
EQSTC= 3.101E 12 EQSTD = 3.487E 12 EQSTE = 4.620E 10 EQSTG = 1.62
EQSTM = 0.25 EQSTS = 4.265E 11
YOS = 1.812E+10 MU = 1.550E 12 YADD = 0.
COSQ = 4.0 C1 = 0.1 C2 = 0.
TENS(1)= -2.000E 11 TENS(2)= -5.000E 10 TENS(3)= -2.000E 11
RHOP = 14.56 14.628 18.45 18.90 20.83 21.0
COSQ = 4.0 4.0 4.0 4.0 4.0
C1 = 0.2 0.2 0.2 0.2 0.2
1 P2 = 1.000E 10 DELP = 0. YADD = 0.
2 P2 = 6.500E 10 DELP = -8.000E 09 YADD = 0.
3 P2 = 8.200E 10 DELP = -2.000E 09 YADD = 0.
4 P2 = 2.000E 11 DELP = 0. YADD = 1.200E 10
EMELT = 6.440E 09 3.000E 09 0. 0.5 0.
AK = 2.100E+12 MUP = 1.050E+12 YO = 0.
NZONES= 1, 30 CELLS IN 1.620E-01 CM, DELX= 3.000E-03
C7 (MN GAGE) RHO = 1.190E+00 NEQST = 1 NPOR = 0 NYO = 0 NCON = 0
EQSTC = 7.816E+10 EQSTD = 1.956E+10 EQSTE = 3.000E+10 EQSTG = 2.000E+00
EQSTM = 2.500E-01 EQSTS = 2.214E+11
COSQ = 2.000E+00 C1 = 0.050E 00 C2 = 0
TENS(1)= -3.000E+09 TENS(2)= 0. TENS(3)= 0.
NZONES= 1, 30 CELLS IN 7.500E-01 CM, DELX= 1.200E-02

```

END

NDATE= 10/23/68 IDENT=1046 TUNGSTEN-TUNGSTEN FOAM IMPACT 13473

STRESS HISTORY AT INTERFACES BETWEEN MATERIALS 1 AND 2 IS FOR COMPARISON WITH
GAGE RECORD OF DAVE SCHMIDT FROM SHOT 13473
COMPUTATIONS WERE MADE WITH SRI PUFF 1 ON THE CDC 3200 AT SRI. THE VERSION
OF SRI PUFF 1 IS EQUIVALENT TO THAT SUPPLIED TO AFWL WITH FINAL REPORT ON
DISTENDED MATERIAL MODEL DEVELOPMENT.

* * * TUNGSTEN-TUNGSTEN FOAM IMPACT * * *

1 NTEDT = 7 NJEDIT = 6 NREZDN = 1 NSEPRAT = 0
2 TEDITS= 5.000E-07 1.000E-06 1.500E-06 2.000E-06 2.500E-06 3.000E-06 3.500E-06
3 JEDITS= 62 71 80 89 98 106
4 NTR = 1
5 JREZDN= 80
6 NEDTM = 10000 NEDIT = 10000 NPERN = 1
7 STOPS JCYCS= 2000 CKS= 3.0 TS = 4.000E-06
8 NMTRLS= 4 MATFL= 2 UZERO = 7.350E 04
PLEXIGLAS RHO = 1.189 NEQST = 1 NPOR = 0 NYO = 0 NCON = 0
EQSTC = 7.816E+10 EQSTD = 1.956E+11 EQSTE = 3.000E+10 EQSTG = 2.000E+00
EQSTH = 0.250E+00 EQSTS = 2.214E+11
COSQ = 2.000E+00 C1 = 0.050E 00 C2 = 0
TENS(1)= -1.000E+10 TENS(2)= 0. TENS(3)= -1.000E+10
NZONES= 1, 30 CELLS IN 1.000E 00 CM, DELFIN= 1.000E-02
TUNGSTEN FLYER RHO= 1.960E 01 NEQST= 1 NPOR = 0 NYO = 1 NCON= 0
EQSTC= 3.101E 12 EQSTD = 3.487E 12 EQSTE = 4.620E 10 EQSTG = 1.62
EQSTH = 0.25 EQSTS = 4.265E 11
YO = 1.812E 10 MU = 1.550E 12 YADD = 0.
COSQ= 2.0 C1 = 0.1 C2 = 0.
TENS(1)= -2.000E 11 TENS(2)= 0. TENS(3)= 0.
NZONES= 1, 20 CELLS IN 1.140E-01
TUNGSTEN FOAM RHOS = 19.6 NEQST= 1 NPOR= 4 NYO= 1 NCON= 0
EQSTC= 3.101E 12 EQSTD = 3.487E 12 EQSTE = 4.620E 10 EQSTG = 1.62
EQSTH = 0.25 EQSTS = 4.265E 11
YOS = 1.812E+10 MU = 1.550E 12 YADD = 0.
COSQ = 4.0 C1 = 0.1 C2 = 0.
TENS(1)= -2.000E 11 TENS(2)= -5.000E 10 TENS(3)= -2.000E 11
RHOP = 14.26 14.328 18.45 18.90 20.83 21.0
COSQ = 4.0 4.0 4.0 4.0 4.0
C1 = 0.2 0.2 0.2 0.2 0.2
1 P2 = 1.000E 10 DELP = 0. YADD = 0.
2 P2 = 6.500E 10 DELP = -8.000E 09 YADD = 0.
3 P2 = 8.200E 10 DELP = -2.000E 09 YADD = 0.
4 P2 = 2.000E 11 DELP = 0. YADD = 1.200E 10
EMELT = 6.440E 09 3.000E 09 0. 0.5 0.
AK = 2.100E+12 MUP = 1.050E+12 YO = 0.
NZONES= 1, 50 CELLS IN 3.100E-01 CM, DELX= 3.000E-03
C7 (MN GAGE) RHO = 1.190E+00 NEQST = 1 NPOR = 0 NYO = 0 NCON = 0
EQSTC = 7.816E+10 EQSTD = 1.956E+10 EQSTE = 3.000E+10 FOSTG = 2.000E+00
EQSTH = 2.500E-01 EQSTS = 2.214E+11
COSQ = 2.000E+00 C1 = 0.050E 00 C2 = 0
TENS(1)= -3.000E+09 TENS(2)= 0. TENS(3)= 0.
NZONES= 1, 30 CELLS IN 7.500E-01 CM, DELX= 1.200E-02

END

REFERENCES

1. Rempel, J. R.; Schmidt, D. N.; Erkman, J. O.; Isbell, W. M.; Shock Attenuation in Solid and Distended Materials, Technical Report No. WL-TR-64-119, Stanford Research Institute, Contract AF29(601)-6040, February 1966.
2. Anderson, G. D.; Duvall, G. E.; Erkman, J. O.; Fowles, G. R.; Peltzer, C. P.; Investigation of Equation of State of Porous Earth Media, Technical Report No. AFWL-TR-65-146, Stanford Research Institute, Contract AF29(601)-6427, February 1966.
3. Linde, R. K.; Schmidt, D. N.; "Shock Propagation in Nonreactive Porous Solids", J. Appl. Phys., 37, p. 3259-3271, July 1966.
4. Linde, R. K.; Schmidt, D. N.; Attenuation of Shock Waves in Distended Materials, Stanford Research Institute Contract AF29(601)-6734, Technical Report No. AFWL-TR-66-13, May 1966.
5. Schmidt, D. N.; Linde, R. K.; Response of Distended Copper, Iron and Tungsten to Shock Loading, Technical Report No. AFWL-TR-68-33, Stanford Research Institute, Contract AF29(601)-7236, July 1968.
6. Gregson, V. G.; Ahrens, T. J.; Petersen, C. F.; Dynamic Properties of Rocks, Final Report, Stanford Research Institute, Contract AF 19(604)-8419, August 15, 1963.
7. Petersen, C. F.; Murri, W. J.; Anderson, G. D.; and Allen, C.F.; Equation of State of Rocks, Interim Technical Report by Stanford Research Institute, Contract AF (04-3) - 115, June 15, 1968.
8. Kormer, S. B.; Funtikov, A. I.; Urlin, V. D.; Kolesnikova, A. N.; "Dynamic Compression of Porous Metals and the Equation of State with Variable Specific Heat at High Temperatures," Soviet Physics JETP, 15, No. 3, September 1962.
9. Krupnikov, K. K.; Brazhnik, M. I.; Krupnikova, V. P.; "Shock Compression of Porous Tungsten," Soviet Physics JETP, 15, No. 3, September 1962.
10. Boade, R. R.; Shock Loading of Porous Tungsten, SC-RR-66-290, Sandia Laboratory, Albuquerque, New Mexico, June 1966.

11. Johnson, J. O.; Wackerle, J.; "Shock-Wave Compression of Porous Magnesium and Ammonium Sulfate," Presented at IUTAM Symposium on Behavior of Dense Media Under High Dynamic Pressures, Paris, France, September 11-15, 1967.
12. Anderson, G. D.; Fahrenbruch, A. L.; Equation of State of Solids II: Aluminum and Teflon, Technical Report No. AFWL-TR-67-43, Stanford Research Institute, Contract AF 29(601)-7214, September 1967.
13. Boade, R. R.; "Compression of Porous Copper by Shock Waves," J. Appl. Phys., 39, p. 5693 (1968).
14. Butcher, B. M.; Karnes, C. H.; Dynamic Compaction of Porous Iron, SC-RR-67-3040, Sandia Corporation, April 1968.
15. Butcher, B. M.; Porous Carbon Materials, SC-DR-66-438, Sandia Corporation, September 1966.
16. Boade, R. R.; " Shock Compression of Foamed Graphite," J. Appl. Phys., 39, p. 1609, February 15, 1968.
17. Jahsman, W. E.; Static and Dynamic Material Behavior of Syntactic Foam, LMSC/6-77-67-32, Lockheed Missiles and Space Company, Palo Alto, California.
18. Lieberman, P.; Studies of Reactor Containment, Vol. II, Determination of the Equation-of-State of Porous Solids, Task Two Final Report, IITRI-578P21-22, Project T6042, October 1967.
19. Lee, L.M.; Some Dynamic Mechanical Properties of Pyrolytic Boron Nitride, SC-RR-67-2947, Sandia Laboratory, Albuquerque, New Mexico, December 1967.
20. Linde, R. K.; DeCarli, P. S.; Polymorphic Behavior of Titania Under Dynamic Loading, J. Chem. Phys. 50, 319-325, January 1969.
21. Von Neumann, J.; Richtmyer, R. D.; "A Method for the Numerical Calculation of Hydrodynamic Shocks," J. Appl. Phys., 21, p. 232, 1950.
22. Richtmyer, R. D.; Morton, K. W.; Difference Methods for Initial-Value Problems, 2d Ed., Interscience Publishers, New York, 1967.

23. Crosby, J. K.; Gill, S. P.; Feasibility Study of An Explosive Gun, Final Report No. 2, Stanford Research Institute Project FGU-4500, Contract NAS2-1361, May 1966.
24. Nance, O.; Smith, H. A.; An X-Ray Effects Code (U), UCRL-5616-T, University of California, Lawrence Radiation Laboratory, Livermore, California, July 1959 (Secret).
25. Nance, O.; Wilkins, M.; Blandford, I.; Smith, H.; SHARP--A One-Dimensional Hydrodynamics Code for the IBM 704, UCRL-5206-T, University of California, Lawrence Radiation Laboratory, Livermore, California, April 1958.
26. Bothell, L. E.; et al.; Equation of State for the PUFF Code (U), AFSWC-TDR-62-147, Research Directorate, Air Force Special Weapons Center, Kirtland Air Force Base, New Mexico, 1963 (Confidential).
27. Bothell, L. E., et al.; Predictions of the Responses of Materials to X-Rays (U), AFSWC-TDR-62-152, Research Directorate, Air Force Special Weapons Center, Kirtland Air Force Base, New Mexico, 1963 (RD).
28. Bothell, L. E.; Theoretical Calculations of Shock Propagation in Ablative Materials (U), AFSWC-TDR-61-63, Research Directorate, Air Force Special Weapons Center, Kirtland Air Force Base, New Mexico, March 1962 (RD).
29. Bothell, L. E.; PUFF III, Variable Time Step, and Mass Absorption Coefficient Codes (U), AFSWC-TDR-62-151, Research Directorate, Air Force Special Weapons Center, Kirtland Air Force Base, New Mexico, 1963 (RD).
30. Bothell, L. E.; Archuleta, C. E.; Franke, R. E.; PUFF IV Hydrocode, Part I (U), Kaman Nuclear Report KN-664-65-1, Contract DA-01-021-AMC-90023(x), November 1965 (RD).
31. Bothell, L. E.; Archuleta, C. E.; PUFF IV-EP Hydrocode, Part I (U), Kaman Nuclear Final Report KN-664-67-1, Contract DA-01-021-AMC-90023(y), January 1967 (RD).

32. Bothell, L. E.; Archuleta, C. E.; PUFF V-EP CODE (U), Kamcan Nuclear Final Report KN-703-67-101(R), Contract DA-01-021-AMC-90029(Y), for Sentinel Systems Command, SENEC-DRS, Redstone Arsenal, Alabama, December 15, 1967 (RD).
33. Grandey, R. A.; PUFF VTS Computer Program (U), AFSWC-TDR-62-76, Research Directorate, Air Force Special Weapons Center, Kirtland Air Force Base, New Mexico, 1963 (Confidential).
34. Allen, R. G.; Goodwin, L. K.; et al.; A Study of X-Ray Counter-measure Methods (U), AFWL TDR-64-42, Air Force Weapons Laboratory, Kirtland Air Force Base, New Mexico, June 1964 (RD).
35. Brodie, R. N.; Hormuth, J. E.; The PUFF 66 and P PUFF 66 Computer Programs, Research and Technology Division, Air Force Weapons Laboratory, Kirtland Air Force Base, New Mexico, May 1966.
36. Herrmann W.; Holzhauser, P.; Thompson, R. J.; WONDY, A Computer Program for Calculating Problems of Motion in One Dimension, SC-RR-66-601, Sandia Corporation, Albuquerque, New Mexico, February 1967.
37. Trulio, John G.; Theory and Structure of the Afton Codes, AFWL-TR-66-19, Nortronics, Division of Northrup Corporation, Contract AF29(601)-6683, June 1966.
38. Thouvenin, J.; "The Effect of a Shock Wave on a Porous Solid," Proc. Fourth Symposium on Detonation, U.S. Naval Ordnance Laboratory, White Oak, Maryland, p. 258, October 1965.
39. Heyda, J. F.; "An Equation of State for Solids Based on a Modified Plate-Gap Model," Presented at IUTAM Symposium on Behavior of Dense Media Under High Dynamic Pressures, Paris, France, September 11-15, 1967.
40. Prindle, H.; Shocks in Porous Materials, D2-125019-1, The Boeing Company, February 1968.
41. Butcher, B. M.; Dynamic Crushup of Foams, SC-RR-66-325, Sandia Laboratory, Albuquerque, New Mexico, May 1967.

42. Fritz, J. N.; Taylor, J. W.; An Equation of State for Adiprene Foam and Its Application in Producing Low Pressure-Long Time Pulses, LA-3400-MS, University of California Los Alamos Scientific Laboratory, 1966.
43. Wagner, M. H.; Brooks, N. D.; Bjork, R. L.; "Impact of a Porous Aluminum Projectile on Aluminum at 20 and 72 km/sec," Proc. Seventh Hypervelocity Impact Symposium, Vol. III, Martin Company, Orlando, Florida, February 1965.
44. Herrmann, W.; Equation of State of Crushable Distended Materials, SC-RR-66-2678, Sandia Corporation, Albuquerque, New Mexico, March 1968.
45. Herrmann, W.; On the Elastic Compression of Crushable Distended Materials, SC-DR-68-321, Sandia Laboratory, Albuquerque, New Mexico, June 1968.
46. Johnson, J. N.; A Theory of Rate-Dependent Behavior for Porous Solids: Steady-Propagating Compaction Wave Profiles, SC-RR-68-151, Sandia Laboratory, Albuquerque, New Mexico, April 1968.
47. Kawakita, K.; Tsutsumi, Y.; "An Empirical Equation of State for Powder Compression," Japanese J. Appl. Phys., 4, No. 1, January 1965.
48. Biot, M. A.; "Mechanics of Deformation and Acoustic Propagation in Porous Media," J. Appl. Phys., 33, No. 4, April 1962.
49. MacKenzie, J. K.; "The Elastic Constants of a Solid Containing Spherical Holes," Proc. of the Phys. Society, Sect. B, Vol. 63, p. 2, 1950.
50. Bull, T. H.; "The Tensile Strengths of Viscous Liquids Under Dynamic Loading," Brit. J. Appl. Phys., 7, p. 416, 1956.
51. Metals Handbook, Vol. 1, American Society of Metals, 1961.
52. Butcher, B. M., Mechanical Properties of Impacted Solid Polyurethane, SC-RR-67-478, Sandia Laboratory, Albuquerque, New Mexico, July 1967.

UNCLASSIFIED

Security Classification

DOCUMENT CONTROL DATA - R & D

(Security classification of title, body of abstract and indexing annotation must be entered when the overall report is classified)

1. ORIGINATING ACTIVITY (Corporate author) Stanford Research Institute 333 Ravenswood Avenue Menlo Park, California 94025		2a. REPORT SECURITY CLASSIFICATION UNCLASSIFIED	
		2b. GROUP	
3. REPORT TITLE DISTENDED MATERIAL MODEL DEVELOPMENT Volume I Experiments and Theory for the Model			
4. DESCRIPTIVE NOTES (Type of report and inclusive dates) 21 April 1967 through 1 March 1969			
5. AUTHOR(S) (First name, middle initial, last name) L. Seaman R. K. Linde			
6. REPORT DATE May 1969		7a. TOTAL NO. OF PAGES 108	7b. NO. OF REFS 52
8a. CONTRACT OR GRANT NO. F29601-67-C-0073		8a. ORIGINATOR'S REPORT NUMBER(S) AFWL-TR-68-143, Vol. I	
8b. PROJECT NO. 5710		8b. OTHER REPORT NO(S) (Any other numbers that may be assigned this report) SRI Project PGU 6586	
8c. Subtasks: 15.018 and 15.025			
8d.			
10. DISTRIBUTION STATEMENT This document is subject to special export controls and each transmittal to foreign governments or foreign nationals may be made only with prior approval of AFWL (WLRP), Kirtland AFB, NM 87117. Distribution is limited because of the technology discussed in the report.			
11. SUPPLEMENTARY NOTES <i>copy to WLRP for review</i>		12. AFFECTING MILITARY ACTIVITY AFWL (WLRP) Kirtland AFB, NM 87117	
13. ABSTRACT (Distribution Limitation Statement No. 2) The research goals were (1) to develop a dynamic response model or constitutive relations for porous materials, (2) to test this model against results from shock wave experiments, and (3) to incorporate the model into a computer program for the analysis of shock wave propagation arising either from impacts or from radiation deposition. The model developed exhibits melting, vaporization, and temperature-dependent compaction resistance, yielding, consolidation, and spalling. The model accounts for loading and unloading, heating and cooling, and any combination of these processes. The computer program (SRI PUFF 1) for analyzing shock wave propagation problems employs artificial viscosity in a modified Lax-Wendroff integration scheme. Flyer plate impact experiments (shock attenuation tests) were conducted on samples of porous iron, copper, and tungsten, and stress histories were recorded at the rear face of the targets. Quasi-static one-dimensional compression tests were made on samples of the same porous metals, using pressures up to 10 kbar. Numerical values of parameters in the model were obtained from the quasi-static tests and from previously reported Hugoniot experiments. Stress histories computed with the code were compared with stress records obtained from the attenuation experiments. The computed (predicted) peak stresses and arrival times of the waves generally agreed to within 20 percent or better with the measured values. Precursor amplitudes and other wave front features were correctly represented in the computed histories. The model appears to adequately represent the dynamic response of porous materials, the major uncertainty being the numerical values of parameters for a given material.			

DD FORM 1473

NOV 66

REPLACES DD FORM 1473, 1 JAN 64, WHICH IS OBSOLETE FOR ARMY USE.

UNCLASSIFIED

Security Classification

~~UNCLASSIFIED~~
~~Security Classification~~

14.

KEY WORDS

LINK A

LINK B

LINK C

ROLE

WT

ROLE

WT

ROLE

WT

Hugoniot
Shock hydrodynamics
Equation of state of metals
Distended materials

UNCLASSIFIED

~~Security Classification~~